TÉCNICO
LISBOA

Temporal Evolution of a NAPL Source Zone Up-gradient of a Pump & Treat System in a Fractured Sandstone Aquifer

Brian Kamau Ndirangu

Thesis to obtain the Master of Science Degree in
Environmental Engineering

Supervisors:
Prof. Dr. Beth Parker
Dr. Maria Teresa Condesso de Melo

Examination Committee
Chairperson: Prof. Dr. Luís Tavares Ribeiro
Supervisor: Dr. Maria Teresa Condesso de Melo
Members of the Committee: Prof. Dr. Jessica Rae Meyer

September 2018

Temporal Evolution of a NAPL Source Zone Up-gradient of a Pump & Treat System in a Fractured Sandstone Aquifer

Master of Science Thesis
by
Brian Kamau Ndirangu

Supervisors
Prof. Dr. Beth Parker
Dr. Maria Teresa Condesso de Melo

Examination committee
Prof. Doutor Luís Tavares Ribeiro
Prof. Dr. Jessica Rae Meyer
Doutora Maria Teresa Condesso de Melo

This thesis is submitted in partial fulfilment of the requirements for the academic degree of
Master of Science in Water Science and Engineering
UNESCO-IHE Institute for Water Education, Delft, the Netherlands
Master of Science in Environmental Engineering
Instituto Superior Técnico, Universidade de Lisboa, Portugal
Master of Science in Hydro Science and Engineering
Technische Universität Dresden, Germany

MSc research host institution
Instituto Superior Técnico, University of Lisbon, Portugal

September 2018

Acknowledgements

First, I would like to thank my supervisors: Dr. Teresa Melo for giving me the opportunity to participate in a collaborative research environment and for her close guidance throughout my master's program and Prof. Beth Parker for welcoming me into her research team, engaging me in a very unique and challenging field of research and equipping me with valuable skills that will continue to serve me beyond this research period. I would also like to thank Prof. Jessi Meyer for the time she took to introduce me to the site, for the numerous discussions whose insights were fundamental to my research and for reviewing my work. I would also like to acknowledge the G^{360} team members who helped me settle in Canada smoothly, coordinated various fieldwork campaigns and who made my time memorable.

The constant support from my family and friends has been very instrumental during this program. I appreciate my parents, Ndirangu and Wanjiru, who despite being far away, have always supported me in my endeavours. Sylvia, for your supportive role throughout my program, especially in Canada, and the many friends that I have made from all over the world who have added life to my years. I would also like to thank the GroundwatCH coordinators from The Netherlands, Portugal and Germany, Tibor Stigter, Luís Ribeiro and Christian Bernhofer for their thoughtful input in creating such an exciting program and for the Erasmus Mundus funding opportunity.

Resumo

O desempenho das tecnologias de remediação de compostos de fase líquida não aquosa (NAPL) depende da caracterização espacial e temporal efetiva das arquiteturas das áreas fonte. Atualmente, poucos estudos publicados avaliaram a utilização de métodos *in situ* para investigar locais de rochas fraturadas cujas condições hidrogeológicas exibem grande heterogeneidade espacial e distribuição complexa de compostos NAPL. O estudo localizou-se no centro-sul do estado de Wisconsin (EUA) e a contaminação resulta de um composto DNAPL multicomponente (compostos orgânicos clorados alifáticos incluindo etenos clorados, etanos e metanos, cetonas e benzeno, tolueno, etil benzeno e xilenos, em resumo BTEX) lançado antes de 1970 e que criou uma pluma de contaminação na formação dos Grés de Tunnel City (TC), com cerca de 2,8 km de comprimento e uma profundidade de 48 a 56 metros sob a superfície do terreno. O DNAPL móvel permanece nos arenitos da TC e existe DNAPL residual na rocha sobrejacente. Três furos de bombagem localizados nos Grés de TC a cerca de 1 km da origem operam desde 2003.

Este estudo caracteriza *in situ* a variabilidade temporal da massa de contaminante utilizando uma amostragem das formações geológicas de alta resolução em 5 sondagens ao longo de uma secção transversal perpendicular ao fluxo de água subterrânea e 80 m águas abaixo do foco de contaminação. Um desses locais inclui três sondagens localizadas no mesmo local em 2003, 2014 e 2017, cada uma monitorizada de forma contínua e amostrada para a recolha de amostras de rocha para análise de compostos orgânicos voláteis (VOCs) nas proximidades e distante de zonas de fraturas para comparação com as amostras de água subterrânea. Também foi estimada a influência da heterogeneidade espacial na avaliação temporal através da utilização de métodos geofísicos e amostragens ao longo da secção transversal de 278 m. Este estudo também avalia caudais de bombagem e dados de concentração dos furos localizados águas abaixo do foco de contaminação para se obter valores de fluxo de massa que foram depois comparados com os observados na secção ao longo da área fonte (SZT).

Os resultados revelam uma redução de massa de 77% dos VOCs na matriz da rocha entre 2003 e 2014 e outros 6% até 2017, mostrando assim uma redução de massa exponencial com o tempo. Uma análise complementar dos dados revela que a redução de massa ocorre a uma velocidade variável com a profundidade e o tempo. Entre 2004 e 2014, a maioria desta redução deu-se nas unidades mais superficiais e entre 2014 e 2017, são as unidades mais profundas que apresentam maior redução. Uma análise das frações molares com a profundidade mostra um aumento de 57% dos compostos clorados e um aumento correspondente nas concentrações de cetonas e BTEX. Estimou-se que a influência da distribuição espacial das três amostras nas interpretações temporais varia de 4 a 6%. Em geral, as concentrações na água subterrânea são diferentes numa ordem de magnitude das observadas na água dos poros das rochas. Este equilíbrio mostra que processos de difusão podem acontecer na matriz em determinadas secções, contribuindo para as reduções das concentrações de contaminantes observadas nas áreas fonte. Os fluxos de massa calculados nos furos de bombagem são cerca de 60x superiores aos fluxos de massa na fonte desde 20154 até à atualidade. A comparação das composições mostra que a composição no furo de bombagem localizado na secção ao longo da área fonte se aproxima da observada nas amostras de rocha da área fonte.

Abstract

Performance of non-aqueous phase liquids (NAPL) remediation technologies rely on effectively characterizing source zone architectures spatially and temporally. Few published studies have used field-focused methods to investigate fractured rock sites whose hydrogeological conditions display large spatial heterogeneity and complex NAPL distribution. The study site is located in south-central Wisconsin and consists of a multicomponent DNAPL (chlorinated aliphatic compounds including chlorinated ethenes, ethanes and methanes, ketones and benzene, toluene, ethyl benzene and xylenes, i.e. BTEX) released prior to 1970 that has created a 2.8 km long plume 48 to 56 meters below ground surface (mbgs) in the Tunnel City sandstones. Mobile DNAPL remains in the Tunnel City sandstones and inferred residual DNAPL in the overlying rock. Three pumping wells screened in the Tunnel City sandstones located ~1 km downgradient of the source zone have been operating since 2003.

This study characterizes the temporal variability of the *in situ* mass using high resolution rock core sampling at five locations along a 278 m long transverse cross-section (i.e. transect) perpendicular to groundwater flow and eighty meters downgradient of the source zone. One of these locations includes three co-located core holes drilled in 2003, 2014 and 2017, each continuously logged and sampled for depth-discrete rock core VOC analyses for total mass concentrations near and away from fractures for comparison to groundwater samples predominantly from fractures from a multi-level systems installed at each hole. The influence of spatial heterogeneity on the temporal evaluations is also estimated using the core and geophysical logs along the 278m long transect. This study also examines pumping rates and concentration data from the downgradient wells to obtain a mass discharge which is then compared to calculated mass flux across the source zone transect (SZT) in the rock matrix up-gradient.

The results show a 77% mass reduction in rock matrix volatile organic compound (VOC) mass between 2003 and 2014 and a further 6% by 2017, representing an exponential mass reduction with time. Further analysis shows that the mass loss occurs at a variable rate with depth and with time. Between 2004 and 2014, most of the mass loss occurred in the upper bedrock whereas between 2014 and 2017, the lower bedrock units recorded the highest declines. Analysis of mole fractions with depth show a 57% decrease in chlorinated compounds and a corresponding increase in ketones and BTEX. The influence of the spatial distribution of the three cores on the temporal interpretations was approximated to be between 4 and 6%. Generally, concentrations of groundwater are within an order of magnitude difference with calculated rock matrix pore water concentrations. This equilibrium shows that back-diffusion processes may be occurring within the matrix in certain sections, contributing to the observed source declines. Mass discharge from the pumping wells was calculated to be approximately sixty times higher than the total mass flux observed at the source zone from the 2014 data. Comparison of the compositions show that the composition of the extraction well closest to the SZT closely matches that observed from the cored holes in the source zone.

The mass lost from the source zone was attributed to a number of mechanisms. First, the reduction of concentrations of higher molecular weight chlorinated compounds and a noticeable increase in daughter products suggests that biodegradation is taking place inside the rock matrix. Further evidence drawn from previous microbial community studies at this site showed the presence of cultures in the rock matrix that support biodegradation as a mechanism for mass reduction. The equilibrium of groundwater and pore water concentrations in certain sections of the profiles suggests that back-diffusion processes could be occurring, leading to rock matrix contaminant declines. The high mass discharge, especially from the well closest to the source zone core holes, and its composition, are evidence that the increased rate of groundwater flushing is contributing to the observed source zone mass declines. Over the entire analysis period, it has been shown that a substantial change in mass and composition occurs in the upper rock rather than in the Tunnel City sandstones where the pump & treat system is screened. Given the large difference in mass discharge and source zone mass flux, it is possible that the pumping wells are capturing mass from the zones above, within and below the screened section, although further capture zone delineation studies are needed to confirm this result. Ultimately, this study provides insights on temporal changes in the mass and composition of contaminants within a source zone, which will be valuable in refining site conceptual models, informing source and plume management strategies and offering insight on remediation strategies.

Table of Contents

List of Figures

List of Tables

Abbreviations

Abbreviations and acronyms are listed in alphabetical order. Abbreviations that appear only once are not included in this list. Acronyms that appear in citations are provided in full in the References.

1,1-DCA	1,1-dichloroethane
1,1-DCE	1,1 dichloroethene
1,1-TCA	1,1,1- trichloroethane
1,2-DCA	1,2-dichloroethane
BTEX	benzene, toluene, ethylbenzene, and xylene
Cis-1,2-DCE	cis-1,2, dichloroethene
CSIA	compound specific isotope analysis
DCM	methylene chloride/dichloromethane
DFN-M	discrete fracture network and matrix
DNAPL	dense non-aqueous phase liquid
f_{oc}	fraction of organic carbon
GC/MS	gas chromatography/mass spectrometry
HBS	hydraulic barrier system
HGU	hydrogeological unit
MEK	2-butanone/methyl-ethyl ketone
MIBK	4-methyl-2-pentanone/methyl isobutyl ketone
MLS	multilevel system
NAPL	non-aqueous phase liquid
PCE	perchloroethene /tetrachloroethene
SCM	site conceptual model
SZT	source zone transect
TCE	trichloroethene
TVOC	total volatile organic compounds
VC	vinyl chloride
VOC	volatile organic compound

1   Introduction

1.1   Motivation and Relevance of the Study

The extensive production and improper handling of household and industrial chemicals such as plastics, paints, gasoline products and pesticides has led to widespread contamination of regional aquifers around the world (Brusseau et al., 2007; O'Connor et al., 2018). In the United States (US), 77,000 such sites have undergone cleanup work and it is estimated that between 235,000 to 355 000 sites will need to be cleaned up in the next two decades at a total estimated cost of $209 billion (U.S. E.P.A., 2004). Of the myriad of contaminants present at hazardous waste sites, organic chemicals in the form of dense non-aqueous phase liquids (DNAPLs), including chlorinated solvents, have been ranked as some of the most challenging to remediate (NRC, 1994). Historical DNAPL releases at a substantial number of impacted sites have included single or multi-component spills from multiple or unknown sources. Further exacerbating this complexity is the presence of such DNAPLs in fractured media which are ubiquitous in the US and are often considered to be the most heterogeneous geology (NRC, 2005). Due to the multiplicity of these complex factors, site management can be very expensive and the effectiveness of planned remediation remains uncertain. It is estimated that restoration of such aquifers within the next century is likely unachievable (NRC, 2013). A major stride towards better decision making for the long-term management of contaminated fractured aquifers lies in understanding the behaviour and spatio-temporal evolution of DNAPLs.

The topic of contaminated aquifers is of central importance especially in light of various aspects of global change. The quadrupling of global population in the last century has resulted into an eight-fold increase in water demand; a further 55% population increase projected by 2050 is likely to increase water stress and shortage (UNESCO, 2014). The resulting socio-economic pressures have exacerbated anthropogenic contamination of water resources at a time when water scarcity is prevailing. Groundwater is not immune to these changes as aquifers around the world continue to be polluted by sources which are sometimes detected decades after the original contamination. Some parts of the US, such as California and Nevada, have exhibited severe droughts, land-use change and economic changes that have threatened their groundwater dependent populations. The fact that California's groundwater systems have reported widespread contamination, including DNAPLs (Pierce et al., 2018), underscores the importance of identifying, characterising, remediating and managing groundwater resources more so in the face of climate change.

1.2   Research Objectives

The overarching goal of this study is to assess groundwater contamination up-gradient of a pump & treat system with a focus on improving the site conceptual model (SCM) to inform on potential remediation technologies (Parker et al., 2018). A field research site located in Cottage Grove, Wisconsin, was selected, where historical releases of multi-component DNAPLs contaminated a fractured sandstone prior to 1970.

Detailed field investigations since 2003 provide several complimentary datasets gathered from high resolution characterisation of volatile organic compound (VOC) concentration profiles in the rock matrix using continuous cores followed by depth-discrete multilevel groundwater sampling from these wells after coring. Downgradient, a pump and treat system has been operational since 2003 to limit the migration of the dissolved-phase plume. Data available from these extraction wells include quarterly groundwater VOC concentrations and pumping rate records. Previous studies at this site since 2003 provide a wealth of other supporting information to strengthen interpretations of this work.

Source zone characterisation has been identified as a crucial step to better inform on the attenuation processes, to understand the spatial and temporal variations of the contaminant mass, zones of varying distribution, and back-diffusion processes from the matrix to fractures. The two key questions which will be examined in this thesis in order to address the research gaps in the science are: 1) what is the long-term temporal evolution of contaminants in the rock matrix within the source zone? and 2) how do mass and composition changes within the source zone compare to that captured by downgradient pumping wells?

Two main objectives were identified and combined with a study approach specifically designed to fill in the scientific gaps and also inform the SCM used to make management and remediation decisions. These objectives are: 1) to characterise the temporal evolution of contaminant mass in the rock matrix just downgradient of the source zone and 2) to compare the contaminant changes downgradient of the source zone to the mass removed by a pump and treat system. The qualitative and quantitative approaches used in this investigation are briefly discussed below.

For the first objective, the temporal evolution is characterised using three co-located vertical boreholes that were cored in 2003, 2014 and 2017. These core holes are located eighteen meters apart along a transect approximately eighty meters downgradient of the source zone where contaminant spills occurred. From each borehole, high resolution sampling methods (at least 3 samples/meter of core) were utilised to collect rock samples from the low permeability matrix which were then tested for thirty-five VOCs. The rock core VOC profiles provided depth discrete and detailed quantification of the contaminant mass in the rock matrix. Groundwater samples representative of the fractures were collected from depth-discrete multilevel systems installed in the same holes after they were cored to complement the rock matrix data. Previous assessment of the rock core data from 2003 and 2014 was performed by Buckley (2017). The results from the 2017 core is added to these analyses to determine how the rock matrix contaminant mass has changed over the fourteen year period. In addition, although the holes are co-located, some of the differences between cores maybe due to spatial heterogeneity rather than change through time. The influence of spatial heterogeneity on the temporal interpretations is evaluated by utilising rock core data from five other holes that were drilled in 2014 and which make up the rest of the source zone transect (SZT).

For the second objective, a detailed comparisons of the mass loss observed along the SZT is compared to the mass extracted by a hydraulic barrier system (HBS) composed of three pumping wells located 573, 1075 and 1296m downgradient of the SZT. The main aim of this comparison is to better understand the

processes and physical conditions that would result in any differences noted. The originality of this study is that it explores multiple lines of evidence using rock core samples from low permeability rock matrix and groundwater samples representative of the fractures collected over various spatial and temporal scales to identify, quantify and suggest suitable mechanisms for mass and composition changes at a contaminated site that is under the influence of a pump and treat system. Attaining this fundamental understanding into source-zone architectures should make an important contribution to depth-targeted subsurface remediation and inform environmental regulation on contaminated zones.

1.3   Approach

The Discrete Fracture Network and Matrix (DFN-M) approach developed by Parker et al. (2012) is a particularly useful approach for investigating fractured rock sites. The DFN-M approach has been successfully applied in numerous contaminated sites in Europe and North America to gain a detailed understanding of contaminant distribution and evolution (Chapman et al., 2018; Meyer et al., 2016; Pierce et al., 2018; Stuetzle, 2014). A major advantage is its emphasis on depth-discrete rock core sampling to delineate vertical contaminant distribution in the low-permeability matrix where most of the contaminant mass resides, especially in mature contaminated sites. The DFN-M approach was adjusted to suit this location based on previous site knowledge on fracture network, matrix porosity, and contaminant distribution.

Preliminary results from rock core analysis including the position and distribution of both fractures and contaminants were combined with borehole geophysics and hydraulic tests to design and install depth-discrete groundwater monitoring systems, typically referred to as multilevel systems (MLSs). An MLS system divides a borehole into multiple monitoring zones for high-resolution acquisition of hydraulic heads and groundwater sampling (Cherry et al.,2007). Beginning in 2015, four annual sampling campaigns for VOCs have been conducted along the SZT. These samples represented groundwater from the fractures and provided complementary datasets to the rock core samples. Nielsen (2005) provides a comprehensive approach on depth-discrete MLSs and a description of the overall high resolution MLS design process is provided by Meyer et al. (2016).

Three pumping wells have been active between 2003 and 2017 and whose data constitutes the bulk of the HBS analysis. Pumping volumes provided information on contaminant mass extracted which was combined with quarterly groundwater concentration data to assess the composition and quantity of extracted VOCs and finally to compute mass discharge.

1.4   Organisation of the Thesis

The thesis is organised into six key sections. Following this introduction is Section 2 that contains the state of the art review for DNAPL contamination in fractured rock, an examination of high resolution characterisation in fractured aquifers and finally narrowing down to source zones studies. Section 3 is

divided into three parts that describe the study site in detail: 3.1 discusses the field location, 3.2 provides an overview of the geology and hydrogeology and 3.3 is an account of the contamination and research history. Section 4 has 3 parts (4.1, 4.2 and 4.3) which provide an overview of the field data collection methods for rock core, groundwater and pumping wells data. Section 5 contains the results and discussion and is divided into 3 parts: 5.1 describes the results from the source zone rock core analysis; 5.2 describes the calculation process to quantify the effect of spatial variability on temporal interpretations; and 5.3 is an analysis of the pumping rate and contaminant concentration from the pumping wells. Section 6 is a discussion related to the two main research questions: 6.1 discusses sources of source zone declines (6.1.1 on effective solubility, 6.1.2 on back-diffusion and 6.1.3 that examines specific analytes) and 6.2 is a comparison of source zone declines with the hydraulic barrier system. Section 7 contains the summary and conclusions and is divided into two parts: 7.1 that summarises the source zone temporal changes and 7.2 which evaluates the efficiency of the pumping wells. Concluding this thesis are recommendations (8) and a list of references used (9).

2   State of the Art Review

The problem of recalcitrant groundwater contaminants and their sclerotic management in the US had been acknowledged as early as 1955 when the US Geological Survey (USGS) compiled nationwide data on the effect of waste disposal practices on groundwater resources. This data was utilised in a report by a task group on underground waste disposal and control (Lynn M. et al., 1957). However, the recognition of groundwater contamination went largely unrecognised in the US until the 1970s when regulation drove the formation of environmental agencies, chiefly the US EPA and the safe drinking water act. These efforts were invigorated in 1980 when Congress enacted the Superfund Act whose goal was to directly respond to issues on hazardous wastes (Mintz, 2011). It is during this period that the ground-breaking research on the behaviour of chlorinated solvents as DNAPLs by Friedrich Schwille was translated from German to English (Schwille & Pankow, 1988). Schwille performed physical experiments where free-product tetrachloroethene (PCE) was released in sand tanks to investigate penetration in porous and fractured media as well as dissolution and subsequent transport by groundwater.

Across the Atlantic at around the same time, a group of researchers set up an experimental facility in Canada, famously referred to as the Borden site, to study contaminants in groundwater. In the late 80s, scientists at the Borden site performed DNAPL controlled-release experiments to understand their behaviour as well as the performance of remediation technologies (Cherry et al., 1996). It is through these experiments that the exceptionally complex behaviour of DNAPLs in fractured rock was elucidated. DNAPLs were found to be capable of migrating far and deep through interconnected fractures where they eventually diffused into the low-permeability matrix as shown in Figure 1 below (Mackay & Cherry, 1989). The persistence of DNAPLs was further reinforced by the futility of pump and treat systems in remediating such impacted aquifers.

In the early 90s, further understanding of DNAPL behaviour led to revision of the conceptual model on transport and fate of immiscible-phase liquids in fractured sedimentary rocks. The pertinent role of diffusive mass transfer from fractures into the matrix and the effect of back-diffusion on the persistence of DNAPL plumes was incorporated into conceptual models (Parker et al., 1994). The researchers used a one–dimensional analytical model to demonstrate possible changes in multi-component DNAPL composition due to differential diffusive fluxes. Such mathematical models laid the base for numerical models that incorporated fracture networks and diffusion into groundwater flow and transport processes, which collectively came to be known as discreet fracture network (DFN) approaches. Field experiments such as that conducted by Parker et al. (2004) in Connecticut later confirmed the occurrence of back-diffusion processes by examining rock core data from an aquitard below a plume. A major implication of this work was reframing remediation approaches by accounting for the relatively immobile DNAPL mass in the matrix as well as accompanying composition changes.
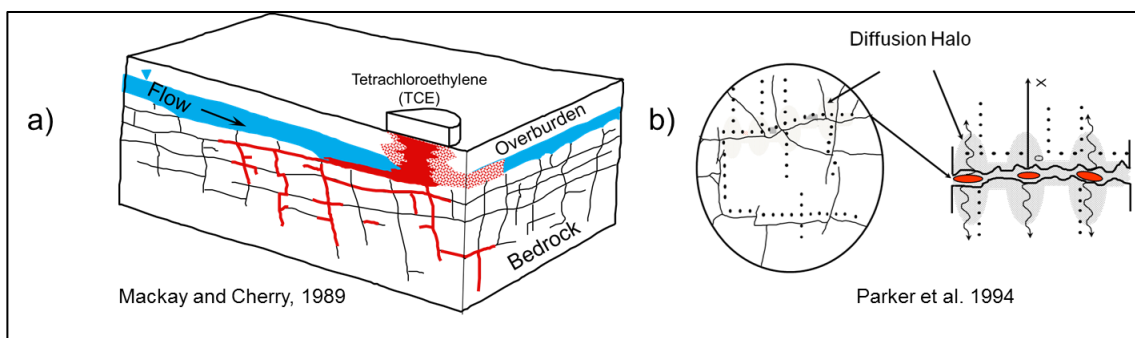
Figure 1: DNAPL, shown in red, migrating through fractured media.

In a) it is dissolved by flowing groundwater where it diffuses into the matrix while in b) the diffused DNAPL serves as a source of persistent contamination through back-diffusion from the matrix to the fractures.

Recent work on characterisation of DNAPLs have used high spatial resolution methods to understand heterogeneous contaminant distribution in the subsurface. These studies began in 1996 through a field focused program in Canada whose aim was to improve site methods for the characterisation of fractured sedimentary rocks. After nearly two decades and over ten site studies, a comprehensive approach, referred to as the DFN approach, was synthesised by Parker et al. (2012) to investigate fractured sedimentary sites. The study areas integrate hydraulic and rock core data from both low permeability matrix and adjacent fractures as well as geophysical methods to understand key drivers of contaminant migration and persistence (e.g Goldstein et al., 2004; Parker et al., 2018a, 2018b; Pierce et al., 2018; Sterling et al., 2005). Of equal importance is the advancement of site conceptual models and fracture numeric models which have played a pivotal role in understanding and simulating the effects of transport and remediation timeframes of impacted aquifers.

In the last decade, novel studies have continued to unearth finer and important characteristics of both spatial and temporal relevance to NAPLs in fractured rock sites. A study performed by Chapelle et al. (2012) estimated that naturally occurring biodegradation rates at a fractured rock site in New Jersey were comparable to mass discharge from a nearby pump and treat system. Natural attenuation had been known to exist at contaminated sites (NRC, 2005; Wiedemeier et al., 1999). It is only in the last decade that researchers have turned their attention to these microscopic yet important organisms capable of degrading contaminants. A recent fractured site study by Lima et al. (2012) characterised the dechlorinating microorganisms in the primary porosity of the rock matrix which are responsible for degrading the *in situ* contaminant mass upon diffusion into the matrix. Given the long duration that contaminant mass is known to reside in the lower permeability matrix, the confirmation of the presence of dechlorinating microorganisms has a profound effect on contaminant evolution and on the required timeframes for such sites to achieve their contaminant cleanup goals.

As a consequence of the paradigm shift on understanding and framing the DNAPL problem, two spatial regions of interest are typically considered: the source-zone and the dissolved-phase plume (Basu et al., 2008; Fure et al., 2006; Parker et al., 1994; Rivett et al., 1994). The source zone is the volume of subsurface that contains the original contaminant, often starting as a large mass in a small volume of the subsurface that over time is dissolved by flowing groundwater creating a plume downgradient (NRC, 2005) (Figure 2). The longevity of these plumes can be sustained by complex and dynamic source-zone architectures through dissolution of the contaminants to flowing fracture water, diffusion-driven mass transfer, abiotic transformation and microbial activity (e.g. Costanza et al., 2005; Darlington et al., 2013; Lenczewski et al., 2003; Lima et al., 2012; Liu & Ball, 2002; Parker et al., 2004, 1994; Şimşir et al., 2017). Such processes increase complexities in characterizing and managing source-zones which then impedes the selection and performance monitoring of appropriate remediation technologies (Kokkinaki et al., 2014; Stroo et al., 2012). Due to these complexities within the source zone as well as the importance of this spatial region to the success of remediation strategies both in the source and plume, the source zone forms the bulk of the work presented in this thesis.
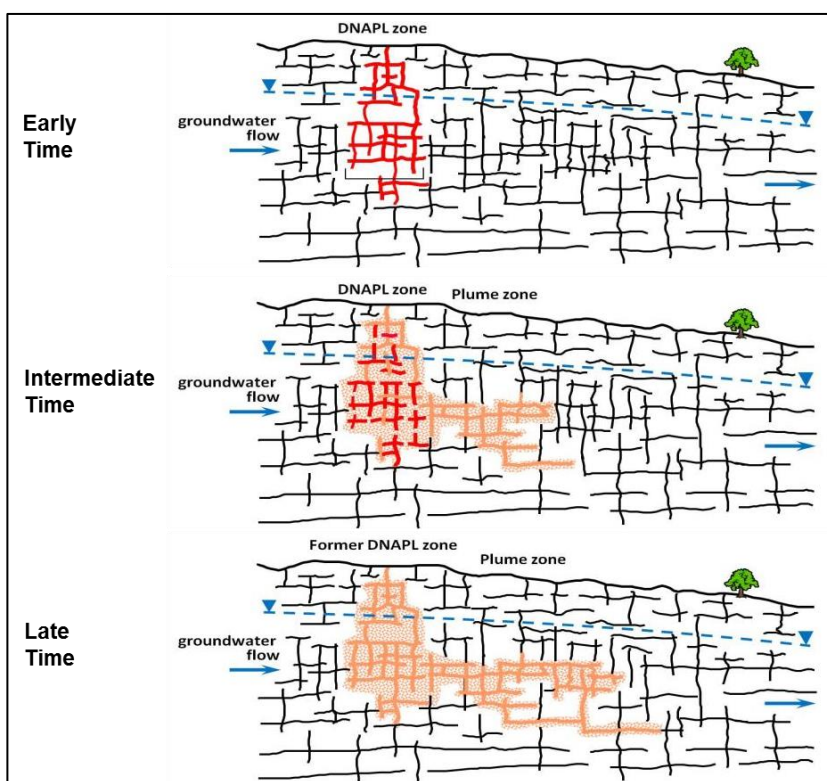

Figure 2: Source zone and plume evolution and stages
(Adapted from Parker et al.,2010)

There has been a growing body of detailed field-focussed investigations at fractured rock sites aimed at characterising spatio-temporal contaminant mass and composition changes within source zones and dissolved-phase plumes as well as evaluating the performance of remediation technologies at both spatial

scales. Lenczewski et al. (2003) conducted a study in a fractured shale bedrock in Tennessee to investigate natural attenuation of trichloroethylene (TCE). The study characterised the temporal variation of TCE using groundwater monitoring within the plume over one year. However, at fractured sites with low permeability matrix, groundwater samples are often representative of contaminants in the fractures and do not capture contaminants that have diffused into the rock matrix. Furthermore, the overall magnitude of natural attenuation processes can be underestimated if the degradation processes within the matrix are not taken into account. The overall effect is a misrepresentation of temporal changes of contaminants which often require longer monitoring timeframes than a year in order to draw robust conclusions on contaminant evolution.

Lima et al. (2012) investigated the presence of dechlorinating microorganisms at different depths within the low permeability rock matrix at a fractured sedimentary rock site by sampling rock core at ~5cm intervals from a vertical borehole in the dissolved phase plume combined with compound specific isotope analysis (CSIA). This study was among the first to investigate the heterogeneity in microbial colonies with depth which demonstrated the importance of high resolution rock core sampling techniques.

Goode et al. (2014) combined high resolution rock core sampling methods with multi-level groundwater monitoring systems to delineate the spatial variability of a TCE DNAPL at a fractured mudstone site in New Jersey. However, the study was not aimed at any particular spatial zone (source zone or plume) because the location of the spill was unknown and suspected to have occurred at multiple locations. The difficulty in pointing out the location of the spill at these and other numerous sites across the US attests to the complexities at fractured sites and highlights the importance of more concerted efforts towards the DNAPL challenge.

Schaefer et al. (2016) performed a field scale study in California using partitioning tracers, discrete interval straddle packer testing and rock cores to examine the role of DNAPL in low-permeability fracture zones on plume longevity. The study also estimated the time needed for DNAPL removal using a constant dissolution rate of a PCE DNAPL. The study reflects on the growing importance of using multiple lines of evidence to quantify contaminant changes in the source zone and their impacts on downgradient plumes In their timeframe estimates, the authors noted that the calculated timeframes did not take into account microbial activity and contaminant mass changes between rock matrix and fractures which have been proven to be significant (e.g. Newell et al., 2006).

Two recent studies have been published that use high-resolution rock core samples and groundwater from multilevel wells to characterise degradation processes at fractured rock sites. In the first study, located in South Carolina, Wanner et al. (2018) used multilevel wells along two transects oriented perpendicular to groundwater flow and high resolution rock core samples to investigate and quantify degradation processes using CSIA. The site was contaminated with a complex mixture of chlorinated ethanes, ethenes and methanes. Similarly, Pierce et al. (2018) used long-term temporal records of groundwater from conventional and multilevel wells in addition to high-resolution rock core sampling to deduce attenuation rates of a TCE

DNAPL. The above list of fractured rock field studies is by no means exhaustive but it does provide insight into the paradigm shift on framing the DNAPL conundrum and the novel techniques constantly being developed by researchers to respond to contaminants that have impacted aquifers, including those close to municipal supply wells.

Within this growing body of literature, there are no detailed investigations, to my knowledge, that combine high resolution rock core sampling with depth-discrete groundwater sampling methods to examine temporal changes in mass and composition of a multi-component DNAPL source zone in a fractured aquifer under the influence of a pump and treat system. These changes are environmentally significant as demonstrated by Chapelle et al. (2012) and can affect the selection, design, delivery and performance evaluation of remediation technologies (Kueper et al., 2014). This study seeks to obtain data which will help to address these research gaps.

3   Study Area

3.1   Site Description

The field site is located in Cottage Grove, a village located approximately 21 km east of Madison, Wisconsin, U.S.A. (Figure 3). The field site is characterised by low to moderate topographical relief associated with Pleistocene lacustrine, fluvial, and drumlinised till deposits (Meyer et al., 2016). It encompasses the DNAPL source zone, surrounding wetlands and agricultural land affected by the migrating plume.
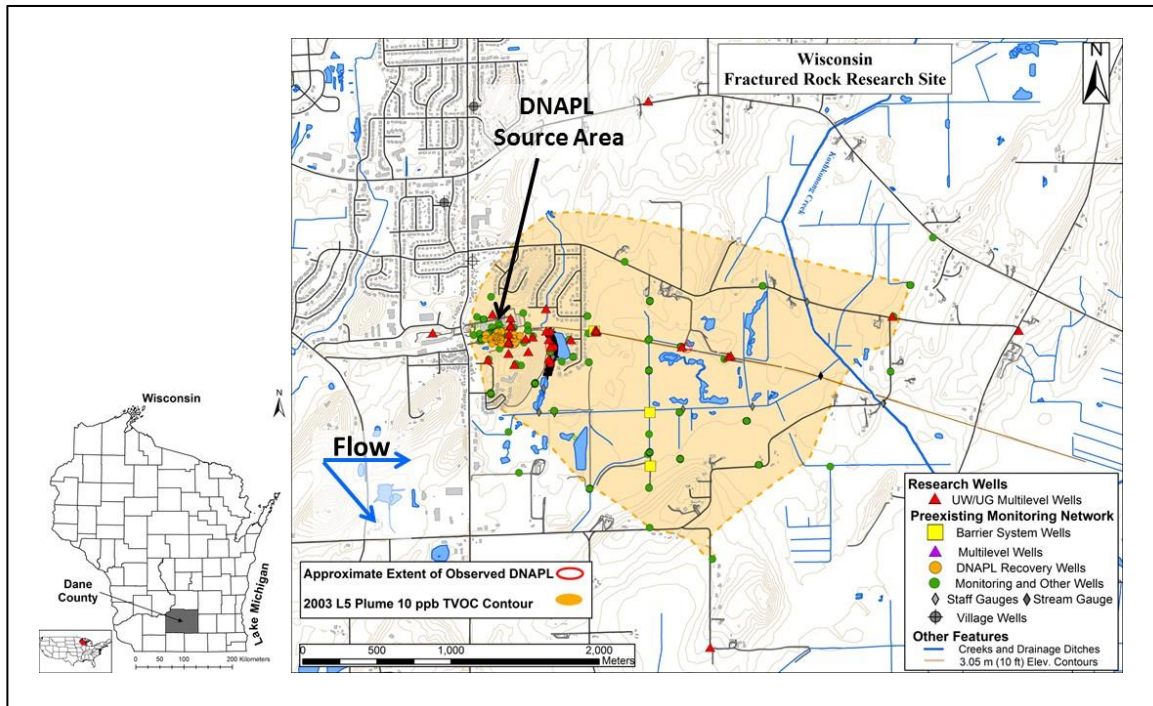
Figure 3: Field location in Dane County, Wisconsin, U.S.A.

(Courtesy of Meyer, 2017)

Data collected from three of the SZT research core holes (MP-7, MP-24S and MP-24D) and 3 pumping wells (P-128, P-130, and P-145) downgradient form the focus of this study with supporting evidence drawn from 6 other cores (MP-22S, MP-23S, MP-23D, MP-25S, MP-25D, MP-26S) within the SZT (Figure 4 and Figure 5).
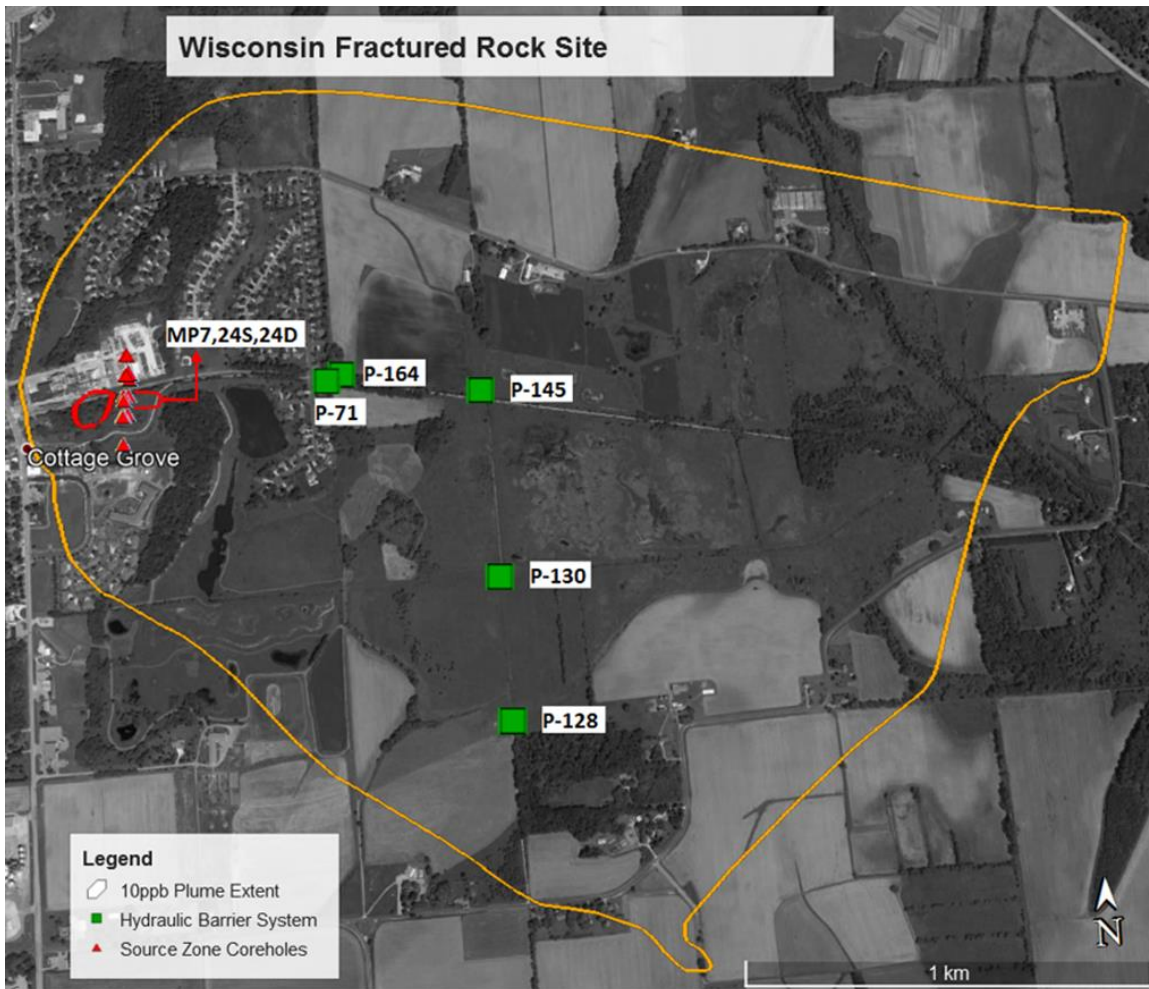
Figure 4: Study area showing the location of the pumping wells and the source zone transect core holes
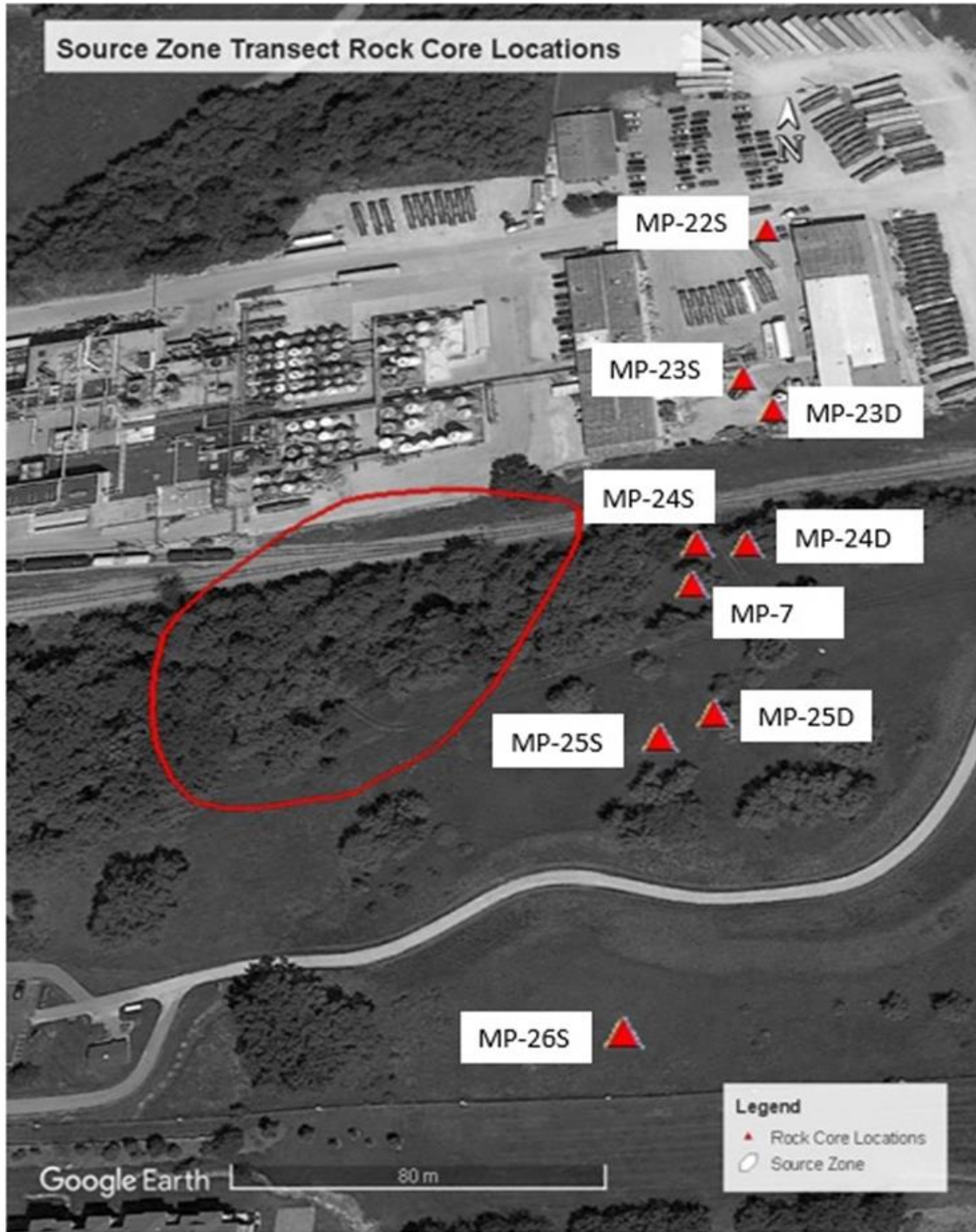
Figure 5: Location of the source zone transect core holes

3.2   Hydrogeological Conditions

The lowermost rocks in Dane County region are crystalline igneous and metamorphic rocks from the Precambrian age overlain by Cambrian-Ordovician sandstone, dolostone, and siltstone bedrock layers (Figure 6). The rocks are generally fractured as a result of stress fields associated with uplift and erosion of minerals such as glauconite and shale as well as dissolution of carbonate bedrock present in Dane County. Detailed descriptions of these units including the unconsolidated sediments, glacial deposits and bedrock geology are provided in various literature (e.g Clayton & Attig, 1997; Cline, 1965; Mai & Dott, 1985; Mickelson, 1983; Odom, 1978; Ostrom, 1970). Literature on the hydrogeology of Dane county including the flow system, groundwater resources and hydrochemistry include works by Bradbury et al. (1999), Cline (1965) and Kammerer (1995). Recent groundwater modelling studies for Dane County have also been performed by Parsen et al. (2016) (Figure 7).
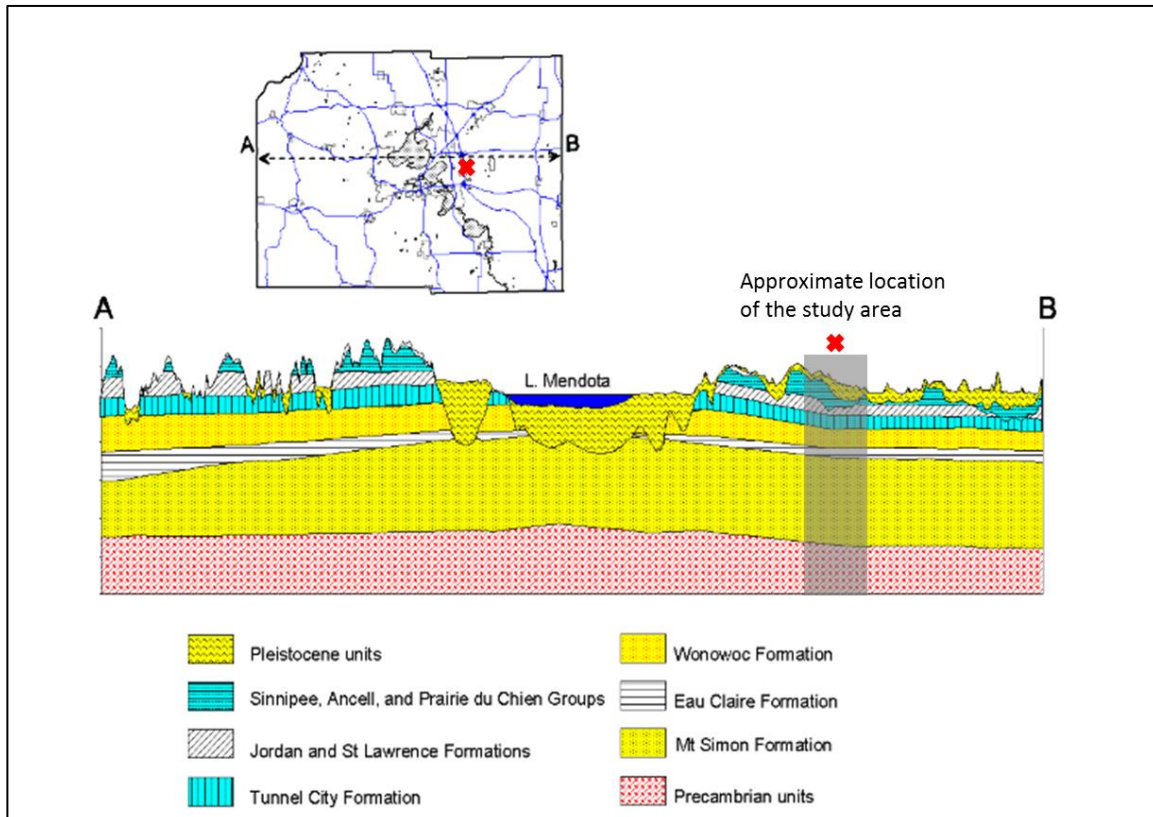
Figure 6: Stratigraphic cross-section across the larger Dane County, Wisconsin.

The figure shows subsurface stratigraphy at the site, including Precambrian units (from Bradbury et al., 1999, first appeared in Massie-Ferch et al., 1997).
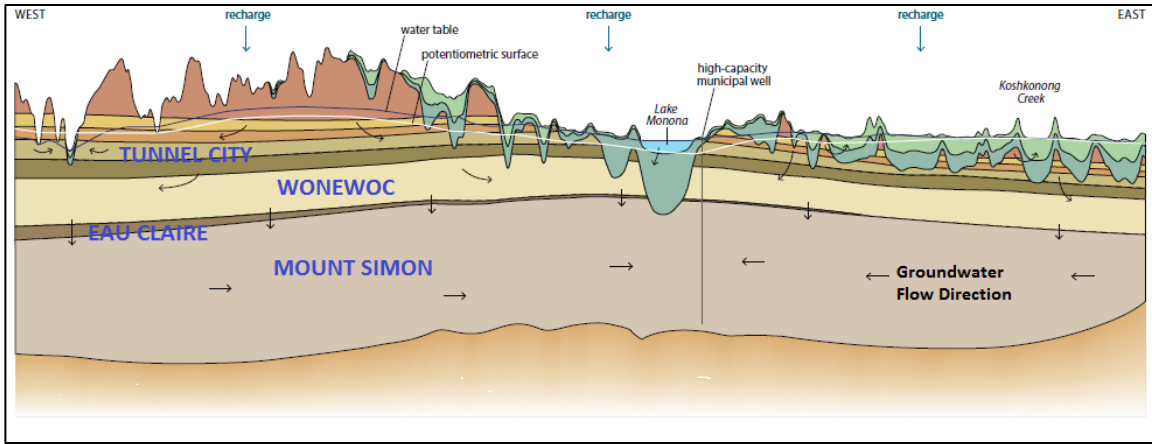
Figure 7: Conceptual Model of Dane County groundwater system
(modified from Parsen et al. 2016)

Detailed descriptions of the geology and groundwater flow system at the Hydrite site were presented by Austin (2005) and Meyer (2005); an abridged discussion is presented below and shown in Figure 8.
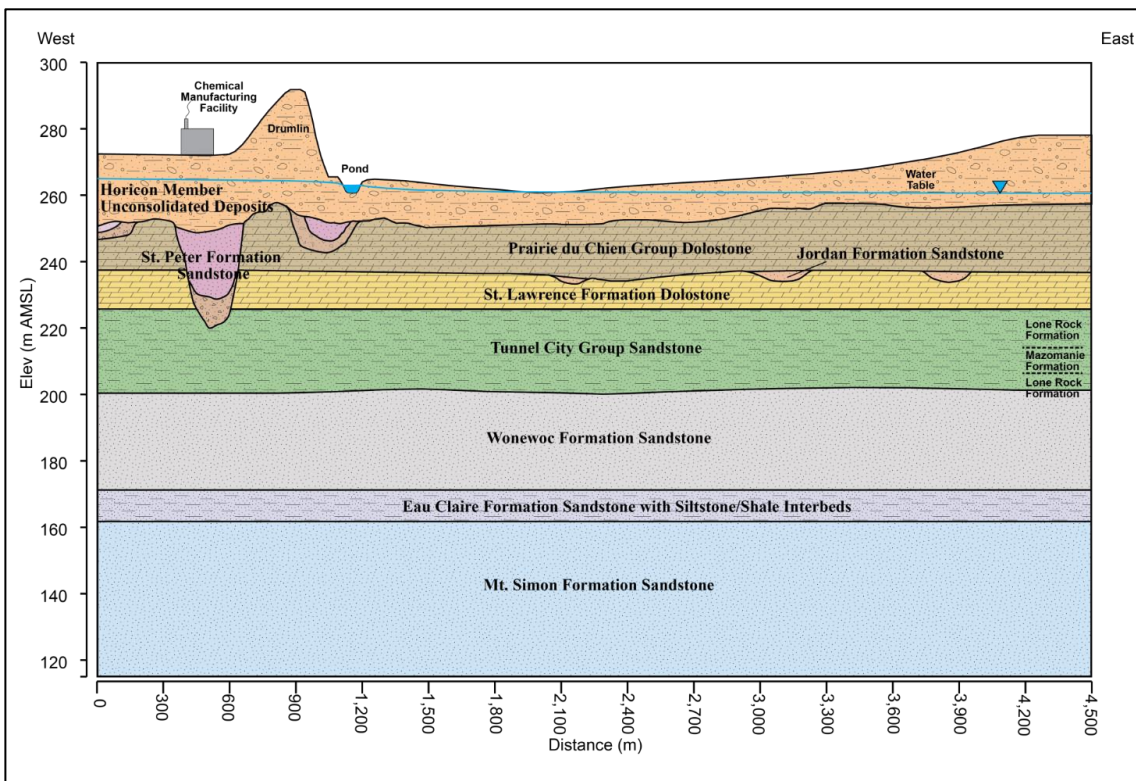
Figure 8: Conceptualisation of the site stratigraphy
*the above units correspond to the stratigraphic column in the results section

The Precambrian rocks are not water-yielding and thus form the base of the regional groundwater reservoir in Dane County (Cline, 1965). Rock core investigations at the Hydrite site performed between

2003 and 2017 identified the Elk Mound Group of Cambrian age as the lowest encountered geologic unit (GeoTrans, 2003; Parker et al., 2015, 2018). It consists of three formations (lowest to uppermost): Mount Simon, Eau Claire, and Wonewoc. Mount Simon Formation is approximately fifty meters thick and consists of well-cemented, coarse to medium grained quartz sandstone with porosity ranging between 7.6-22.6% (Austin, 2005; Cline, 1965). The overlying Eau Claire formation is composed of very fine to medium-grained feldspathic, glauconitic and dolomitic sandstone with variable amounts of siltstone and mudstones (Aswasereelert et al., 2008). Core analysis at Hydrite performed by Austin (2005) showed that some sections of the Eau Claire formation display a high contrast of matrix vertical hydraulic conductivities between the sandstone and shaley intervals, 6.4×10^{-5} cm/s versus 8×10^{-10} cm/s. At the site, the Wonewoc Formation overlies the Eau Claire Formation. It consists of the Galesville (lower) and Ironton (upper) Members which are well-rounded and well-sorted sandstones with poor cementation (Bradbury et al., 1999; Brown et al., 2013).

The above three sandstone formations of the Elk Mound Group form the principal aquifer in Dane County (Bradbury et al., 1999). Groundwater moves primarily through fractures, which are large and abundant but flow also occurs through the interconnected pore spaces, through fractures and along bedding planes (Cline, 1965). Mount Simon Formation is a confined aquifer important for municipal, industrial, agricultural, and domestic water supply. Groundwater recharges the Mount Simon aquifer where the water table is higher than the potentiometric surface (Bradbury et al. 1999; Meyer et al. 2014) whereas discharge occurs when the potentiometric surface is above the water table with upward hydraulic gradients. Wells in the Eau Claire Formation have the least specific capacity of the three formations and it has been reported to act as a heterogeneous and anisotropic regional aquitard (Aswasereelert et al., 2008; Parsen et al., 2016).

The Tunnel City Group overlies the Elk Mound Group at the site. It is a permeable Cambrian age siliciclastic rock characterized by fractured glauconitic sandstone with thin interbeds of siltstone and shale. It consists of two distinct facies that intertongue, namely a glauconitic facies, the Lone Rock Formation, and a nonglauconite facies, the Mazomanie Formation (Ostrom, 1970). These 2 formations are hypothesised to have been deposited in the same time frame via similar sub-tidal mechanisms (Odom, 1978). Site investigations conducted in the Lone Rock formation by Austin (2005) reported an average porosity of 19%. Meyer (2005) showed that the hydraulic conductivities of the matrix and horizontal fractures differ by four orders of magnitude ($1.2 \times 10^{-7}$ vs 8.6×10^{-3} cm/s) indicating that most of the groundwater flows through the dominant hydraulically active horizontal fractures. Estimates of organic carbon fractions (f_{oc}) reported by Lima et al. (2012) at this study site were below the 0.1% threshold for organic carbon dominated sorption as reported by Odutola & Walsh (2002). However, sorption processes differ depending on the solubility of the compounds: low fractions of organic carbon can control sorption of very hydrophobic compounds whereas highly soluble compounds are not sorbed in geologic media with low organic carbon content (Banerjee, 1984).

The St. Lawrence Formation of Cambrian age overlies the Tunnel City Group and is composed of a dolomitic siltstone with trace amounts of glauconite (Brown et al., 2013). In the source zone area, this formation is partially to fully eroded and is deeply undercut by the St. Peter Formation. Very low matrix hydraulic conductivity values ranging from 4 to 8 x 10^{-7} cm/s (Austin, 2005) suggest that most of the flow occurs within the fractures, many of which are horizontal or oblique (Runkel et al., 2006).

The Jordan Formation is the youngest of the Cambrian age rocks and it lies on top of the St. Lawrence Formation. This formation is absent from the source zone area and is therefore not discussed in detail. The Prairie du Chien Group is a dense, massive and hard dolostone of Ordovician age whose base is at the top of the Cambrian sandstones (Ostrom, 1970). It has been presumed to be deeply eroded in sections of the source zone but it is present in downgradient positions within the site (Hydrite database). At both the site and around Dane county, the rocks are heavily fractured(Austin, 2005; Bradbury et al., 1999).

The St. Peter Formation is the youngest bedrock unit encountered below the unconsolidated glacial sediments (Horicon Till Member) and overburden at depths of between 15.4 and 26.8 mbgs. It consists of two members(a fine to coarse-grained sandstone with total porosity of approximately 17-19.5% (Austin, 2005) which reduces as the degree of cementation increases; secondary porosity features such as fractures are present, with most of them being horizontal or oblique. The vertical matrix hydraulic conductivity of approximately 10^{-5} cm/s (Austin, 2005) is amongst the highest observed at the source zone. However, most of the groundwater flow occurs in the fractures (Meyer et al., 2008).

Generally, the shallow and deep groundwater systems are in Dane County are connected (see Figure 7). Key surface water bodies at the site include Koshkonong Creek, a man-made pond and drainage ditches that run east to west. The groundwater flow system follows the classical description of Toth (1963) with influences from topography, soils and climate, heterogeneity and pumping effects (Bradbury et al., 1999). Groundwater originates from rainfall and snowmelt and flows east towards Koshkonong Creek within the unconsolidated deposits and shallow bedrock whereas it flows towards the south in the deep bedrock (Meyer et al., 2016).

3.3 DNAPL Contamination

In 1970, Hydrite Chemical Co. (Hydrite), a chemical manufacturing and waste management company, purchased a site in Cottage Grove, Wisconsin. Previous occupants over the last two decades operated businesses that involved the use or storage of waste solvents and chemicals (GeoTrans, 1999). During site construction activities in 1982, the soil, and later groundwater, were found to be contaminated with DNAPLs. These contaminants were released into the subsurface prior to 1970 before Hydrite acquired the property.

After the discovery of the contamination, environmental consultants performed numerous field studies to characterise the nature and extent of the contamination. Between the 1982 and 2003, over 151 extraction wells and monitoring wells were drilled to monitor the groundwater quality and to further determine the extent of contamination in the lower bedrock. These site characterisation studies by GeoTrans (1999)

showed that the contaminants migrated through the unconsolidated glacial sediments and into the upper bedrock units, before settling at a depth of between 45 to 56 m below the surface in the upper part of the fractured Tunnel City sandstones (Figure *9*).
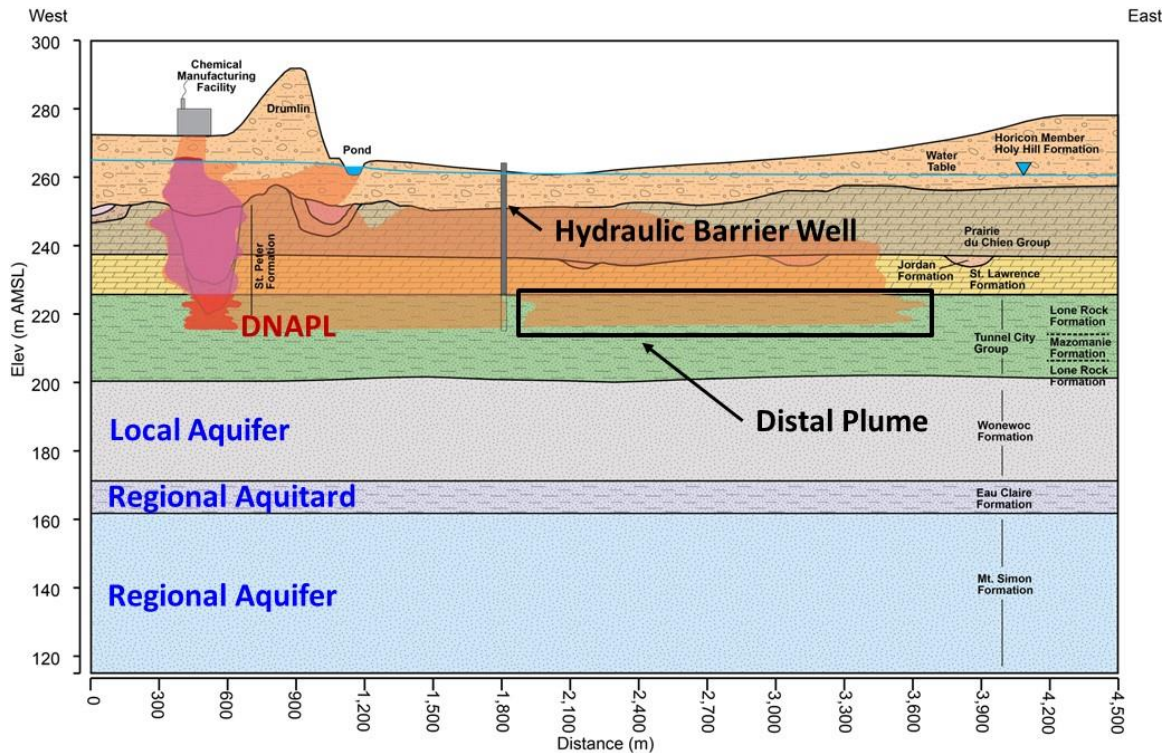
Figure 9: Stratigraphic Cross-Section showing the DNAPL.

The figure shows major hydrogeological units and the HBS cutting off the downgradient plume from the DNAPL source zone (modified from Meyer et. al 2017)

Density differences are likely to have been a key driving force for this downward movement. The consultants hypothesised that the DNAPL did not migrate deeper into the bedrock because of decreasing fracture intensity, increased clay content or as a result of the interfacial tension of the contaminants (GeoTrans, 1999). An updated SCM suggests an additional mechanisms that may have contributed to the DNAPL migration. In the above summary of the geology, it was noted that the Prairie du Chien Group consists of hard dolostones that have been eroded in many sections of the source zone. Geophysical evidence show the existence of isolated dolostone towers surrounded by sections of the St. Peter Formation (Parker et al., 2018). This spatial heterogeneity in erosion which created hard resistant dolostones separated by the mud-rich St. Peter Formation may have influenced the migration and settling of the DNAPL. The current location where the DNAPL resides, hereafter called the source zone, is located between 40 and 100m south of the release area. West-East groundwater flow through the source zone has resulted into a dissolved-phase plume that has migrated downgradient and measured 2.8 km long at its maximum lateral extent in 2003. To avoid the plume, the private wells in the plume's path were deepened. Four municipal wells that are cross-gradient with respect to the dissolved phase plume pump water from

the deeper Mount Simon formation and have not reported any contamination from this plume. A hydraulic barrier system (HBS) consisting of three pumping wells was installed in 2003 to cut off the plume from the source zone and prevent further migration down-gradient.

The oily-phase DNAPL was sampled in 1999 and in 2004. The laboratory results showed that the contaminants predominantly consisted of chlorinated solvents including tetrachloroethene (PCE), trichloroethene (TCE), 1,1,1- trichloroethane (TCA), and their daughter products: *cis*-1,2, dichloroethene (cis-1,2-DCE), vinyl chloride (VC), 1,1 dichloroethene (1,1-DCE), and 1,1-dichloroethane (1,1-DCA) (Austin, 2005; GeoTrans, 1999, 2003). Other VOCs present include ketones: acetone, methyl ethyl ketone (MEK), methyl isobutyl ketone (MIBK) and some aromatics: benzene, toluene, ethylbenzene, and xylene (BTEX compounds).

Since the discovery of the contamination, a variety methods have been utilised to recover the DNAPL from the soil and the subsurface, especially the upper Tunnel City sandstones. These efforts included DNAPL pumping from recovery wells, a soil vapour extraction system and aeration of the vadose zone. Consultant records indicate that by 1999, 26 289L of DNAPL had been pumped from seven recovery wells (GeoTrans, 1999). By 2002, another 7 779L was pumped out from wells within the source zone, bringing the total extracted volume from the source zone to 34 068L. The volume extracted by the HBS is not included in this extracted mass but is calculated, presented and analysed in this thesis. Given that the volume of the original spill is not known, it can only be assumed that it was greater than 34 068L. However, consultants attempted to provide estimates of the total DNAPL that could have existed in the deep bedrock, based on studies of the fracture network; they put a probable figure of 72 680L (GeoTrans, 2003). The remaining volume is believed to be the major DNAPL reservoir at the Hydrite site. The large volume of contaminated aquifer makes this site an important study candidate for advanced characterisation of source zone conditions that influence contaminant transport and fate.

In 2003, the Parker/Cherry research team under the framework of the University Consortium for Field Focused Groundwater Contamination Research began research at this site. The work continues to advance the understanding of the geological framework, hydrogeological units and flow system, contaminant fate and transport, and DNAPL source zone to continuously update, refine and inform the SCM. This thesis fits within this larger framework.

4   Materials and Methods

4.1   Rock Core Sampling

Between 2003 and 2017, eleven research holes were drilled to investigate the vertical distribution of contaminants within the low permeability rock matrix near the source zone. These core holes were drilled along a North-South transect eighty meters downgradient of the source zone and roughly perpendicular to the West-East groundwater flow direction. Two of the holes were cored in the unconsolidated formation and were not utilized in this study. Figure 5 shows the location of nine SZT research core holes: MP-7 drilled in 2003; five shallow bedrock holes (designated with an 'S') drilled in 2014 (MP-22S, MP-23S, MP-24S, MP-25S and MP-26S); and three deep bedrock holes (designated with a 'D') drilled in 2017 (MP-23D, MP-24D, and MP-25D). Of these core holes, MP-7, MP-24S and MP-24D cored in 2003, 2014, and 2017 respectively are co-located within a nine meter radius. They serve as the central focus of this study by providing a unique opportunity to evaluate temporal changes of the contaminant mass and distribution within the source zone. MP-22S, MP-23S, MP-25S and MP-26S form the secondary set of research core holes used to understand the effect of spatial variability on the temporal analysis of the three main core holes. Concentration data from these five shallow cores were also used to calculate the total mass flux from the SZT in 2014.

The drilling, coring and sampling process is similar to that described by Meyer et al. (2008) and detailed in the University Consortium research progress reports (Parker et al., 2015, 2018). The drilling and coring method for the SZT holes is outlined and generalised below to capture the overall process for both shallow and deep wells. A visual summary of this process is presented in Figure 10 below.
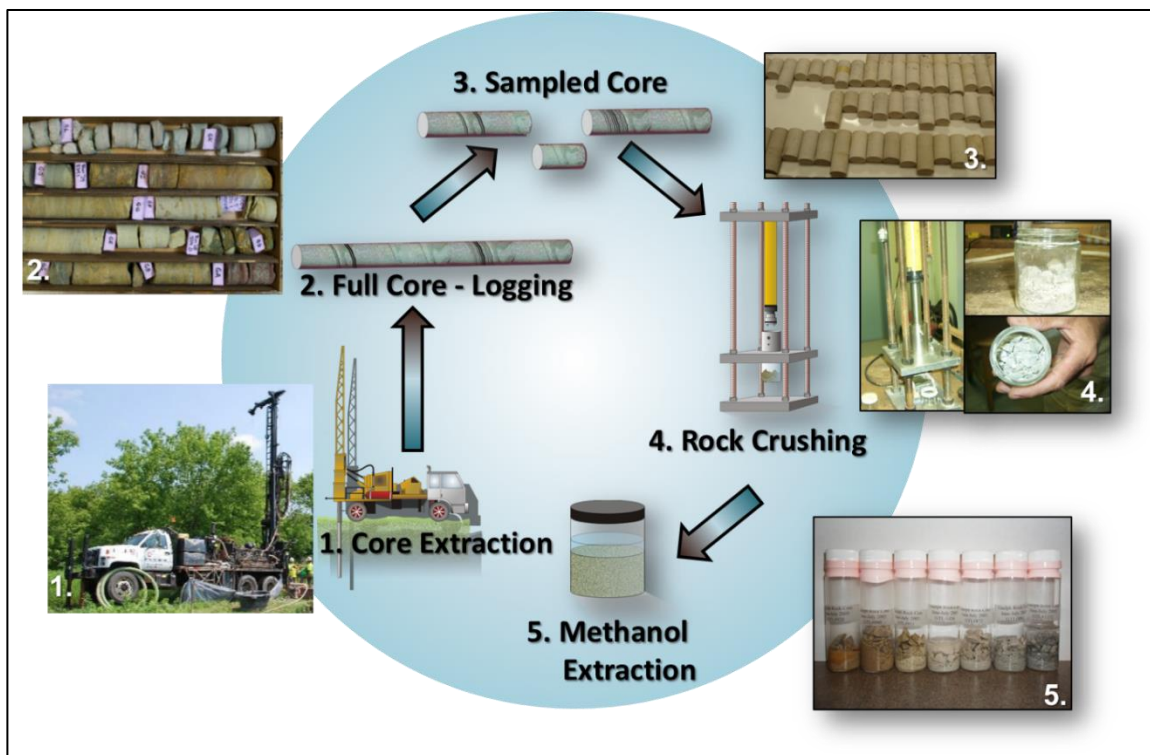
Figure 10: An overview of the rock core drilling, sampling and VOC extraction process (Modified from Hydrite Consutant Reports)

In the first stage, a mud rotary drilling technique with a tricone drill bit was used to drill from the ground surface to the coring start depth. The start depth was selected based on the subsurface locations of interest and designed to avoid re-coring the sections previously cored. A temporary casing was installed in preparation for coring. Cuttings and fluid produced during drilling were captured in drums, screened and thereafter disposed.

The second stage of drilling utilized a rotary rig and a wireline HQ3 triple-tube coring system designed to maximize core recovery in soft formations. Tap water was used as a drilling fluid. Cores were retrieved and the continuous coring was completed in 1.5 m increments up to the target depth. The diameter of the core barrels were selected to maximise core recovery. The coring rods and the temporary HWT casing were then removed. The well was reamed and a steel casing installed and cemented into place. Tap water was used as a drilling fluid except in the softer sands of the Wonewoc Formation (for the deep wells) where a polymer was added to improve borehole stability.

Specifically for the deep wells, a third drilling stage was completed using a HQ3 triple-tube coring system and cores collected until the final target depth was reached. The final coring depth was selected in order to minimise cross-contamination between any transition zones from high to low contaminant concentrations.

With the completion of each core run, the inner core barrel that collected the sample was lifted to the surface using a wireline retrieving system for core sampling and analysis. Buckley (2017) provides a

detailed account of the sampling process and a summary is presented below. The stainless steel core sleeve that lines the barrel was extracted using water pressure and the core was carefully laid onto a PVC tray lined with aluminium foil and wrapped to minimize VOC loss by volatilization. Four criteria for selecting sampling points along the core have been elaborated by Meyer (2005). Major sampling points were on one side of an identified fracture surface, along bedding plane partings, in zones exhibiting distinct lithological changes and a series of samples that step away from the fracture surface with a view to characterise the diffusion halo. In addition, spacing samples were collected in zones where the criteria above resulted in 2-3ft of unsampled core. Field duplicate samples were also collected. The identified samples were extracted using a hammer and chisel, wrapped in aluminium foil and placed in a resealable plastic bag. The samples were stored in a cooler with ice packs. A few chunks of the representative sample were crushed using a hydraulic press and a small mass of crushed sample was transferred into a 40 mL VOA vial pre-filled with 15-18 mL of HPLC grade or purge and trap grade methanol. Methanol was used to extract and dissolve rock core VOCs (Goode et al., 2014; Sterling et al., 2005). During core sampling, duplicate samples were collected to ascertain the repeatability of the results by providing two practically identical samples. The samples were split along the axis and processed using the same steps as the original sample. Extra samples designated as matrix spike (MS), matrix spike duplicate (MSD) and time-series samples were collected for quality assurance and quality control measures (QA/QC) of the laboratory analysis. Other QA/QC measures included a 5-step decontamination process for the equipment after each core run. This consisted of washing with soapy water, rinsing with distilled water, rinsing with wash grade methanol and a final rinse with distilled water after which the equipment was left to dry.

All the samples were shipped to a commercial laboratory certified by the National Environmental Laboratory Accreditation Program (NELAP) for analysis. They were first sonicated and then shaken using an orbital shaker for one hour per week over a minimum period ranging from 3-15 weeks. Shaking expedited the rate of VOC extraction from the rock samples into the methanol. Time-series samples were analysed at every few days to monitor the rate of VOC extraction into the methanol. These results were compared to the VOC concentrations from the minimum shaking period to ensure that VOCs were fully extracted. Except during shaking, samples were stored in a freezer. Once the extraction phase was complete, the samples were diluted to ensure their concentrations fell within the calibration ranges. The shallow "S" wells and deep "D" wells were analysed using US EPA SW846 Method 8260C (SW-846), Volatile Organic Compounds by Gas Chromatography/Mass Spectrometry (GC/MS) whereas MP-7 was analysed using the older SW-846 method 8260B using GC/MS. Ion monitoring mode was selected since the quantitation limits are below the normal operating range of the MS.

The laboratory reported the final rock core contaminant concentrations in micrograms of VOC per litre of methanol used to extract the wet rock contaminant mass$(\mu g/L\ MeOH)$. The total concentration of each compound i in µg of VOC per gram of wet rock sample was determined using the mass of wet rock and the concentration and volume of the methanol.

$$C^i_{wet\ rock}\left(\frac{\mu g_{VOC}}{g_{wet\ rock}}\right) = \frac{C^i_{methanol}\left(\frac{\mu g_{VOC}}{L}\right)V_{methanol}\,(L)}{M_{wet\ rock}\,(g)}$$

where C^i is the concentration of a VOC, V the volume of methanol used and M the mass of wet rock sample from the rock matrix.

This value was converted to moles per gram of wet rock in order to better account for changes in the loss of hydrogen during reductive dechlorination which would be harder to detect when working in mass units. The conversion was done as shown below.

$$C^i\left(\frac{mol_{VOC}}{g_{wet\ rock}}\right) = \frac{C^i\left(\frac{\mu g_{VOC}}{g_{wet\ rock}}\right)}{MW\left(\frac{10^6\,\mu g_{VOC}}{mol}\right)}$$

where MW is the molar mass of each compound in micrograms per mole.

The total mas for each rock core sample concentration was also calculated by assuming that each sample has an volume of influence represented by a vertical length (half the distance between the upper and lower samples) and an area of 1m², chosen to simplify calculations. This steps are illustrated below:

$$C^i(mol) = C^i\left(\frac{mol}{g_{wet\ rock}}\right)\rho_{wb}\left(\frac{g_{wet\ rock}}{m^3}\right)A(m^2)\frac{Y}{2}(m)$$

where ρ_{wb} is the wet bulk density of the sample, Y is the distance between the upper and lower samples, and A is the area of influence of the core sample, taken as $1m^2$ as shown below in Figure 11 .
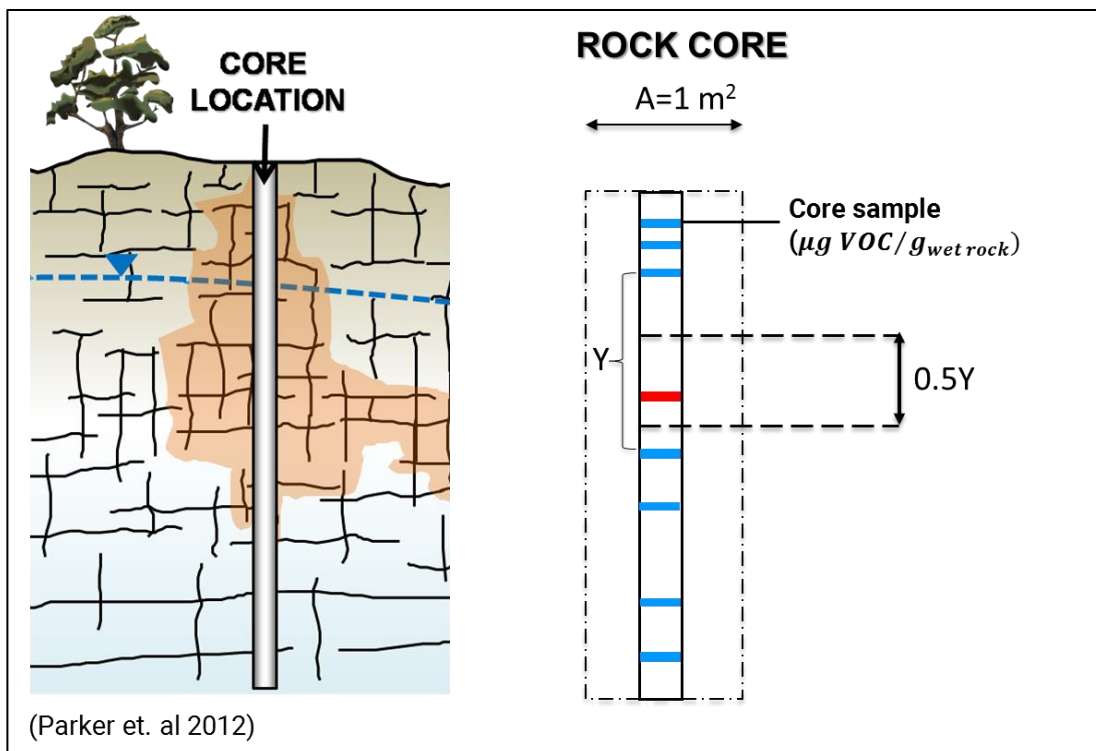
Figure 11: Illustration of rock core contaminant mass calculation

4.2   Groundwater Sampling

Depth-discrete multilevel systems (MLSs) are powerful yet cost-effective engineered solutions for complex fractured rock sites because they maximize the quantity of data obtained from a single borehole. Cherry et al. (2015) and Einarson (2006) discuss some MLS brands commercially available in North America along with their utilization. The Westbay® System offers the largest number of monitoring zones within the typical borehole dimensions used in this study (Meyer et al., 2014). Westbay Systems®, henceforth termed Westbays were selected to facilitate depth-discrete measurement of hydraulic pressure and collection of groundwater samples at MP-7 in 2005 and MP-24S in 2015 and 2016. The position and length of the desired monitoring intervals and packer seals were identified based on core analysis and complimentary datasets (Meyer et al., 2014). Once the design was complete, all of the necessary parts were shipped to the site and the MLS was assembled one piece at a time and lowered into the hole. Once the entire system was assembled and installed in the hole it was zeroed based on the design specifications and tested to ensure the casing was not leaking and all of the monitoring ports were positioned as per the design and operating properly. Then, the packers were inflated with water to seal between each monitoring interval thus preventing cross-contamination or blending between zones in the Westbays.

After the installation of the Westbay system, a complementary system composed of one or more sampling canisters and a pressure probe connected to a user interface was used for sampling. The wireline-operated MOSDAX pressure probe was mounted on a winch and connected to a MAGI user interface

control unit complete with a built-in LCD display (www.westbay.com). A 250mL groundwater sampling container was screwed onto the wireline operated probe. In monitoring zones where duplicate samples were collected, two containers were attached in parallel. Groundwater was purged prior to sampling at MP-7. A peristaltic pump attached in-line was used to evacuate air from the container to a pressure of 3 psi and thereafter lowered into the plastic casing to the desired sampling level. The valve at the measuring port was opened and due to pressure difference between the container and the formation fluid pressure in the annular space between the borehole wall and the Westbay system casing, groundwater flowed into the container. The valve was closed once the two pressures equalized and the container was reeled in to the surface. A small valve-operated tap located at the bottom of the container was opened and a multi-parameter device was used to measure physical parameters consisting of temperature, pH, electrical conductivity and oxidation reduction potential (ORP). Samples were then collected in labelled 40 mL volatile organic analysis (VOA) vials ensuring no headspace to minimize volatilization. Each VOA vial was labelled, wrapped in bubble-wrap, placed inside resealable plastic bags and packed in coolers with ice packs. The samples were shipped overnight to the laboratory and analysed within 7 days of sampling using gas chromatography-mass spectrometry (GC/MS) method 8260C. Since no preservatives were added to the samples, it was necessary to get them analysed within a week of collecting them. Similar to the rock core sampling procedure, QA/QC measures included collecting equipment blanks, trip blanks for each cooler and duplicate samples

4.3   Hydraulic Barrier System Measurements

Five pumping wells that constitute an HBS were installed in 2003-2004 to cut off the plume from the source zone and prevent further contaminant migration downgradient. These pumping wells are located between 0.5-1.2 km downgradient from the SZT and are screened between 38-48mbgs corresponding to the Tunnel City Group where most of the residual DNAPL lies.

As of December 2017, only 3 pumping wells (P-164, P-128, and P-130) were operational and constitute the HBS. P-145 was deemed redundant and taken offline in 2008 because P-164 that is located 383 m up-gradient was capturing most of the groundwater VOCs. P-71 was replaced with P-164 since the former was not performing to its full capacity. The site overview map (see Figure 4) shows the locations of the pumping wells.

The volume of groundwater extracted by the HBS was measured in US gallons using mechanical flow meters installed at each well. The pump start and stop times were also recorded. The pumping schedule was periodically interrupted due to shutdown of the pumps for repair, testing and maintenance, replacement of flow meters and generators, high water levels at the lift station, planned treatment of the wells to reduce slime bacteria and installation of new pumps to induce higher pumping rates. Groundwater VOC sampling results from the HBS were collected and reported on a quarterly basis (Tetra Tech, 2017). With the exception of P-70 that had between 40-44 VOCs analysed in 1996 and 1997, all subsequent reporting

quarters for all the pumping wells consisted of 35 VOC analytes. Pumping volumes recorded were combined with groundwater concentration data to glean information on mass discharge and the quantity and composition of the extracted VOCs.

Table 1: Pumping well operation duration and sampling campaigns

Pumping Well	Sampling start date	Last utilised sampling campaign	Number of quarterly sampling events (as of Dec 2017)
P-128	Feb-01	Dec-17	61
P-130	Feb-01	Dec-17	56
P-145	Mar-04	Sep-08	18
P-164	Sep-04	Dec-17	50
P-71	Mar-96	Jun-17	66

5   Results

5.1   Temporal Changes in Mass and Composition of rock-core contaminants

The first objective of this thesis was to characterise the temporal evolution of contaminant mass in the rock matrix just downgradient of the source zone. Results of rock core VOC sampling show that the total contaminant mass per square meter of core declined from 8.78 moles (815.70 g) to 1.89 moles (163.91 g) between MP-7 cored in 2003 and MP-24S cored 2014 and to 1.46 moles (121.54 g) in MP-24D cored in 2017. These declines represent changes of 78.5% between MP-7 and MP-24S and 22.7% between MP-24S and MP-24D as shown in Figure 12 below. The overall decrease in moles over the fourteen-year period was 83.4% measured with MP-7 results as the baseline. Over this time period, chlorinated methanes and ethenes recorded the highest declines, 99% and 95% respectively, whereas ketones displayed the lowest decline of 42%. The mass of chlorinated ethanes declined by 89% and that of BTEX compounds by 77%.
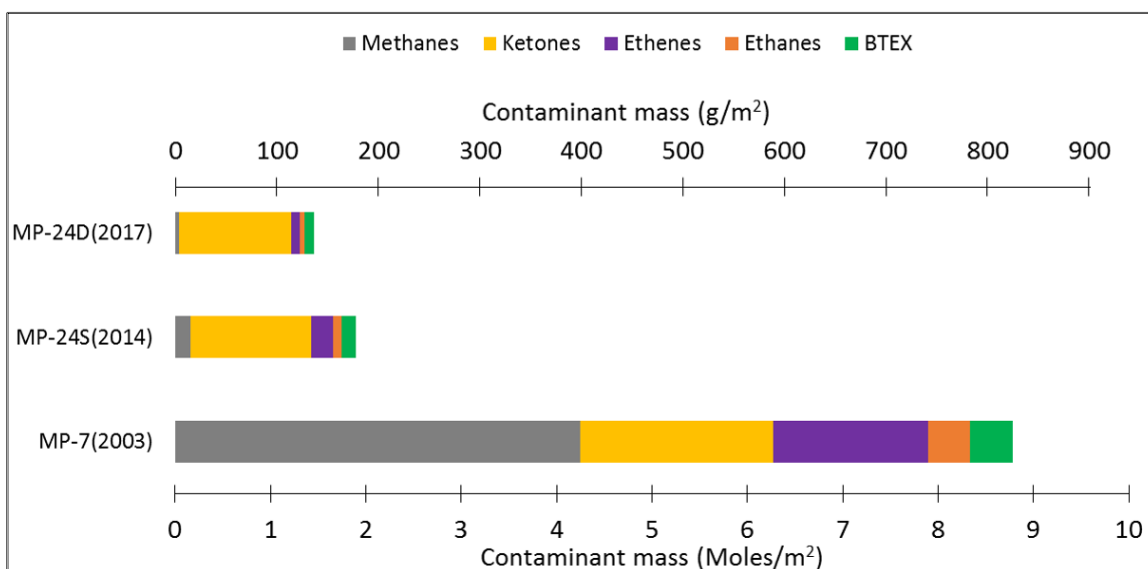
Figure 12: Temporal rock matrix contaminant mass and composition changes.

The figure shows changes for the 3 locations cored over the fourteen year period. Chlorinated methanes recorded the highest decline in mass, from 4.3 moles/m^2 in MP-7 to 0.041 moles/m^2 in MP-24D, representing a 99% mass loss. Ketones, relative to the other contaminant groups, declined at the slowest rate and were seen to persist. At 2.02 moles/m^2, ketones constituted 23% of the contaminant mass at MP-7 and because of the slow declining rate relative to the other groups, the MP-24D mass of 1.18 moles/m^2 represented 80.6% of the total contaminant mass.

The figure above is a summation of all the contaminant mass in each rock core. Contaminants in fractured rock have preferential zones of mass distribution that necessitates analysis over short vertical intervals. Therefore, depth-discrete results were analysed for approximately every 24cm increase in depth for the entire core length (Table 2).

Table 2: Coring interval and sampling rate for the three locations

Well ID	Coring Start Date	Elevation (masl)*	Coring Depth (m)		Samples collected	Sampling interval (m)
			From	To		
MP-7	Dec-2003	271.28	29.39	73.78	170	0.26
MP-24S	June-2014	270.78	30.46	54.73	110	0.22
MP-24D	Jun-2017	270.89	28.9	96.99	276	0.25

*masl: meters above sea level

Figure 13 below shows the moles recorded for depth-discrete sampling of total volatile organic compounds (TVOCs) and the five key contaminant groups: chlorinated methanes, chlorinated ethanes, chlorinated ethenes, ketones and BTEX. The vertical profiles show that despite TVOC moles decreasing over the fourteen years, the rate varied with depth in addition to time. TVOC in the upper bedrock (Tonti Member, 30-48m bgs) exhibited the highest declining rates of up to four orders of magnitude between MP-7 and MP-24D whereas in the lower rock (Tunnel City, 50-55m bgs), the contaminants persisted or had minor variations over the same period. Chlorinated methanes, ethanes and ethenes had the highest declining rates throughout the profile with the highest declines registered in the upper bedrock where concentration and mass decreased by up to 5 orders of magnitude. BTEX and ketones were generally persistent throughout the entire profile and registered the slowest declines amongst the five contaminant groups.
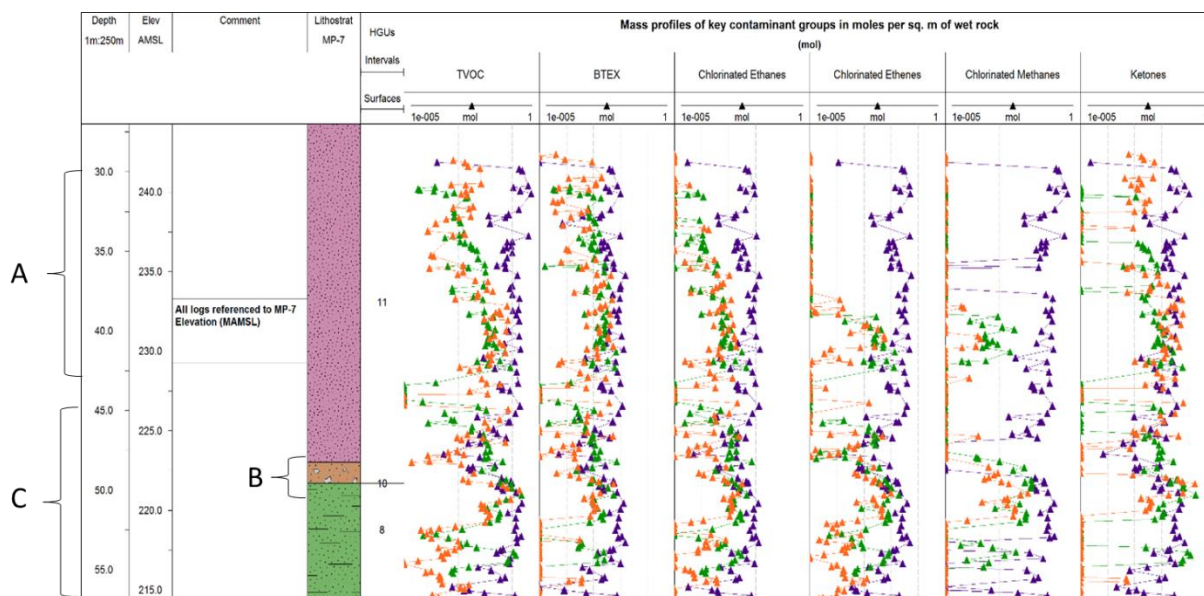
Figure 13: Mole profiles of contaminant groups with depth (moles/m^2 of rock core).

The 3 locations showed are: MP-7 (2003) ▲, MP-24S (2014) ▲ and MP-24D (2017) ▲. The plots show contaminant changes with depth for total VOCs (TVOCs), BTEX, chlorinated ethanes, chlorinated ethenes, chlorinated methanes and ketones. In 2003, contaminant mass was evenly distributed in the

profiles except in section B (47-49m bgs) where there was a sudden reduction. 2014 results show that most of the contaminant mass was preferentially lost from upper sections of the bedrock in section A (30-42m bgs) while the 2017 profile shows that most of the mass loss occurred in section C which is the upper Tunnel City formation (45-55m bgs). Temporal changes show that chlorinated methanes, ethanes and ethenes declined fastest, whereas BTEX and ketones changed the least.

In addition to contaminant mass changes with depth, the relative composition of the five key contaminant groups (as a percentage of TVOC at every ~30cm interval) is shown in Figure 14 below. MP-7's profile was comparatively consistent with depth: chlorinated methanes, ethenes, and ketones dominated the composition at most depths. The composition changed in MP-24S and MP-24D where ketones and BTEX compounds dominated most of the profile, especially in the upper bedrock units. Within lower units, the percent molar composition of chlorinated ethenes increased significantly whereas the ketones and BTEX composition was generally below 5%.
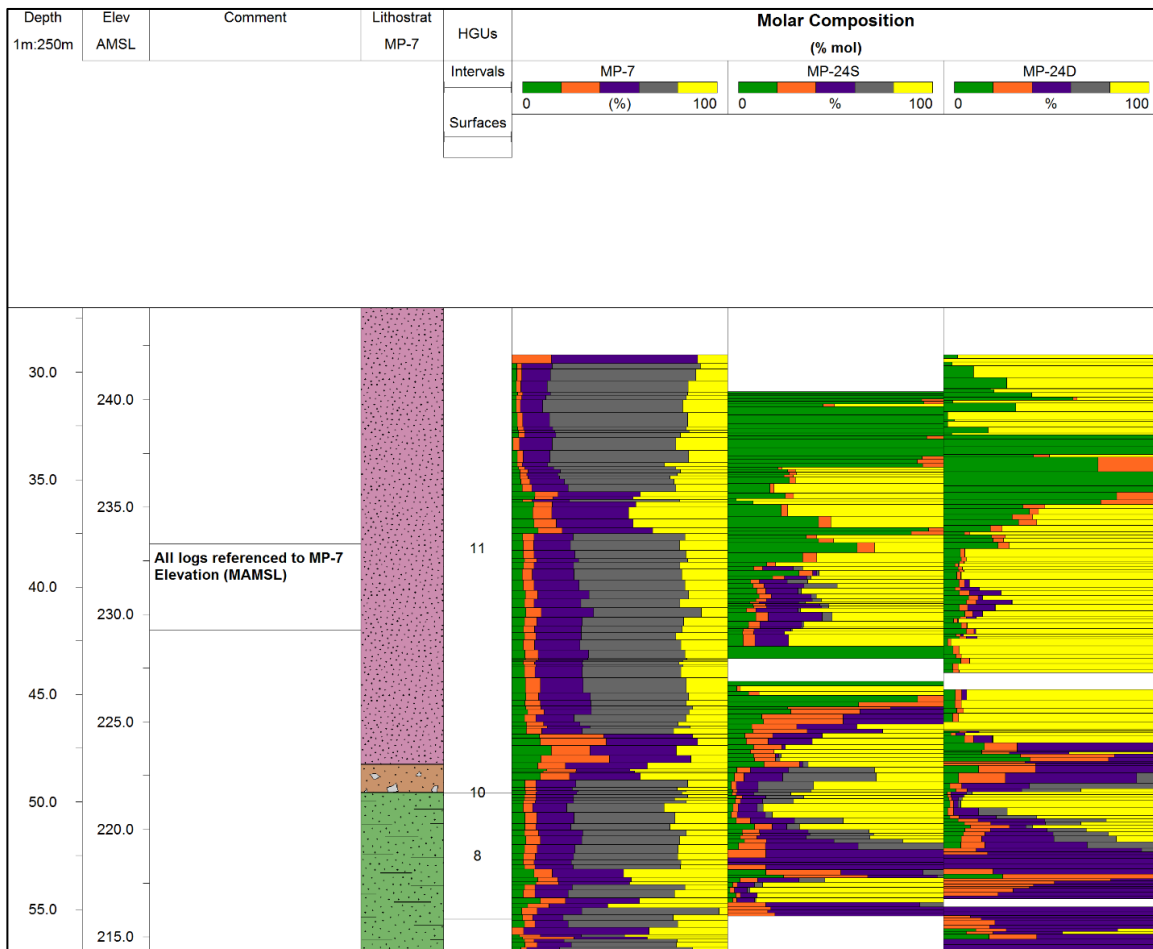
Figure 14: Contaminant groups profiles for each of the three core holes.
BTEX ▮, Chlorinated Ethanes ▮, Chlorinated Ethenes ▮, Chlorinated Methanes ▮ and Ketones ▮. At MP-7, chlorinated methanes dominated the composition in most sections of the profile followed by

ketones and chlorinated ethenes. In the upper bedrock (30-36m bgs) of subsequent cores, percent molar composition of chlorinated methanes reduced throughout the profile to become a minor constituent whereas BTEX and ketones increased to become dominant contaminant groups. In the lower bedrock (45-55m bgs), chlorinated ethenes dominated the composition.

Of the 35 contaminants analysed, 15 accounted for 99.99% of the rock matrix contaminant mass at the three locations as shown in Table 3. The remaining 20 compounds were either reported as non-detect concentrations in all the three core analysis or only constituted less than 0.01% of the total mass in the rock core. This subset of 15 compounds were selected for further analysis on the temporal variations rather than the full suite of reported analytes. Of the 15 compounds, 12 exhibited declining trends while 3 displayed increases in mass.

Table 3: Fifteen contaminants as a percentage of the total contaminants at three core locations. Methylene chloride (DCM) constituted 48.3% of the MP-7's mass followed by MIBK at 22.6% and cis-1,2-DCE at 17.1%. By 2017, DCM declines by 4.2 moles/m2 of core, the highest decline of all contaminants. 3 contaminants (vinyl chloride, chloroethane, and 2-butanone) increase in mass over the fourteen-year period.

Contaminant Group	Contaminant	15 selected VOCs as % of total VOCs (actual moles/m^2 in parenthesis)			Δ (moles/m^2) 2003 to 2017
		MP-7 (2003)	MP-24S (2014)	MP-24D(2017)	
Chlorinated Ethenes	Tetrachloroethene	0.237 (0.021)	0.08 (0.002)	0.04 (0.001)	-0.020
	Trichloroethene	0.377 (0.033)	1.002 (0.019)	0.594 (0.009)	-0.024
	cis-1,2-Dichloroethene	17.139 (1.505)	9.627 (0.182)	3.808 (0.056)	-1.450
	1,1-Dichloroethene	0.694 (0.061)	0.633 (0.012)	0.298 (0.004)	-0.057
	Vinyl Chloride	0.128 (0.011)	0.941 (0.018)	1.267 (0.019)	0.007
	Sub-Total	18.58 (1.631)	12.28 (0.232)	6.01 (0.088)	-1.544
Chlorinated Ethanes	1,1,1-Trichloroethane	2.591 (0.228)	0.75 (0.014)	0.4 (0.006)	-0.222
	1,2-Dichloroethane	0.026 (0.002)	0.014 (0)	0.031 (0)	-0.002
	1,1-Dichloroethane	2.336 (0.205)	2.778 (0.053)	1.014 (0.015)	-0.190
	Chloroethane	0 (0)	1.222 (0.023)	1.986 (0.029)	0.029
	Sub-Total	4.95 (0.435)	4.77 (0.090)	3.43 (0.050)	-0.385
Chlorinated Methanes	Methylene Chloride	48.343 (4.246)	8.468 (0.16)	2.793 (0.041)	-4.205
Ketones	2-Butanone	0.376 (0.033)	40.282 (0.762)	54.389 (0.795)	0.762
	4-Methyl-2-pentanone	22.64 (1.988)	26.626 (0.504)	26.209 (0.383)	-1.605
	Sub-Total	23.02 (2.022)	66.91 (1.266)	80.60 (1.178)	-0.843
BTEX	Toluene	4.346 (0.382)	6.027 (0.114)	5.799 (0.085)	-0.297
	Ethylbenzene	0.183 (0.016)	0.275 (0.005)	0.185 (0.003)	-0.013

Contaminant Group	Contaminant	15 selected VOCs as % of total VOCs (actual moles/m² in parenthesis)			Δ (moles/m²) 2003 to 2017
		MP-7 (2003)	MP-24S (2014)	MP-24D(2017)	
	Xylenes	0.58 (0.051)	1.27 (0.024)	1.18 (0.017)	-0.034
	Sub-Total	5.109 (0.449)	7.572 (0.143)	7.163 (0.105)	-0.344
	Total	99.997 (8.783)	99.996 (1.892)	99.991 (1.462)	-7.321

Within each of the five major contaminant groups, each individual analyte displayed unique temporal trends that were examined in detail. Figure 15 below shows the mole profiles with depth of the five analytes that constitute chlorinated ethenes. From the highest to lowest molecular weight, the five analytes are PCE, TCE, dichloroethene isomers (cis-DCE and 1,1-DCE) and VC. Between MP-7 and MP-24D, the moles of PCE decreased by an average of 95% in almost all sections of the profile. TCE decreased by 73% except in a 5 m zone in the upper Tunnel City group where the mass persisted or slightly increased. Despite an overall decrease of 96% for cis-DCE, the mass at two sections (38-43 and 48-55 mbgs) declined by <5% and at some intervals showed slight increases in mass. 1,1-DCE mass decreased by over 2 orders of magnitude consistently throughout the profile except in the same two zones as cis-DCE but with shorter intervals (40-42 and 50-52 mbgs). VC was one of three exceptions out of the 35 compounds analysed whose overall mass increased between 2003-2017, from 0.0072 to 0.0113 moles/m² of core representing a 64% increase. VC is a known carcinogen with stringent US EPA drinking water guidelines of 2µg/L. As a comparison, the maximum concentration of VC in MP-24D was 2 401 µg/L.
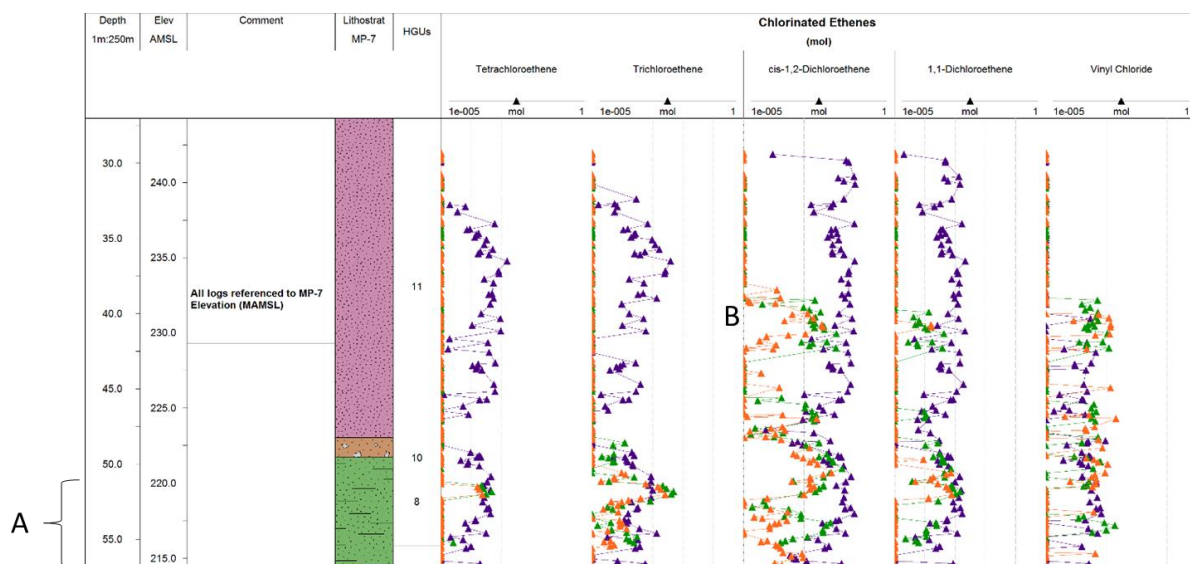

Figure 15: Profile of moles with depth for chlorinated ethenes.

The profiles shown are MP-7 ▲, MP-24S ▲ and MP-24D ▲. In 2003, PCE, TCE, cis-DCE and 1,1-DCE were the dominant chlorinated ethenes. The MP-7 profiles show that the vertical distribution in terms of the magnitude of concentration of these four compounds is fairly consistent with depth. The 2014 and

2017 profiles show that most of the mass is distributed in the upper Tunnel City group (section "A", 52-55m bgs). Between 2003 and 2017, higher molecular weight chlorinated ethenes (PCE and TCE) decreased in moles by 2-3 orders of magnitude except in section "A" where mass was seen to persist. Cis-DCE showed a similar temporal trend with the exception of a second zone between 38-42m bgs (section "B") where the mass persisted. An increase in the mass of VC was noted in most sections of the profile except in the upper bedrock where VC concentration was non-detect. It could be plausible that VC present in the upper bedrock was completely degraded to ethene, which subsequently escaped as a gas. However, a contrasting possibility is the absence of microbial colonies in the upper bedrock that are capable of dechlorinating VC. Despite 16S rRNA tests conducted by Lima et al. (2012) at this site which identified the presence of Dehalococcoides capable of dechlorinating VC to ethene, a comprehensive review of the VC recalcitrant nature presented by Bradley (2010) showed that 16S rRNA techniques are insufficient to fully identify the specific Dehalococcoides populations capable of this terminal dechlorination.

The second contaminant group, chlorinated ethanes, consisted of TCA, 1,1-DCA, 1,2-DCA and chloroethane. Figure 16 below shows the temporal changes in moles with depth for the four compounds. The moles of TCA declined by up to 3 orders of magnitude (97%) in the upper bedrock whereas in the lower bedrock (50-55 mbgs), the mass changes were minimal. Of the two isomeric dichloroethanes, the mass of 1,1-DCA was originally higher than 1,2-DCA with the former displaying slower mass declines in 2 zones: one in the upper bedrock and the other in the lower Tunnel City Group. The lowest molecular weight compound, chloroethane, was reported as non-detect at MP-7 but the moles in MP-24S and MP-24D increased by 2-3 orders of magnitude throughout the entire profile.

Figure 16: Profile of moles with depth for chlorinated ethanes.

The profiles shown are MP-7 ▲, MP-24S ▲ and MP-24D ▲. The mass of TCA declined by up to 3 orders of magnitude in most sections of the profile except in the lower bedrock (section B, 50-55m bgs), where the mass changes were minimal. The mass of 1,1-DCA was originally higher than 1,2-DCA with the former displaying slower mass declines in 2 sections: one in the upper bedrock (section "A", 30-37m bgs) and the other in the lower Tunnel City group (section "B", 50-55m bgs). The lowest molecular weight daughter product, chloroethane increased in mass by 2-3 orders of magnitude throughout the profile.

In the third contaminant group, chlorinated methanes, DCM was the only chlorinated methane whose mass was greater than 0.01% of the total contaminant mass or was not non-detect in the three rock core results. The moles of DCM decreased by up to five orders of magnitude, from a maximum of 1 mole/m^2 of core in MP-7 to non-detect in MP-24S and MP-24D (Figure 17). However, as in most other contaminant groups, this reduction was least in two zones within the upper and lower formation where the mass was seen to persist or slowly decline.
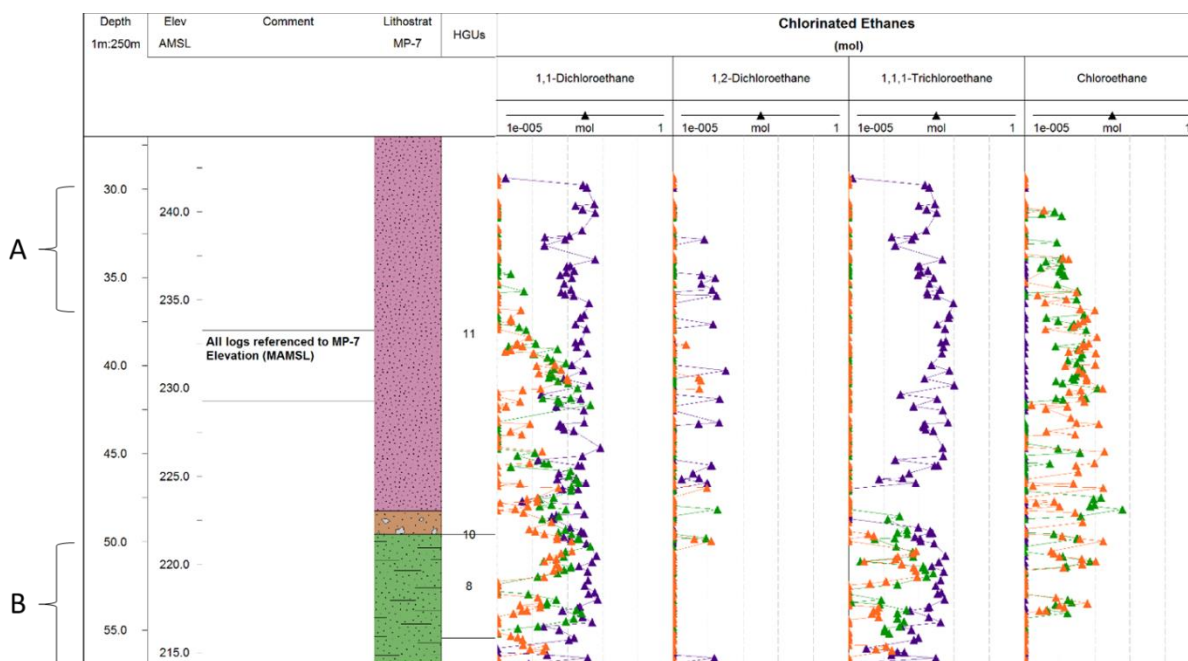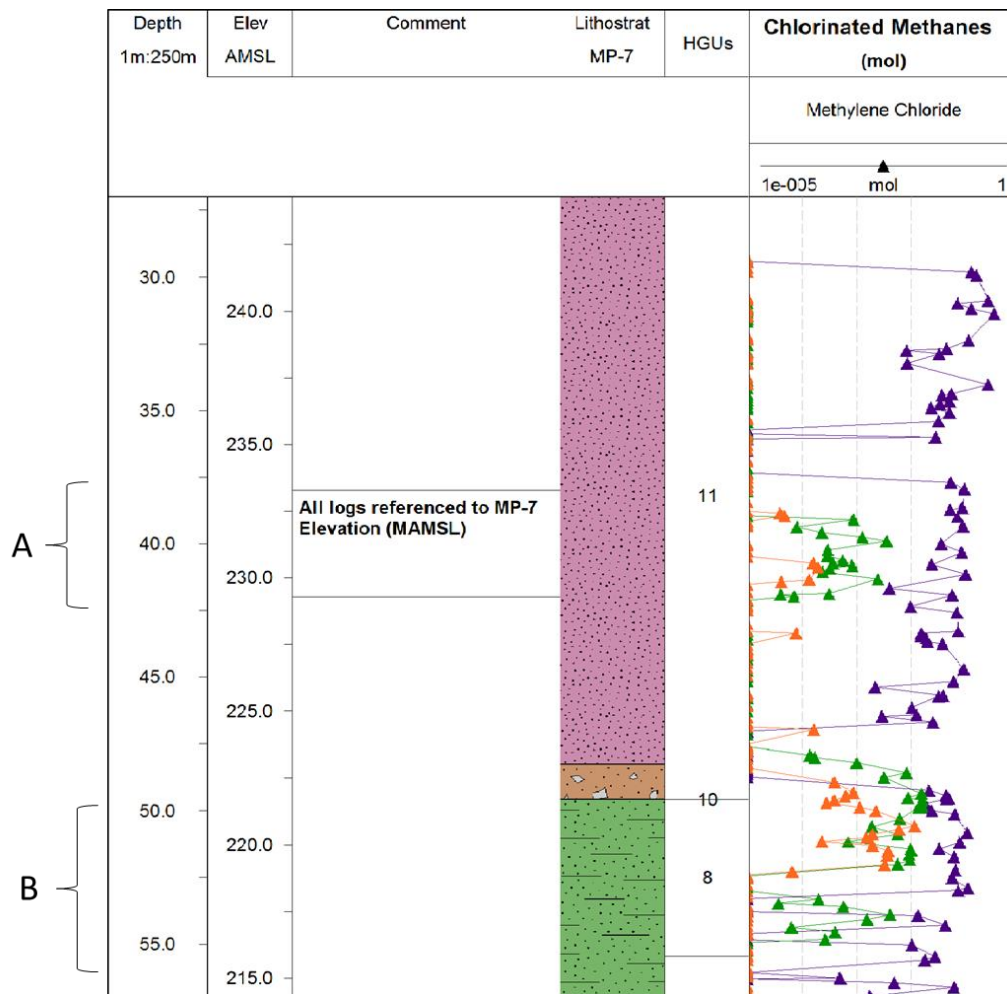

Figure 17: Profile of moles with depth for chlorinated methanes.

The profiles shown are MP-7 ▲, MP-24S ▲ and MP-24D ▲. The mass of chloromethane declines in most sections of the profile by up to 5 orders of magnitude except for two sections ("A" and "B" located at 38-42 and 49-55m bgs respectively) where the mass is seen to persist or slowly decline. This huge decline could be a result of microbial degradation, discussed separately in section 6.1.

Of all the contaminant groups analysed, ketones display the highest overall mass and concentration increases. Figure 18 below shows that the mass of 2-butanone (MEK) in 2003 was almost non-detect but both the 2014 and 2017 results show a consistent 3-4 order of magnitude increase throughout the profile. MIBK mass declined over the fourteen-year period except in some sections where the mass persisted or displayed slight increases compared to the 2003 benchmark.
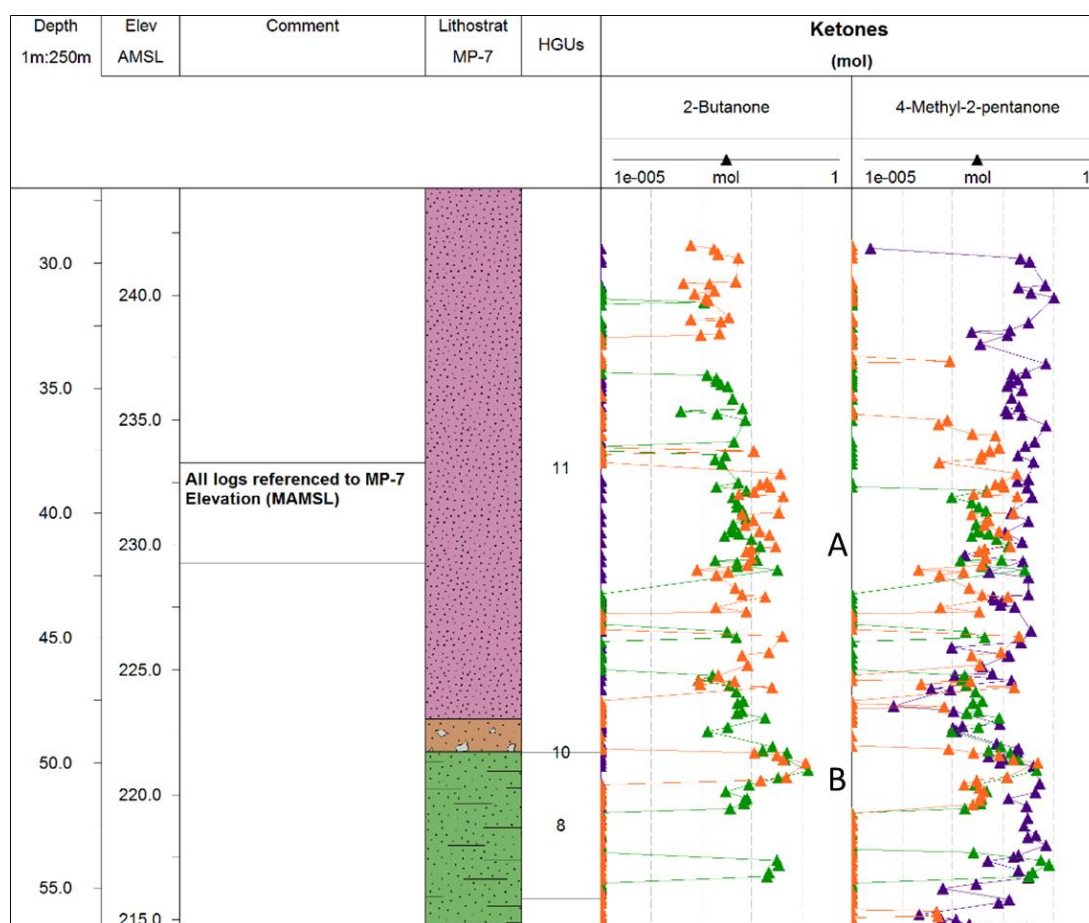
Figure 18: Profile of moles with depth for ketones

The profiles shown are MP-7 ▲, MP-24S ▲ and MP-24D ▲. Of all the contaminants analysed, ketones display the highest overall mass and concentration increases. The mass of MEK in 2003 was almost non-detect but both the 2014 and 2017 results show a consistent three to four-fold increase throughout the profile. MIBK was persistent and its mass slowly declined over the fourteen-year period. This decline is noticeable in most sections of the profile except at section A and B, between 39-43 and 50-52m bgs, where the decline was slower. It is interesting to note that sections A and B, where mass is seen to

either persist or increase, corresponds to zones where DCM, 1,1-DCA and cis-DCE also increase (see previous figures).

Figure 19 below shows mass profiles for BTEX compounds (note that benzene was excluded since its concentration was reported as non-detect in all three core holes), toluene, ethylbenzene and total xylenes (meta, para, and ortho xylenes) are generally persistent throughout the profiles. For instance, xylenes declined at a rate 17% lower than the average decline rate for the overall profile. However, of the three, the mass of ethylbenzene had the fastest declines whereas both toluene and xylene mass changes are minimal.
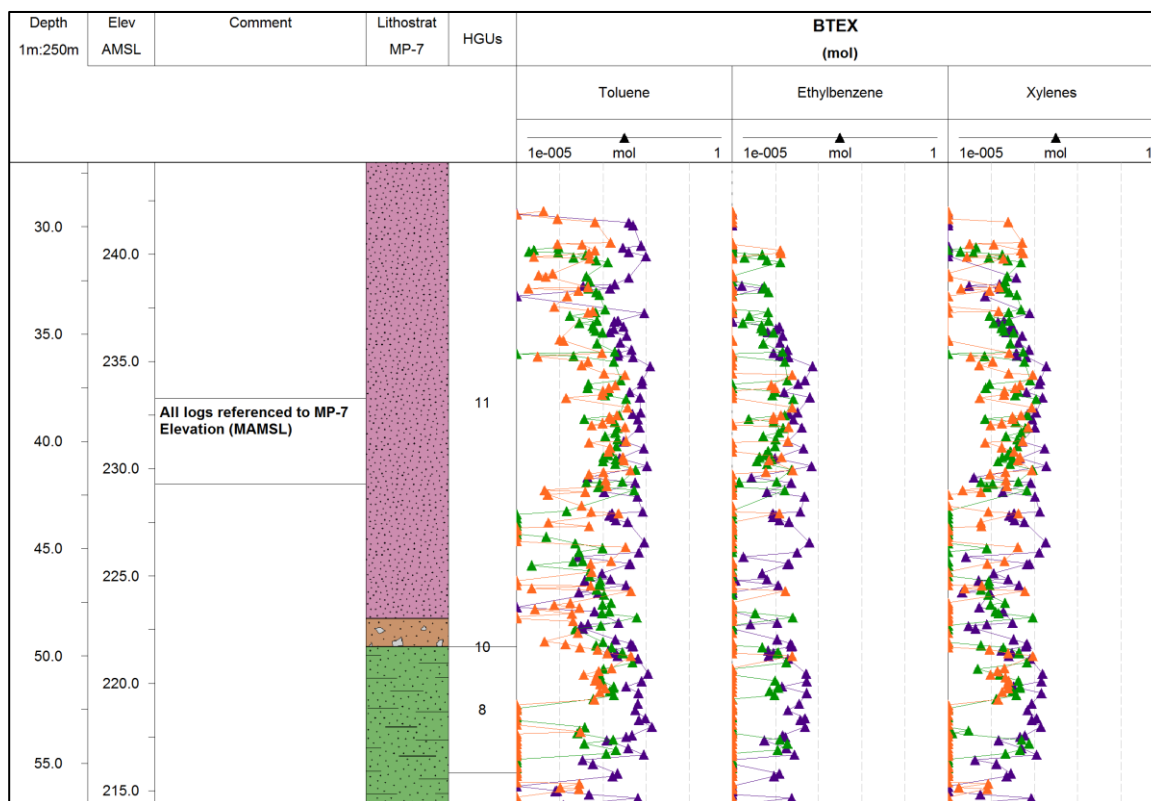
Figure 19: Profile of moles with depth for select BTEX compounds.

The profiles shown are MP-7 ▲, MP-24S ▲ and MP-24D ▲. Benzene was excluded since the concentrations from all three locations were non-detects. From the MP-7 contaminant analysis, toluene had the highest VOC mass of the BTEX compounds. Mass declined fastest in the lowest zone where concentrations at MP-24S are non-detect. The mass of ethylbenzene reduced to non-detect concentrations in almost all sections of the profile in MP-24S. MP-24D results show a slight increase in concentration and especially in the shallow bedrock.

During the analysis of TVOC and the five contaminant groups at MP-24S and MP-24D, a mass distribution pattern emerged. There was a high variability of mass changes with depth: certain sections had

very high contaminant mass and high rate of contaminant mass loss while in other sections, the total mass was low and it either persisted or declined at a slow rate. Graphs of cumulative contaminants with depth were used to identify these distinct zones of mass loss: vertical lines show zones where most of the mass accumulated while nearly horizontal lines show zones where the mass was non-detect or accumulated very slowly over intervals. MP-7 was only used as a baseline to compare the changes in contaminant mass within the four identified zones at MP-24S and MP-24D. Figure 20 shows four distinct zones that were identified through this process and Table 4 shows the total mass in each of the four zones for the three locations as well as the decline of contaminants in each of the four zones measured as a percentage of the total mass in that zone. It is important to clarify that the delineation of zones only took into account the 13/15 contaminant mass that showed declining trends (Table 3 in section 5.1). Contaminants whose mass increased during the analysis period were excluded to reduce interference and cancelling out of the effects of decreasing contaminants. However, a quick check was performed (not shown) and the zones of mass accumulation coincide with the zones of mass decline. Therefore, zones delineated in Figure 20 are representative of both decreasing and increasing contaminants.
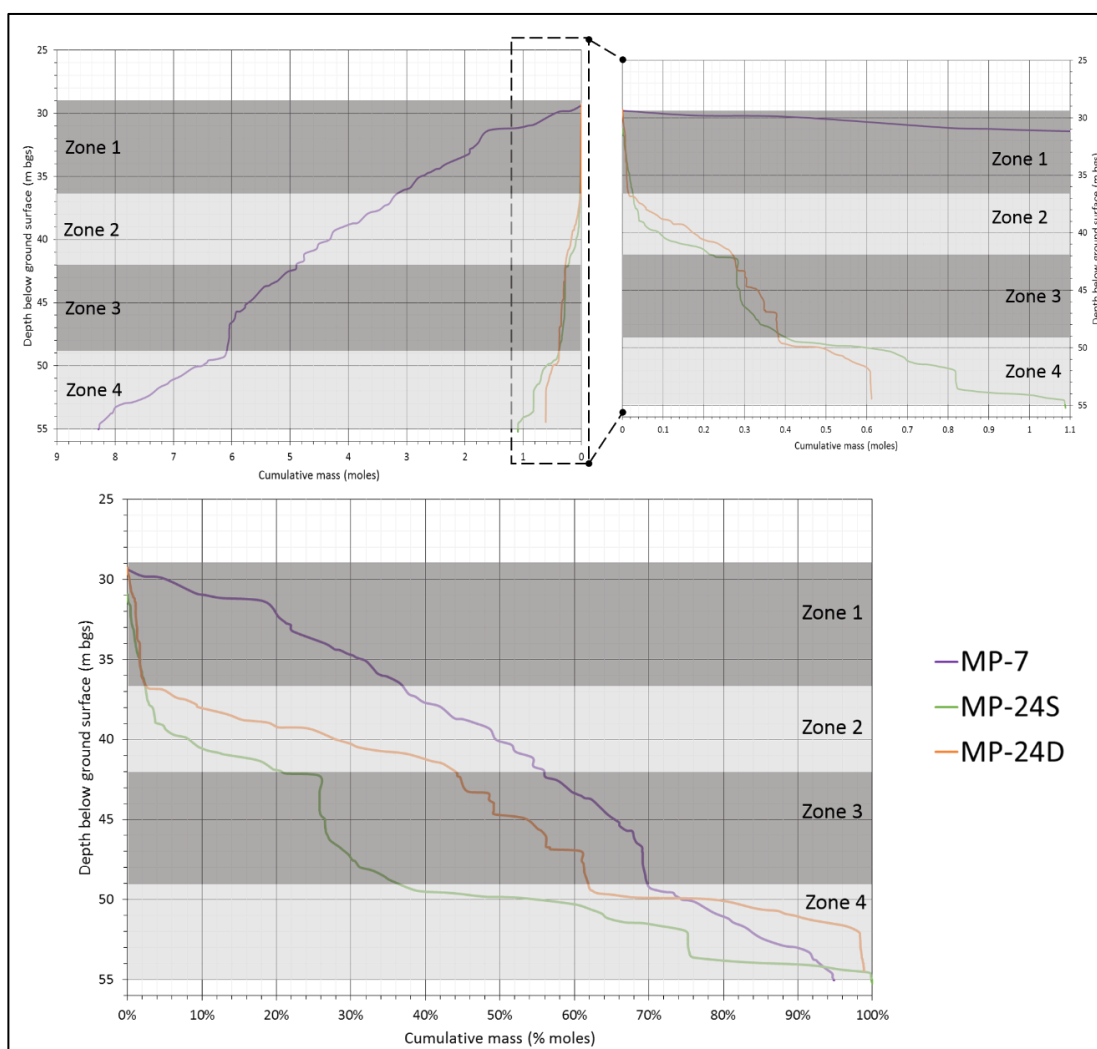
Figure 20: Identification of four zones of mass change.

The profiles of MP-24S and MP-24D are compared to the profile of MP-7. The two figures at the top show cumulative moles with depth while the bottom figure represents the same data as a percentage of the TVOC in the respective core hole. The darker zones (1 and 3) are sections with the lowest mass distribution due to the very high rate of mass reduction that occurred between 2003 and 2017 whereas the lighter zones (2 and 4) have the highest mass distribution due to a low rate of mass reduction over the same period. MP-7's profile reflects the areas of preferential contaminant mass distribution with depth when the NAPL entered the subsurface. With the exception of 47-49m bgs where very little mass was distributed, MP-7's profile shows an even distribution of mass with depth. The curves of MP-24S and MP-24D represent deviations from MP-7's profile which reflects the areas of preferential mass loss (zone 1 and 3) and preferential mass persistence (zone 2 and 4).

Table 4: Percent mole changes in the four identified zones across the three core locations.

Between 2003 and 2014, most of the contaminant decline occurred in the upper bedrock (zone 1) whereas between 2014 and 2017, most of the contaminant decline occurred in the lower bedrock (zone 4)

Zone	Depth (mbgs)		Contaminant mass (moles/m^2 of core)			Changes in contaminant moles (%)		
	From	To	MP-7	MP-24S	MP-24D	MP-7 to MP-24S	MP-24S to MP-24D	Overall Δ
1	29	36.5	3.20	0.04	0.03	-99.1	-35.9	-99.4
2	36.5	42	1.56	0.24	0.24	-83.8	+2.5	-83.4
3	42	49	1.32	0.19	0.11	-85.3	-43.7	-91.7
4	49	55	2.21	0.63	0.23	-72.2	-63.1	-89.7

Between MP-7 and MP-24S, the mass in zones 1 and 3 had the highest decline while between MP-24S and MP-24D, most of the mass lost occurred in zone 4 in the Tunnel City group (49-55 mbgs). Three take-away messages are worth noting from this zonal delineation. The first is that across all three locations, contaminant mass in zone 3 is lower compared to zones 2 and 4 and could be termed as a transition zone. Secondly, Zone 1, in the upper bedrock, had the highest total contaminant mass in 2003 as well as the highest overall rate of contaminant decline. However, most of the mass decline occurred between 2003 and 2014 as opposed to 2014 to 2017. A probable reason is that by 2014, most of the contaminant mass in the shallow bedrock was so depleted (evidenced by many non-detect concentrations) that the potential for change was less between 2014 and 2017. Finally, residual DNAPL is known to have accumulated in the formation and depth corresponding to zone 4. Given the transmissive nature and lateral continuity of this formation, it is likely that lateral transport of contaminants from upgradient location leads to the noticeable contaminant persistence in Figure 20. This result also confirms a previous postulation by Meyer (2005) regarding contaminant characteristics in this zone.

5.2   The Effect of Spatial Distribution on Temporal Contaminant Analysis

The influence of spatial heterogeneity on the temporal interpretations was a subset of the first objective of the thesis. The temporal analysis presented in section 5.1 utilised data from three core holes, MP-7, MP-24S and MP-24D, which are located within 18.3m of each other. Despite being close together to assume that any differences in rock core contaminant mass changes were due to temporal variations, it was necessary to understand the effect of spatial variability on the temporal interpretations. This spatial variability calculation contained a number of assumptions and therefore, it served as an assessment of the probable magnitude of the spatial variability effect rather than provide exact values.

The spatial variability calculation is described below. Overall mass decline results between MP-7 and MP-24S was calculated to be 78.5%. Similarly, mass decline between MP-24S and MP-24D was 22.7%. These declines were assumed to uniformly apply across the entire SZT i.e. at all points within the entire SZT, the mass decline between 2003 and 2014 was 78.5% and 22.7% between 2014 and 2017. The five boreholes cored in 2014 (MP-22S, MP-23S, MP-24S, MP-25S and MP-26S) were used as the baseline for the comparison. The contaminant mass in each of the "S" core holes was calculated for 2014, the year they were all cored. The 78.5% mass decline between 2003 and 2014 was then applied to back-calculate the hypothetical mass of the contaminants in the shallow core in 2003. Similarly, the 22.7% mass decline between 2014 and 2017 was used to calculate the hypothetical mass of the shallow cores in 2017. The results are in Table 5 and in Figure 21 below.

Table 5: Temporal contaminant mass in Shallow core holes in moles

Well ID	Distance from MP-22S	From	To	TVOC ($moles/m^2$ of core)		
	(m)	(mbgs)	(mbgs)	2003	2014	2017
MP-22S	0	18.18	54.74	0.0012	0.0003	0.0002
MP-23S	55	25.07	54.42	3.3260	0.7019	0.5172
MP-24S	111	30.46	54.73	8.9639	1.8918	1.3939
MP-25S	168	31.48	57.71	8.1625	1.7227	1.2693
MP-26S	242	33.47	62.00	1.9013	0.4013	0.2957
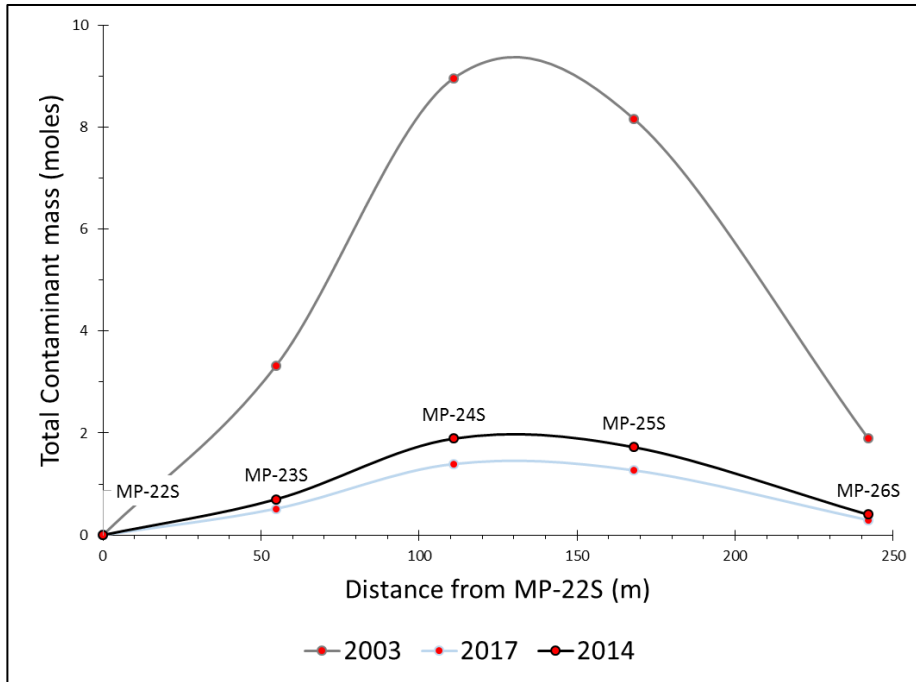
Figure 21: Total contaminant mass for each shallow core hole

In order to evaluate the effect of spatial heterogeneity, the known MP-7 total contaminant mass was added to the hypothetical 2003 profile at 124 m from MP-22S. The hypothesis was that spatial distribution would cause the MP-7 point to lie outside the plotted 2003 curve. The difference between the actual MP-7 total contaminant mass and that from the 2003 curve was assumed to result from spatial distribution. These steps were repeated with MP-24D at 110 m. The results are shown below in Figure 22 and Table 6.
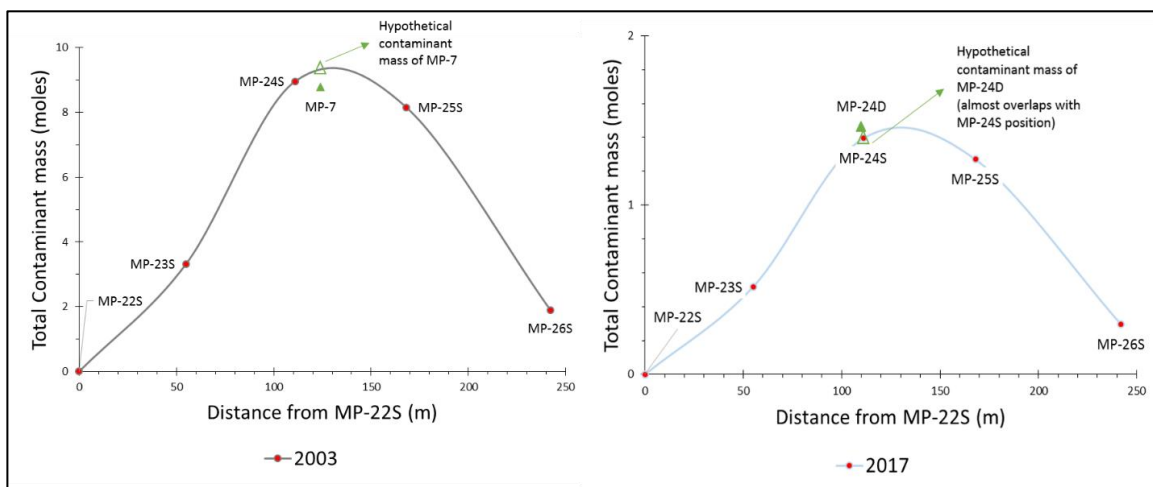
Figure 22: Differences between the actual and calculated contaminant mass values.
The curves show MP-7 and MP-24D spatial variation. These differences were attributed to the spatial distribution of these core holes with respect to the transect line from MP-22S to MP-26S.

Table 6: Effect of spatial distribution on temporal analysis

Core hole	Actual Mass (moles/m^2)	Hypothetical Mass (moles/m^2)	Absolute Difference (%)
MP-7	8.78	9.32	6.1%
MP-24D	1.46	1.39	4.9%

Through this analysis, it can be stated that the spatial heterogeneity accounted for 6.1% of the contaminant mass changes between 2003 and 2014 analysis and 4.9% of changes between 2014 and 2017.

5.3   Analysis of the Hydraulic Barrier System

The second objective of this thesis was to compare the contaminant changes downgradient of the source zone to the mass removed by the HBS. Groundwater samples and pumping rates from the HBS were analysed and reported. Between 2003 and 2017, the five pumping wells that originally constituted the HBS pumped out approximately 3225.8 megalitres (ML, x106L) of groundwater and extracted 260 573 moles (23 693 kg) of TVOCs as shown in Table 7 and Table 8 below. 91.6% of the TVOC mass was extracted between 2003 and 2014 before the SZT cores were collected, with the exception of MP-7 cored in 2003 before the HBS came online. As discussed in section 3.4, two pumping wells, P-71 and P-145, were taken offline in 2004 and 2008. They constitute less than 5% of the groundwater volume pumped out and 13% of the total mass of TVOCs extracted. Consequently, only pumping wells P-164, P-130 and P-128 currently constitute the HBS and therefore were the only ones analysed in detail.

Table 7: Pumping wells operating conditions.
P-164 that is the longest operating well closest to the source zone has extracted the highest volume of groundwater as well as the highest contaminant mass

Well ID	Distance from the SZT(m)	Sampling Period*		Groundwater pumped (x10^6 L)	TVOC removed (kg)
		Start	End		
P-128	1296	Oct-2003	Dec-2017	805.44	294.08
P-130	1075	Oct-2003	Dec-2017	816.03	851.58
P-145	947	Oct-2003	Sep-2008	119.455	1,134.90
P-164	573	Aug-2004	Dec-2017	1459.193	19,383.94
P-71	541	Mar-2004	Sep-2004	25.669	2,028.67
				3225.78	23,693.17

*End of the sampling period refers to the last sampling round used for this study. P-128, P-130 and P-164 are still in operation

Table 8: Summary of VOC Contaminant mass pumped out in kg from each pumping well.

P-164 extracted the highest mass of VOCs with chlorinated ethenes as the highest constituent.

Well	TVOC(kg)	Chlorinated Ethanes	Chlorinated Ethenes	Ketones	BTEX	Chlorinated Methanes
P-128	294.08	105.28	188.45	0.33	-	0.02
P-130	851.58	311.39	537.27	1.32	0.33	1.27
P-145	1,134.90	344.90	523.69	164.09	59.46	42.77
P-164	19,383.94	4,445.13	7,377.36	3,906.27	2,557.31	1,097.87
P-71	2,028.67	419.59	604.25	571.24	225.48	208.11
Total	23,693.17	5,626.28	9,231.03	4,643.25	2,842.58	1,350.03

Relative to the SZT core holes, P-164, P-130 and P-128 are located 563.4, 1075 and 1296m down-gradient respectively. Figure 23 below shows that distance from the SZT influences the mass and composition of the contaminants. The composition of the closest well to the SZT, P-164, consisted of the same five contaminant groups as those observed from the SZT whereas the composition of P-130 and P-128 was mostly dominated by two contaminant groups. P-164 was the most efficient at extracting contaminants. It removed 13.28 kg of VOCs/megalitre of groundwater, over ten times the efficiency of P-130 (1.04kg/ML) and P-128 (0.37kg/ML).
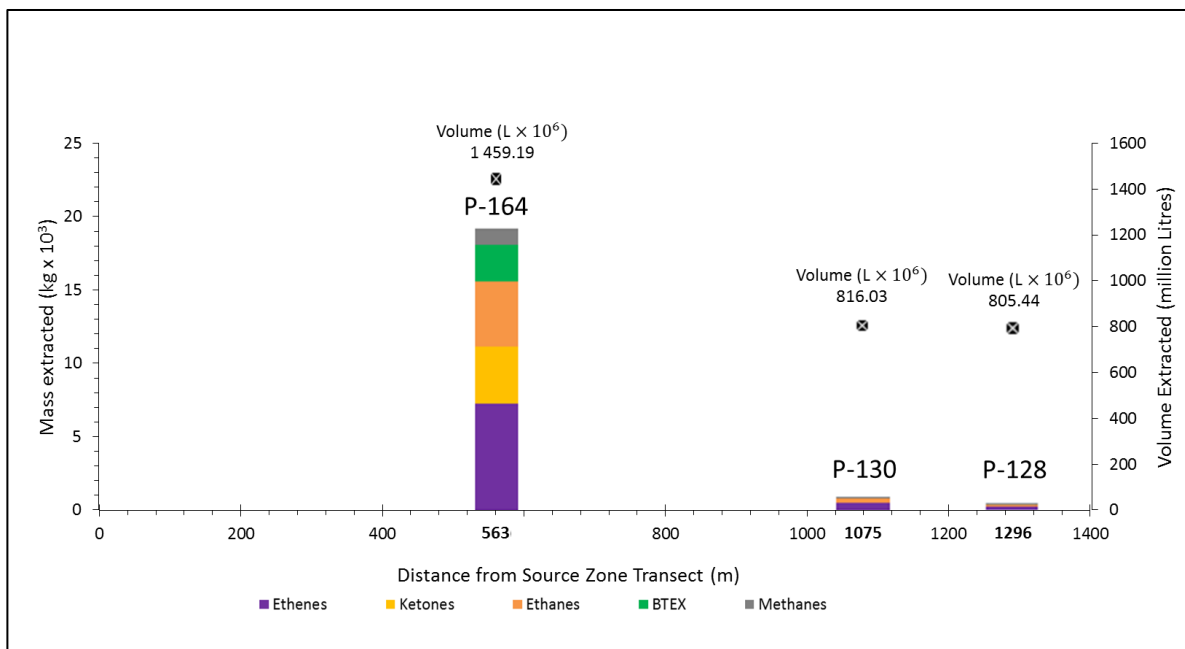
Figure 23: Mass and composition of extracted contaminants from the HBS.

P-130 and P-128 are located furthest from the SZT. These wells were less efficient than P-164 in capturing contaminant mass as shown by the disparity between groundwater pumped and contaminants extracted.

In order to understand the capture zone and consequently, the efficiency of the HBS in capturing mass from the source zone, it is necessary to examine each of the three wells in detail. At 573.9m, P-164 is the closest pumping well to the SZT core holes. Figure 24 below shows the changes in concentration and pumping rates at P-164 between September 2004 and December 2017. Between 2004 and 2007, the concentration of TVOCs extracted was greater than 10 000 µg/L with a peak value of 84 210 µg/L in March 2005. Between 2007 and 2017, the TVOC concentration declined to steady values of below 5 000 µg/L with the lowest TVOC concentration of 4 079 µg/L registered in June 2014. Time series analysis of the pumping rate at P-164 showed that an increasing step trend exists between August 2004-January 2009 and January 2009-December 2017. In the first period, the mean pumping rate was 2.96 L/s while in the second period, the mean pumping rate was 3.59 L/s, an increase of 0.63 L/s (t-value of 12.20 > t_α 2.0 at a confidence of α=0.05).
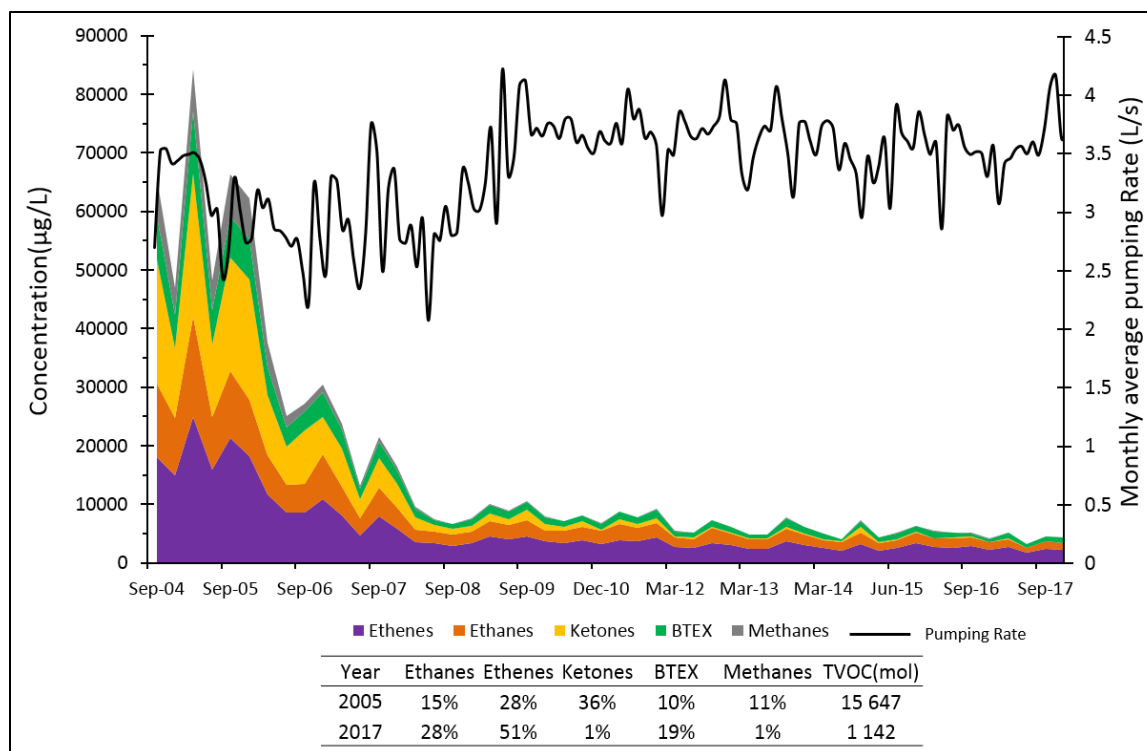
Figure 24: Time-series of the contaminant concentration and pumping rates at P-164.

When the well commenced operation, the concentration of contaminants peaked at 84 210 µg/L. This high initial concentration may have been due to the sudden groundwater flushing of VOCs from the plume and source zone. Over time, the concentration reduced to less than 5mg/L. The table below the graph shows a snapshot of the total VOCs and contaminant composition at the beginning and end of the analysis. Ketones dominated the 2004/2005 composition but these declined by 35% to 1% of the VOCs in 2017 while ethenes increased by 23% over the same duration. The pumping rate experienced a step trend increase of 0.63L/s in January 2009

The molar composition of contaminants extracted between 2004 and 2010 consisted of chlorinated ethenes, ethanes and ketones as the most dominant contaminants and BTEX and chlorinated methanes as minor constituents. The change in molar composition of VOC groups was analysed by comparing two sampling rounds, one at the beginning in 2005 and another in a recent sampling event in 2017 (Table part of Figure 24). The composition of ketones reduced from 36% of the TVOC moles extracted in 2005 to 1% of the TVOC extracted in 2017. The reduction in chlorinated methanes over this duration was from 11% to 1%. For all sampling rounds after 2012, chlorinated ethenes made up over 50% of the contaminant moles extracted compared to an average of 37% prior to 2012. These changes in both mass and composition are important for the evaluation of well performance and offer a glimpse of the processes occurring within the up-gradient source zone. The complete set of specific analytes that were detected at P-164, including the mass extracted, are shown in Figure 25 below.
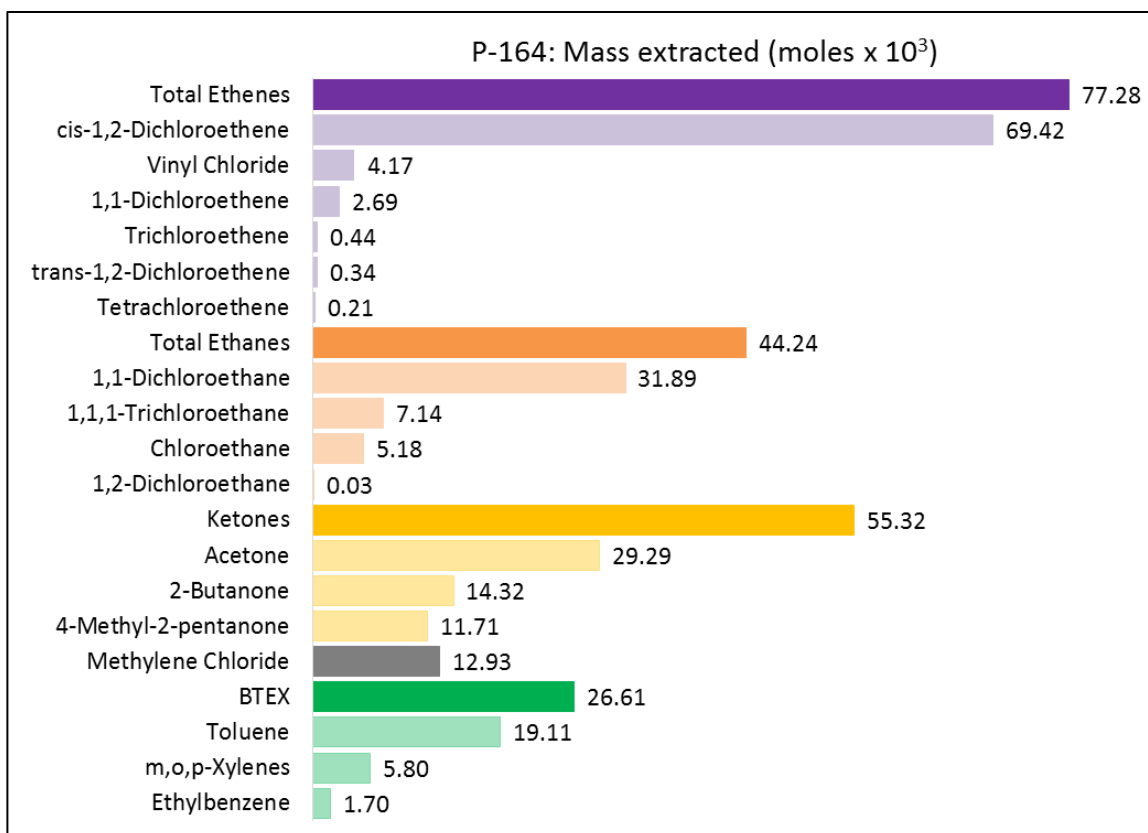
Figure 25: Overall mass and composition of 17 contaminants analysed from P-164.

Cis-DCE was the dominant VOC followed by 1,1-DCA, acetone and toluene. Together, they constitute 74% of the TVOC from the well since it commenced operation.

P-130, located further down-gradient at 1075m from the SZT had very different contaminant mass, composition and pumping conditions from P-164 (Figure 26). 99.5% of the total VOC mass that was extracted over the fourteen-year period constituted chlorinated ethenes and ethanes. Figure 27 shows a detailed breakdown of the individual contaminants analysed at P-130.
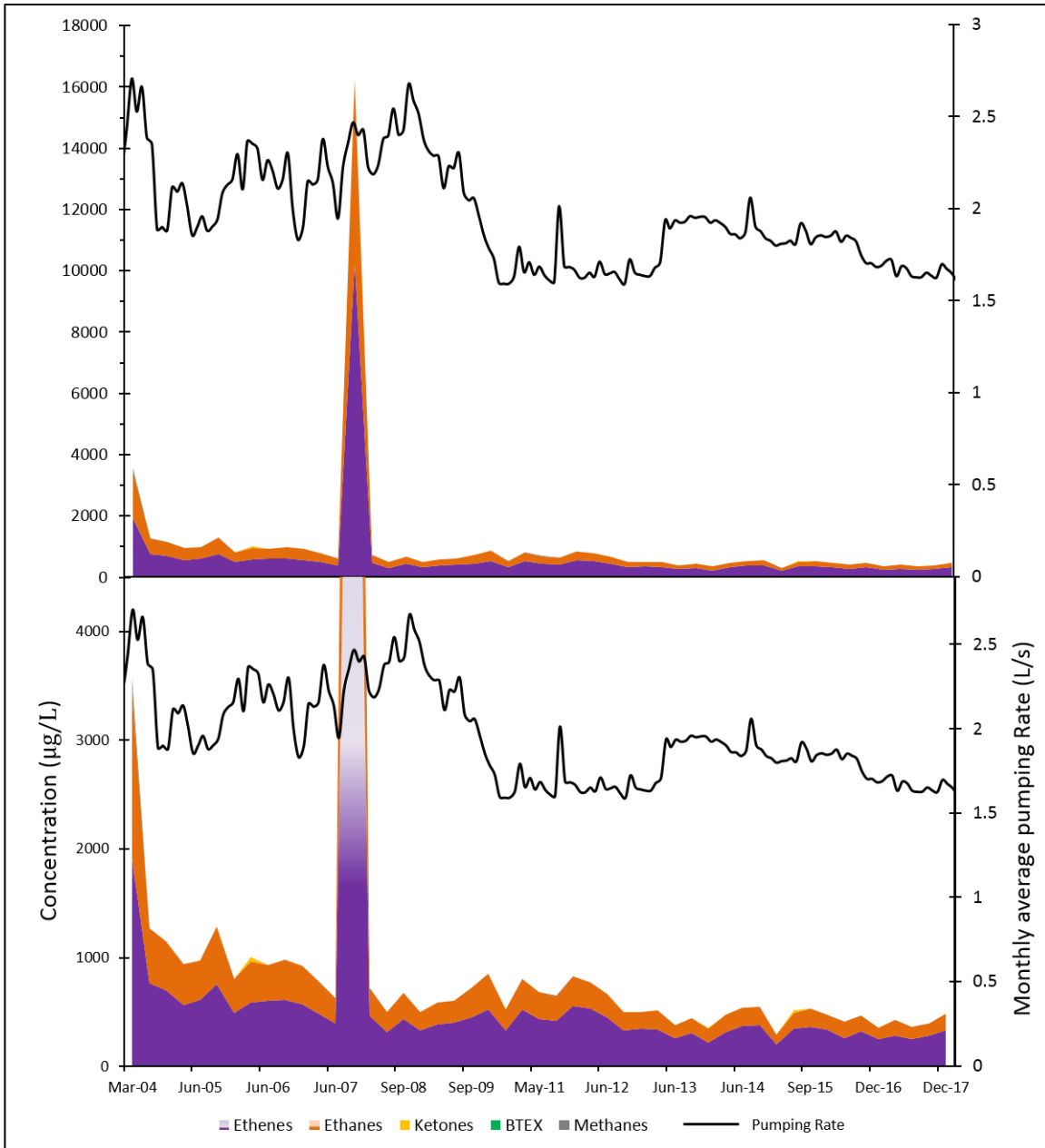
Figure 26: Time-series of the contaminant concentration and pumping rates at P-130.

The top section shows the time series with the outlier peak in 2004 while the bottom section is zoomed in to show the trend of the lower concentration points. The high concentration could have resulted from a high concentration slug within the plume that was within P-128's capture zone. Other alternatives are that groundwater flushing could have caused contaminants in hydraulically active fractures to flow to the well or the laboratory analysis method had much lower detection limits than that used in other samples or field contamination during sampling. A decreasing step trend is seen in January 2009 where the pumping rate decreased by 0.42L/s.

P-130: Mass extracted (moles x 10^3)

Total Ethenes	5.46
cis-1,2-Dichloroethene	4.93
1,1-Dichloroethene	0.27
Trichloroethene	0.17
trans-1,2-Dichloroethene	0.05
Tetrachloroethene	0.03
Vinyl Chloride	0.004
Total Ethanes	2.43
1,1,1-Trichloroethane	2.05
1,1-Dichloroethane	0.38
Ketones	0.02
2-Butanone	0.01
Acetone	0.01
Methylene Chloride	0.01
Toluene	0.004
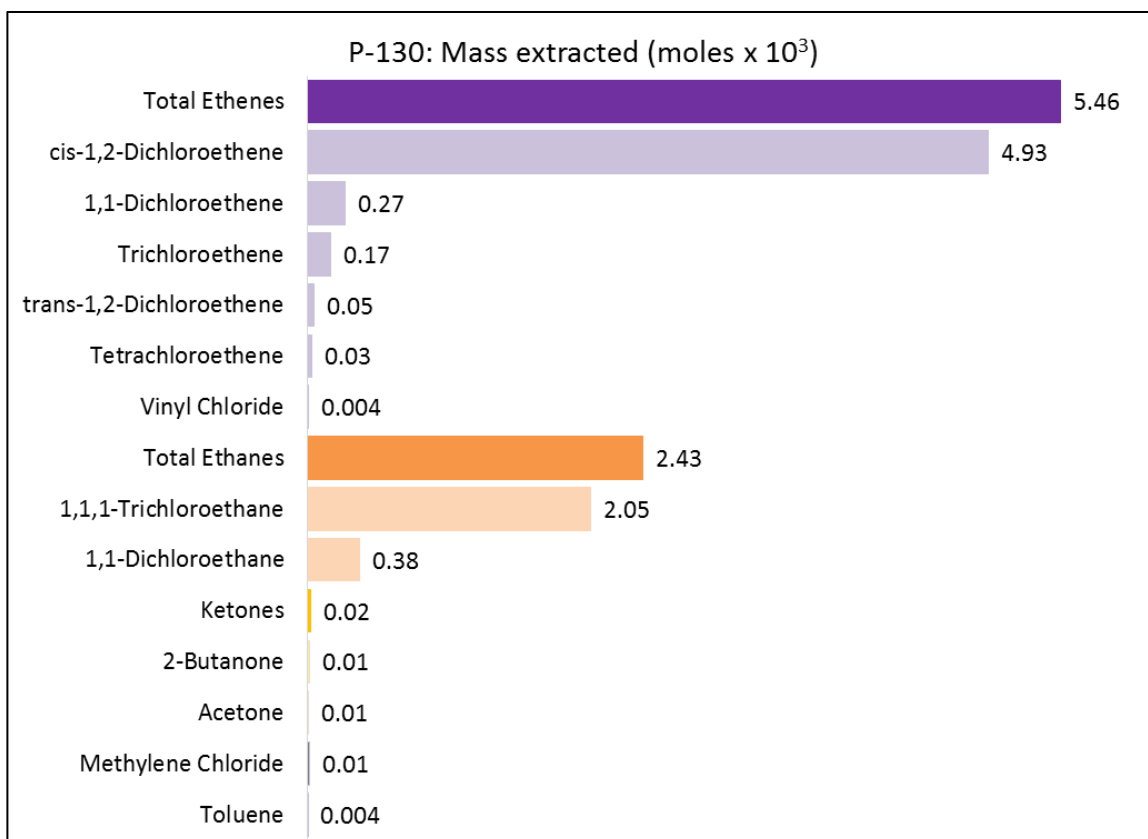
Figure 27: Overall mass and composition of 13 contaminants analysed from P-130.
Cis-DCE and TCA dominate the composition. This composition is very different from P-164 which contains the five contaminant groups in high concentrations.

The highest TVOC concentration of 3568 µg/L was detected in 2004. However, sampling results from Q3-2007 recorded an outlier TVOC concentration of 16 245 µg/L. Laboratory records show that this sample was analysed at a dilution factor of 100 compared to 2.5-10 in other sampling rounds. Such high dilution factors are typical for groundwater of high concentrations, such as the 2004 and 2005 samples. This means that it is likely that the laboratory was not a source of contamination. A hypothesis for the outlier could be that a high concentration slug was moving through the plume and was detected in that sampling round. Given that the average linear groundwater velocity at the site ranges between 1-2.8 m/day, a slug moving through the pumping well zone would not be detected 3 months later in other sampling rounds. This slug could have been moving from its source since the commencement of pumping over three years ago. The slug could alternatively have originated from the fractures upgradient that were plugged with the oily contaminant phase which later became hydraulically active. Time series analysis of the pumping rate at P-130 showed that a decreasing step trend exists between August 2004-January 2009 and January 2009-December 2017 (t-value of 13.52 > t_α 2.0 at a confidence of α=0.05). In the first period, the mean pumping rate was 2.22 L/s while in the second period, the mean pumping rate was 1.80 L/s, a decrease of 0.42 L/s.

P-128, at 1296 m from the SZT, is the furthest located pumping well. Due to its location, the concentration of contaminants extracted were much lower than at P-164 and P-130. In 2004, the concentration of TVOC was 5088 µg/L which decreased to 172.5 µg/L in September 2005 (Figure 28). It is interesting to note that, contrary to the decreasing trends observed at P-164 and P-130, the concentration at P-128 steadily increased between 2005 and 2017 to a local maximum of 519.3 µg/L in the last sampling campaign in December 2017.
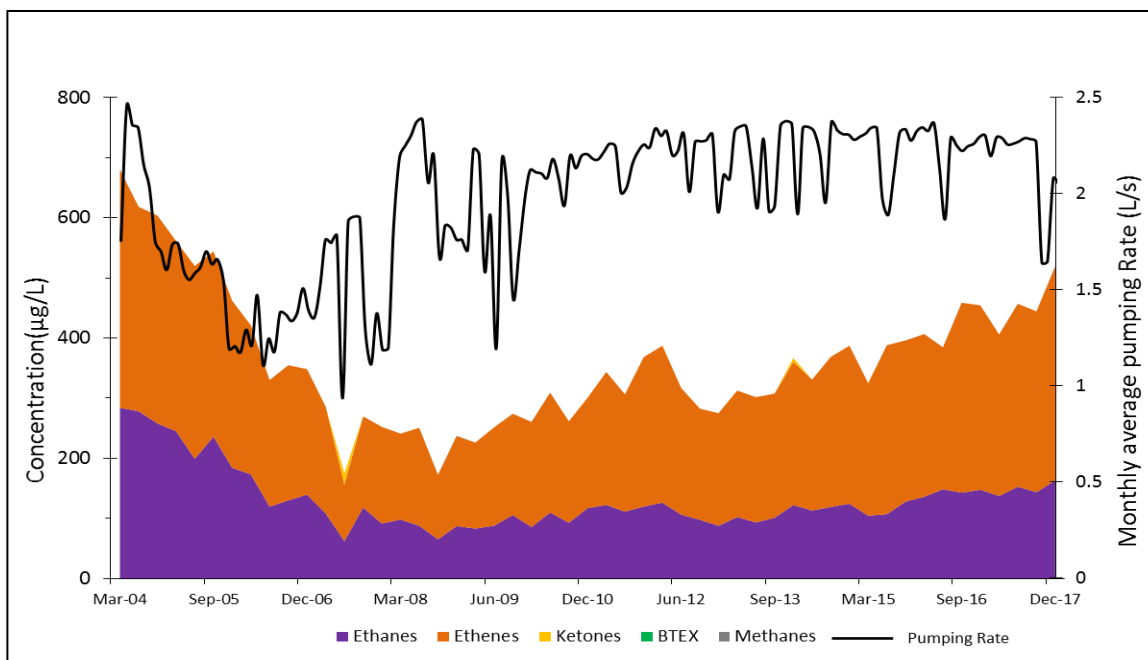
Figure 28: Time-series of the contaminant concentration and pumping rates at P-128

Of the five contaminant groups, chlorinated ethenes and ethanes constituted 92.7% of the total contaminant moles extracted. Figure 29 shows the mass and composition of all the individual VOCs that were analysed. Trend analysis of the pumping rate showed an increasing step trend between January 2004-March 2008 and March 2008-December 2017. The trend was significant at a 5% confidence level (t-value of 12.93 > tα 2.0). In the first period, the mean pumping rate was 1.58 L/s and in the second period, the mean pumping rate increased to 2.14 L/s. This increasing step trend plays a significant role in the analysis of mass discharge in section 6.2.
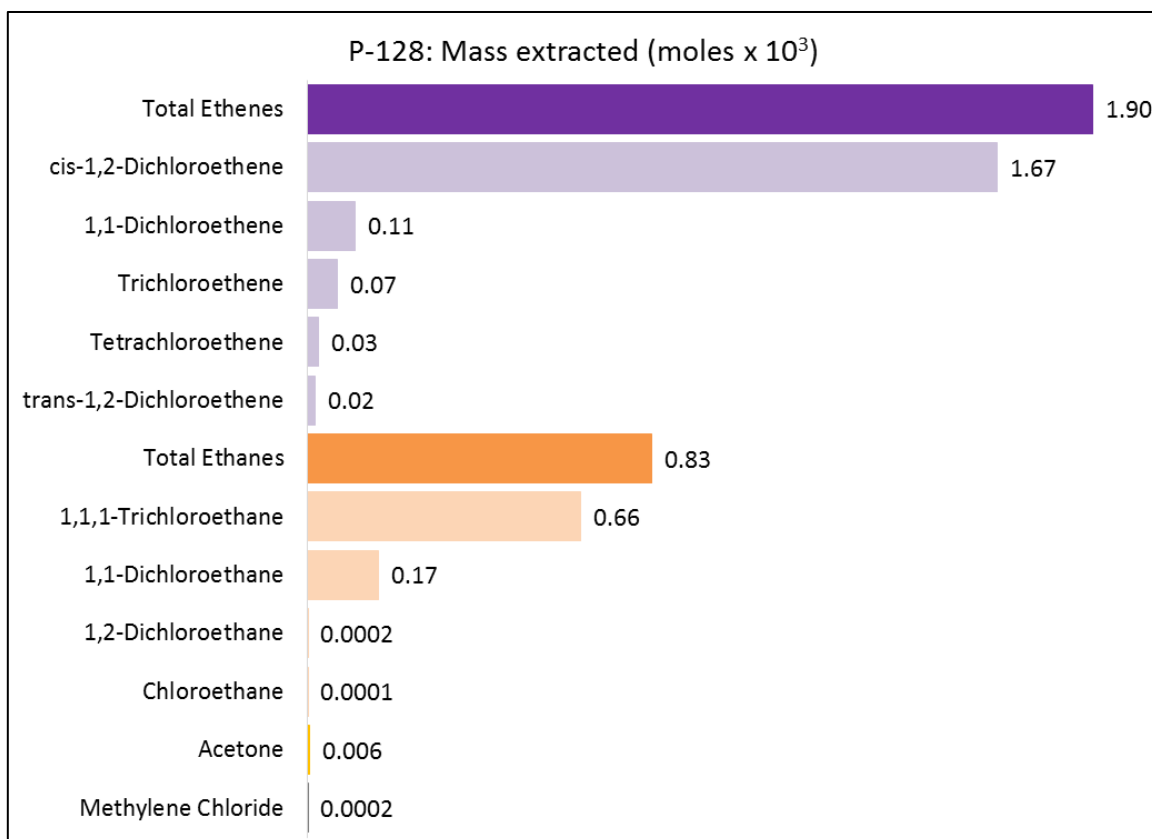
Figure 29: Overall mass and composition of 11 contaminants analysed at P-128.

Similar to P-130, cis-DCE and TCA were the primary constituents, making up 99.8% of the composition of extracted contaminants.

6   Discussion

6.1   Causes of the Source Zone VOC Declines

A key research objective of this study was to understand the processes responsible for the 83% mass decline observed at the three core holes as well as the composition changes of the analytes reported in section 5.1. Multiple lines of evidence were drawn to gain a deeper understanding on possible mechanisms occurring in the up-gradient source zone and the influence of the HBS on the contaminant changes observed in the SZT core holes. The key pillars for investigating source zone declines were: 1) the role of DNAPL composition on the effective solubility of VOCs and the effect on mass persistence patterns; 2) possible zones of back-diffusion processes from the low-permeability matrix into the fractures upon which groundwater transports the contaminants downgradient and 3) the influence of the pumping wells on source zone mass declines. Supporting evidence from previous studies on microbial-mediated natural attenuation mechanisms were also examined as they play a role in degrading contaminants *in situ* within the low permeability matrix to produce different by-products and secretions.

6.1.1   Variations in the Effective Solubility of the Oily-phase NAPL Components

Information on the composition of the original VOCs that were spilled at the site prior to 1970 is of central importance to understanding mass changes in the source zone. Effective solubility is useful in predicting the dissolution and mass distribution patterns of contaminants under the influence of flowing groundwater. This information can be used as one line of evidence to understand, and to an extent, explain the changes exhibited in the source zone. The hypothesis is that contaminants ranked as having very high effective solubility values will dissolve much faster than those with relatively low values which will tend to persist.

Researchers and consultants working at the site directly sampled the oily phase NAPL, hereafter referred to as "original NAPLs", in 1999 and in 2004 from two research wells (RW), RW-58 and RW-111, which are located inside the source zone. The sampling concentrations in mg/L were converted to mole fractions and are shown in Figure 30 below. Eleven compounds were detected at RW-111 and ten in RW-58; 1,1-DCA was not detected in the latter.
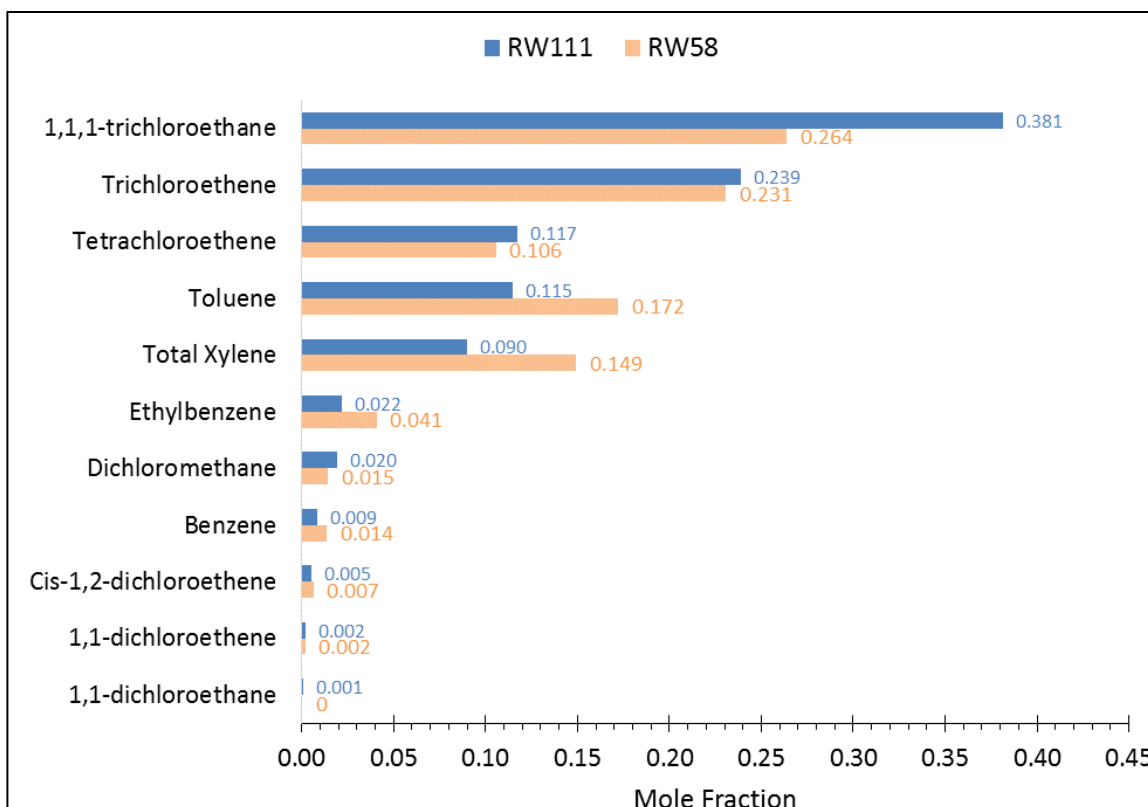
Figure 30: Original composition of the oily-phase VOC samples.

The results were obtained from two research wells inside the source zone. Both sampling results show similar contaminant composition and slight variations in the dominant mass. TCA, TCE, PCE, toluene and xylenes composed majority of the spill.

The above compounds were assumed to be representative of the original NAPLs that contaminated the site and were used to inform on the changes exhibited among VOC contaminant mass at MP-7, MP-24S and MP-24D. In order to understand the preferential dissolution and transport of each VOC, it is necessary to examine the aqueous solubility data that influences this process. The standard aqueous solubility values report the pure-phase solubility of organic nonelectrolytes in pure water. Pure phase solubility values can only be used for VOCs that contain a single NAPL component. For samples from a multi-component NAPL spill, such as that known to have occurred at this site, it is expected that each component will dissolve in water until an equilibrium between the dissolved phase and the NAPL phase is achieved. Consequently, instead of using the pure phase solubility, effective solubility is used. This is the solubility of a component in water that is evaluated by taking the product of its pure phase solubility and the mole fraction of that compound in the mixture (Pankow & Cherry, 1996). Effective solubility for the components in Figure 30 were calculated using the equation below and are displayed below:

$$S_e^i = \chi S_w^i$$

where (S_e^i) is the effective solubility of a component i in a NAPL mixture, (S_w^i) is the pure-phase solubility of a component i in pure water and χ is the mole fraction.

Table 9: Contaminants from the oily-phase NAPL ranked in descending order of effective solubility. Despite some VOCs having very high pure phase solubility, their low abundance as shown by the mole fractions cause their effective solubility to decrease.

Well ID	Analyte Name	Mole Fraction (χ)	Pure Phase Solubility S_w^i (mol/L)*	Effective Solubility S_e^i (mol/L)
RW111	Dichloromethane	0.02	2.31E-01	4.51E-03
	1,1,1-trichloroethane	0.381	9.73E-03	3.71E-03
	Trichloroethene	0.239	1.12E-02	2.67E-03
	Tetrachloroethene	0.117	9.05E-03	1.06E-03
	Toluene	0.115	5.75E-03	6.61E-04
	Benzene	0.009	2.29E-02	1.99E-04
	Cis-1,2-dichloroethene	0.005	3.61E-02	1.86E-04
	Total Xylene	0.09	1.00E-03	9.01E-05
	1,1-dichloroethene	0.002	2.50E-02	5.30E-05
	Ethylbenzene	0.022	1.58E-03	3.43E-05
	1,1-dichloroethane	0.001	5.11E-02	2.61E-05
RW58	Dichloromethane	0.015	2.31E-01	3.35E-03
	Trichloroethene	0.231	1.12E-02	2.59E-03
	1,1,1-trichloroethane	0.264	9.73E-03	2.57E-03
	Toluene	0.172	5.75E-03	9.91E-04
	Tetrachloroethene	0.106	9.05E-03	9.58E-04
	Benzene	0.014	2.29E-02	3.13E-04
	Cis-1,2-dichloroethene	0.007	3.61E-02	2.35E-04
	Total Xylene	0.149	1.00E-03	1.50E-04
	Ethylbenzene	0.041	1.58E-03	6.46E-05
	1,1-dichloroethene	0.002	2.50E-02	5.13E-05

* Pure phase solubility data obtained from The Handbook of Aqueous Solubility Data (Yalkowsky et al., 2010)

6.1.2   Back-Diffusion of VOCs from the Rock Matrix into the Fractures

Diffusion is recognised as the mechanism responsible for contaminant mass transfer from the fractures to the rock matrix (Parker et al., 2004; Sterling et al., 2005). In mature contaminated sites where most of the NAPL phase in the fractures has been dissolved by flowing groundwater, the concentration gradient changes which causes back-diffusion of the contaminants from the matrix to the fractures. To investigate whether back-diffusion could have contributed to the observed rock core contaminant mass declines,

concentration of groundwater sampled from the fractures in the core holes (C_{gw}) was compared to the hypothetical pore water concentration (C_{pw}) - the concentration of aqueous-phase contaminants in the rock matrix that would be in equilibrium with the groundwater in the adjacent fractures. This pore water concentration can be expressed as:

$$C_{pw}\left(\frac{mol}{L}\right) = C_t\left(\frac{mol}{g_{wet\ rock}}\right)\frac{\rho_{wb}\left(\frac{g_{wet\ rock}}{L}\right)}{R \times \theta_m}$$

where (C_t) is total concentration of the wet rock core, (ρ_{wb}) the wet-bulk density, (θ_m) the interconnected matrix porosity and (R) the retardation factor which is defined in Pankow & Cherry (1996) as:

$$R = 1 + \frac{\rho_{db}}{\theta_m}K_{oc}f_{oc}$$

where (ρ_{db}) is the dry-bulk density, (K_{oc}) is the organic carbon sorption coefficient and (f_{oc}) is the fraction of organic carbon.

The wet bulk density and matrix porosities shown in Table 10 were used to calculate the pore water concentrations for MP-24S and MP-7.

Table 10: Physical properties for the calculation of equivalent pore water concentration

Well ID	Stratigraphy	HGU	Average wet-bulk ρ_{wb} (g/cm3)	Matrix Porosity (Øm)
	Tonti	11	2.347	18.18%
	Readstown	11	2.535	18.18%
	Tunnel City	8	2.403	18.91%
MP-7	Tunnel City	7	2.446	18.91%
	Tunnel City	6	2.345	18.91%
	Tunnel City	5	2.441	12.66%
	Wonewoc	5	2.441	12.66%
MP-24S	Tonti	9	2.374	18.18%
	Readstown	8	2.403	18.91%

The values were derived from laboratory analysis performed on rock cores from either selected lithologies or hydrogeological units (HGUs, Meyer et al., 2016). Sorption of VOCs was assumed to be primarily governed by the solid-phase organic carbon content and very little by other aquifer solids such as oxides. Laboratory results for the f_{oc} were generally below the method detection limit (0.004-0.012%) and therefore, retardation of $R = 1$ was assumed (Austin, 2005). This conservative estimate means that, for the same physical properties, the calculated pore water concentration values will reflect the maximum possible value i.e. $C_{pw} = C_{pw,max}$. This comparison can serve as an indicator of the processes responsible for mass loss from the rock matrix. If $C_{pw} \geq C_{gw}$, the concentration gradient may act as a driving force for back-

diffusion mass transfer from the matrix to the fractures thereby suggesting a potential mechanism for the observed rock core mass loss. However, the inverse result ($C_{gw} \geq C_{pw}$) may not be enough to disqualify back-diffusion. This is because of various sources of error in comparing rock core pore water concentrations to the fracture groundwater concentrations which are listed below and discussed in detail later: 1) the rock core VOC data and groundwater concentration data were collected in different points in time; 2) the presence of fractures may cause blending of concentrations from groundwater at different sampling depths; and 3) the calculation steps has assumptions and simplifications in the parameter values. Therefore, unless big discrepancies are noted, it cannot be said with confidence whether pore water concentrations are greater than groundwater concentrations

Figure 31 below shows the comparison of rock core total VOC equivalent pore water concentrations to the groundwater concentrations sampled from depth-discrete MLS at both MP-7 and MP-24S. Groundwater was sampled in 2015 and in 2016 at MP-24S, allowing further analysis of the temporal variation of VOCs in groundwater and presents an opportunity to assess the ranges of this variability. The vertical changes in hydraulic head measured from the MLS are also displayed. The groundwater concentrations are generally higher than the rock core pore water concentrations by 0.5-1 order of magnitude with the exception of point A on MP-24S where the groundwater concentration was 3-4 orders of magnitude higher. In theory, the aqueous concentration of contaminants in the rock matrix and at adjacent fractures is expected to be at equilibrium due to concentration-driven mass transfer at the interface. The differences in groundwater and rock matrix aqueous concentration are close to equilibrium given that exact similar concentrations are difficult to achieve in a field setup due to a number of reasons enumerated below.

Rock core analyses provide point concentration values for the contaminants within the matrix while concentrations from groundwater fractures are subject to blending and cross-connection through other hydraulically active fractures within the zone. The average sampling interval within the MLS ports installed at MP-24S is 1.08m. Studies performed at the Hydrite site by Meyer (2005) showed that fracture intensity increased with depth and the fracture spacing was between 9.1 and 21.3 cm, with an average spacing of 15.2 cm. Therefore, the groundwater sampling interval contained as many as 12 fractures which could have acted as conduits for groundwater blending of different concentrations.
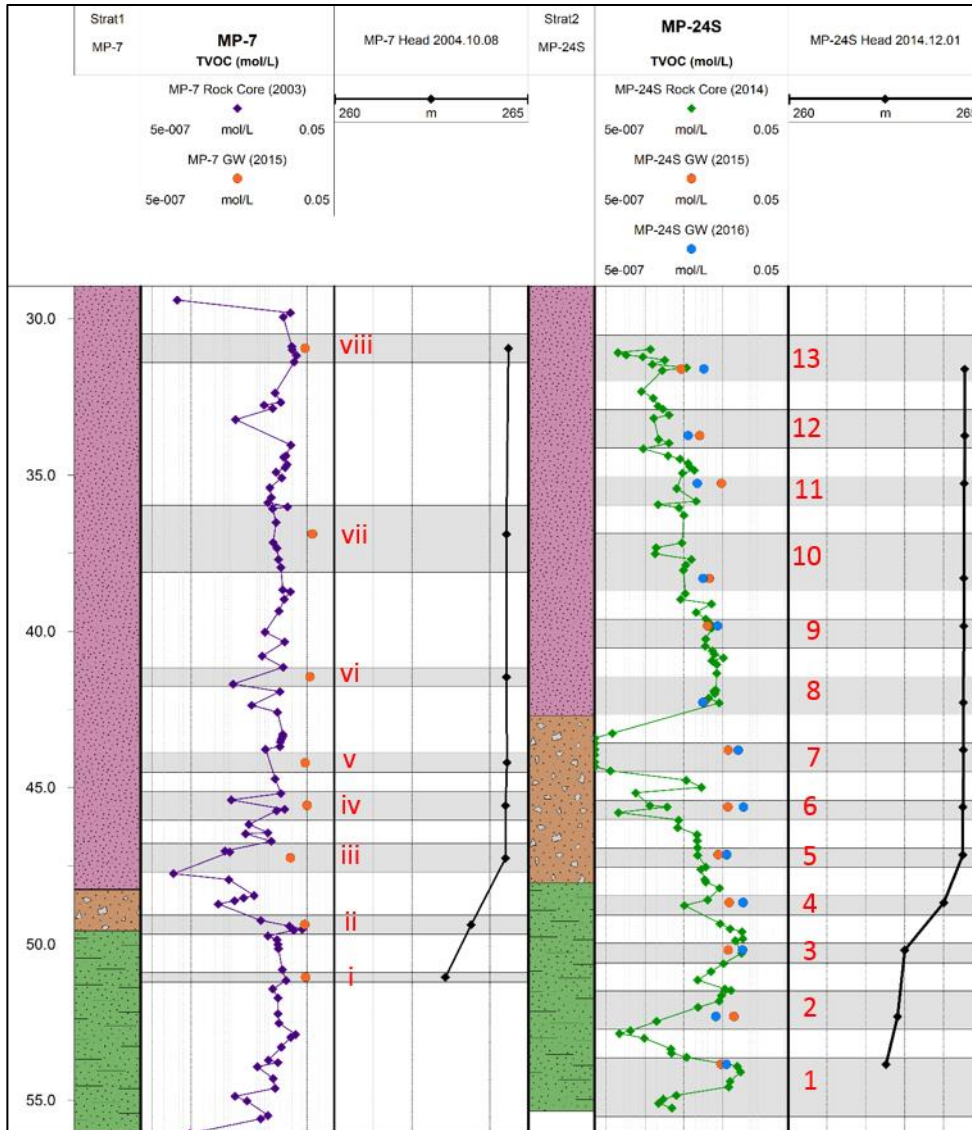
Figure 31: Comparison of groundwater and equivalent pore water concentrations.

Comparison is done for MP-7 and MP-24S on log-scale for total VOCs in mol/L. The hydraulic head profiles are shown beside the TVOC profiles. The grey boxes represent the interval over which groundwater samples are collected which corresponds to the length of the opening in the multilevel sampling ports. At MP-7, TVOC concentration in groundwater is roughly half an order of magnitude higher than the rock matrix pore water in all sections of the profile except port (ii) and (viii) where the groundwater and pore water TVOC concentrations are comparable. At MP-24S, groundwater and pore water concentrations have a much higher variation. At ports one, three, eight and nine, TVOC concentration in groundwater and pore water can be approximated to be in equilibrium while in the other nine ports, groundwater TVOC concentration is higher by roughly half an order of magnitude except in port 7 where TVOC concentration in groundwater is over three orders of magnitude higher than in the rock matrix pore water. Groundwater samples from 2015 and 2016 at MP-24S show slight variability in

concentration. Out of the thirteen ports, eight (ports one, three to seven, nine and thirteen) show that groundwater sampled in 2016 was at a higher concentration than the 2015 samples.

The vertical gradients in Figure 31 for both MP-7 and MP-24S show potential for downward flow of groundwater, which is especially strong in the lower Tonti, Readstown and Lone Rock formations (48-51 mbgs). This downward gradient may induce flow leading to possible blending of fracture-water over the open monitoring intervals shown by the grey boxes, compared to the rock core pore water concentrations which represent point variability. However, it is important to note that the component of downward flow is small compared to the bulk lateral groundwater flow in these formations and locations. Therefore, the groundwater samples should therefore be used as a proxy to assess whether forward or back diffusion processes are occurring and should be assessed with some caution. A check was performed to ascertain whether the 2015 and 2016 sampling rounds were statistically different before examining the differences in the results. The variance of TVOC concentration between 2015 and 2016 was found to be unequal (F 4.97 > F critical one tail 2.69 at α of 0.05) and a two-tail t-test rejected the null hypothesis ($\mu_{2016} = \mu_{2015}$) showing that the mean of the 2015 and 2016 sampling results are statistically significant (t 1.18 < t critical two-tail 2.11 at α of 0.05). Most of the ports where 2016 groundwater sampling results were greater than 2015 results are located in the lower bedrock units. This was expected because most of the rock matrix mass loss between 2014 and 2017 occurred in the lower formation (see Table 4). In the upper bedrock, rock matrix concentrations reduced to non-detect between 2003 and 2014. It was therefore expected that in the upper bedrock, the groundwater sampled in 2016 had lower concentration than the 2015 results.

Figure 32 below shows MP-24S rock core TVOC profile, the 2015 and 2016 sampling results displayed as vertical bars and the horizontal bars representing the range between the two sampling campaigns (Figure 31 above shows the variation between 2015 and 2016 groundwater samples). In zones 1 and 3 which were shown to have the highest declines in rock core TVOC mass, the groundwater concentrations are higher than the rock core pore water concentrations whereas in zones 2 and 4 where contaminant mass was observed to persistent or slowly decline, the groundwater concentrations are within the same range as the rock pore water concentrations.
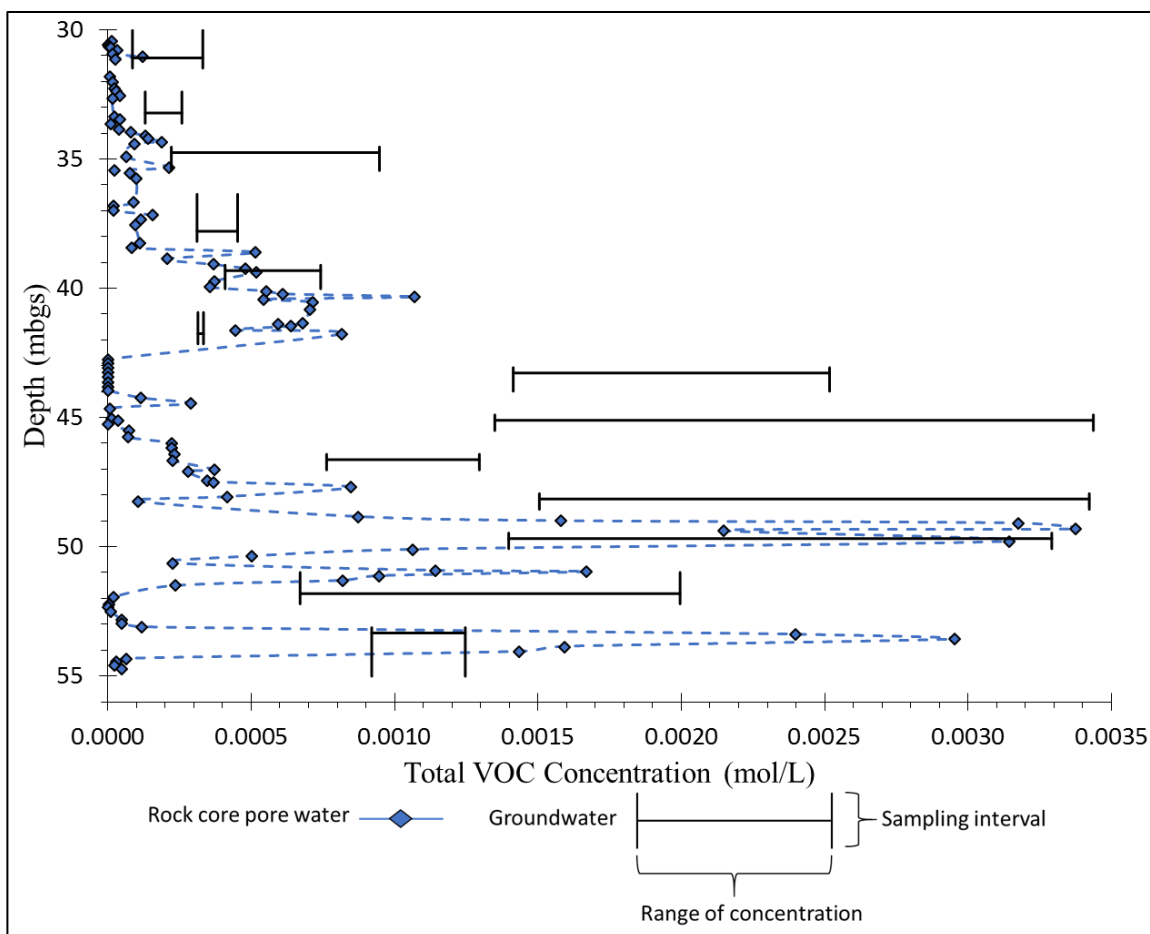
Figure 32: Rock-core pore water and groundwater concentrations.

The comparison shows total rock core VOC concentration at MP-24S compared with groundwater concentrations sampled in 2015 and 2016 from a multi-level system with 13 ports.

One hypothesis for the differences in groundwater concentrations with depth is that of preferential zones of molecular back-diffusion. Prior to 2003, the water in the fractures was laden with contaminants leading to molecular diffusion into the rock matrix throughout the profile (Parker et al., 2010; Parker et al., 1994). The fact that the MP-7 profile showed very comparable mass distribution among the four zones bolsters this hypothesis (see Table 4). After 2003, when the HBS came online, pumping increased groundwater flushing which caused contaminants in the fractures to decline. This observed decline was variable: faster declines in more hydraulically active fractures and less in the fractures that have either healed or are not interconnected with the local groundwater flow system such that the pumping has had a less pronounced effect. Over time, the concentration of contaminants in the fracture-water declined, shifting the concentration gradient which caused back-diffusion of VOCs that resided in the rock-matrix pore water. Most of the back-diffusion occurred in zones 1 and 3 which would explain why the mass in these zones declined by 99% and 96% respectively between 2003 and 2017; from quantifiable to non-detect concentrations. In these zones, the 2015 and 2016 groundwater sampling results are higher than in the

matrix, showing that back-diffusion is no longer a dominant process. In zones 2 and 4, most sections of the profile display either an equilibrium of contaminant concentration between groundwater and matrix pore water or higher concentrations in the rock matrix, alluding to the possibility of ongoing back-diffusion processes. This could explain why most of the mass decline occurred in these zones between 2014 and 2017. These groundwater results are evidence that back-diffusion from the rock matrix in the lower bedrock (upper portion of the Tunnel City group, 49-55m bgs) to the fractures is currently occurring. This process may be partly responsible for the mass loss observed in MP-24S and MP-24D.

In general, higher VOC concentrations in fracture groundwater compared to adjacent rock matrix pore water is meant to serve as one line of evidence for the possibility of back-diffusion. However, significantly high groundwater concentrations could represent upgradient sources of origin rather than represent groundwater adjacent to the rock matrix. For instance, higher groundwater concentrations could indicate that NAPL-phase is likely present upgradient where it is being dissolved and transported downgradient and detected at high concentrations in the multilevel systems. Higher groundwater concentrations compared to matrix pore water could also be because the downgradient pumping wells are inducing groundwater flushing from the source zone where concentration of contaminants is highest. This groundwater of high concentration could be detected by the multilevel wells downgradient. In summary, this comparison is very useful in understanding back-diffusion sources but other competing mechanisms should be appreciated and examined in order to make sure that the right conclusions are drawn.

6.1.3 Possible Causes of Mass Changes in Individual Contaminants

Changes within each of the five contaminant groups were analysed to understand feasible process contributing to the observed source-zone declines. The contaminant groups ranked in descending order based on the observed source zone declines of that group across time are: chlorinated methanes (99%), chlorinated ethenes (95%), chlorinated ethanes (89%), BTEX (77%) and ketones (42%).

Chlorinated methanes declined by 99% between MP-7 and MP-24D - the highest overall decline among the five contaminant groups. Of all the chlorinated methanes, DCM was the only quantifiable analyte. The other constituents (bromodichloromethane, chloroform, chloromethane, dibromochloromethane, bromomethane and chlorodibromomethane) had non-detect concentrations and were not examined. The mole fraction of DCM in the original NAPL at both RW-58 and RW-111 was very low; an average of 1.5 and 2% of the total VOCs respectively. It is therefore interesting to note that despite this low concentration, DCM composed 48% of the contaminant mass at MP-7 in 2003. However, amongst all analytes in the original VOCs, the effective solubility of DCM in groundwater is the highest. A hypothesis is that groundwater in the fractures dissolved and transported DCM at a faster rate down-gradient of the source zone. As fracture-water got saturated with DCM, the concentration gradient favoured molecular diffusion of aqueous DCM from the fractures into the adjacent low-permeability matrix. This migration could explain the high DCM accumulation in MP-7 (48.3%, see Table 3). Between 2003 and 2017, most of the DCM from the source zone could have been dissolved and transported into the down-gradient plume or degraded by

autochthonous bacterial communities or a combination of both. Studies performed by Lima et al in 2012 at this study site showed the presence of bacterial communities residing in the rock matrix. Of the microbes reported, *Acetobacterium* and *Pseudomonas* have been observed at the site and are capable of degrading DCM (Wright et al., 2017). *Acetobacterium* correlates strongly with high DCM concentrations and has been shown to thrive in cultures of DCM (Magli et al., 1995). These two colonies are a likely candidate for attenuating the DCM mass. DCM could also have been used as an electron donor by *Methylophilus* (Lima et al., 2012) for the dechlorination of PCE and TCE, especially at such a site where the contaminants are comingled. DCM mass residing in the low-permeability matrix could also have back-diffused into the fracture-water especially under pumping conditions from the closest well, P-164. The increased the rate of groundwater flushing may have increased the concentration gradient between the matrix and the fractures, enhancing the mass decline observed at the core holes. DCM degradation can also occur in the groundwater fractures along the flow path from the source zone to the downgradient plume (Lima et al., 2012).

Chlorinated ethenes recorded an overall decline of 95% between MP-7 and MP-24D. The analytes in this group are PCE, TCE, cis-DCE, 1,1-DCE and VC. The original NAPL composition results showed the presence of TCE, PCE, cis-DCE and 1,1-DCE at an average % mole fraction of 23.5, 11.2, 0.6 and 0.2 respectively. VC was not detected in the NAPL samples. In the core samples from MP-7, cis-DCE was the dominant chloroethene despite its low mole fraction in the original NAPL. A combination of various mechanisms may have been responsible for this result. The effective solubility of PCE and TCE in the NAPL is approximately ten times higher than that of cis-DCE. These two compounds were dissolved by flowing groundwater and transported to down-gradient locations where they eventually diffused into low permeability matrix. Active solvent-tolerant microbes that thrive in the matrix degraded PCE and TCE, transforming them into cis-DCE, a daughter product of anaerobic reductive dechlorination. This process involves the sequential replacement of a chlorine atom from higher to lower molecular weight chloroethenes and tends to occur more readily in higher chlorinated compounds (EPA, 2000; Pankow et al., 1996). The concentration of PCE and TCE between 2003 and 2017 reduced to non-detect in most sections of the profile, showing evidence of microbial action. That 1,1-DCE did not show drastic mass increase compared to the cis-isomer could indicate that the microbial cultures preferentially produce cis-DCE from respiration of TCE (Miller et al., 1997). The cis-DCE produced from reductive dechlorination of PCE and TCE in addition to the cis-DCE that was originally present in the NAPL could have contributed to the high detections at MP-7. However, there are likely to be other controlling mechanisms that contribute to cis-DCE's relative abundance in all three pumping wells down-gradient than can be accounted for by the above processes. VC was not detected in the original NAPL and the concentrations were non-detect at MP-7. However, both MP-24S and MP-24D display increasing trends. A probable reason is that once most of the PCE and TCE was reduced to cis-DCE, microbial colonies began reducing the cis-DCE to VC. Studies have shown that the reductive dechlorination of PCE and TCE occurs more readily than dechlorination of less chlorinated compounds and this could help explain the degradation time lag (EPA, 2000).

The main chlorinated ethane in the original NAPL was TCA which constituted 38 and 26% of the mole fraction at RW-111 and RW-58 respectively. At the down-gradient core holes, TCA, 1,1-DCA and 1,2-DCA were the major constituents and comprised 5% of the TVOC at MP-7. The three analytes reduced in mass compared to MP-24S and MP-24D results. Chloroethane (CA) was non-detect in MP-7 but was detected in MP-24S and MP-24D where it became the dominant chlorinated ethane. The effective solubility of TCA was amongst the highest in the original NAPL which may have led to faster dissolution and transport down-gradient and through molecular diffusion, it accumulated in the low-permeability matrix. Microbial consortia are likely to have degraded TCA and 1,1-DCA to CA, which would explain its increase in mass over time.

BTEX compounds are very persistent owing to their high sorptive capacity and very low solubility, relative to other VOCs. Measurements of the fraction of organic carbon (f_{oc}) at this site by Lima et al. (2012) showed that out of the 120m of rock matrix tested from nine formation sections, five yielded non-detect f_{oc}(%) while four had f_{oc} ranging from 0.010-0.015%. Due to the very low f_{oc}, it is likely that the low solubility is a more controlling process compared to sorption. Despite benzene being present in the original NAPL and having an effective solubility comparable to the other three compounds, it was non-detect in all three core holes. Of the BTEX compounds, toluene had the highest presence in the original NAPL which could explain its high presence in MP-7. Toluene also recorded the fastest declines within the BTEX group compared to MP-24S and MP-24D samples. This could be because toluene acted as an electron donor (reductant) in the anaerobic reductive dechlorination of TCE, cis-DCE and VC in groundwater (McCarty et al.,1998).

Tests conducted at RW-58 and RW-111 did not show any ketones present in the NAPL. However, at all three core holes, MEK and MIBK are not only present but they account for 80% of the TVOC at MP-24D core hole. In the 170 samples analysed for MEK at MP-7, 99% were reported as field blank contaminated. None of the samples from MP-24S were contaminated but 7% of 278 samples were field blank contaminated at MP-24D. Due to this fluctuation in MEK contamination from field processes, it is difficult to fully ascertain the integrity of the MEK samples. However, if MEK was indeed present at the locations, two suggestions are put forward to account for the presence and the subsequent temporal increase in the mass of MEK. The first is that microbial communities use toluene as an electron donor to dechlorinate TCE, cis-DCE and VC can convert some of the organic matter in the aquifer to MEK. Fowler et al. (2011) elucidated this possibility by examining four sites under active remediation where acetone and MEK were noted to increase in the groundwater. One of the main conclusions of the study was that some microbial communities secrete acetone and MEK as metabolic intermediates especially in the absence of methanogenic conditions. However, very scarce research has been published on ketones in contaminated aquifers and the corresponding microbes that secrete them. The second possibility for the increase in the mass of MEK is that there may be another source zone nearby whose spill contained copious amounts of MEK. This theory is feasible given that the exact NAPL spill components, locations and times are not well documented or understood. If another source zone exists, it could be responsible for the ketones observed at MP-24S and MP-24D.

6.2   *Comparison of the Source Zone to the Downgradient Pumping Wells*

The second key research question was to investigate how the mass and composition changes within the source zone compare to that captured by downgradient pumping wells. To answer this question, mass flux and mass discharge comparisons have been identified from literature as a good candidate for this evaluation and have been applied at various source and plume scales (e.g Einarson & Mackay, 2001; Guilbeault et al., 2005; C J Newell et al., 2003). The transect method was used to estimate the mass flux across the SZT using a similar approach to those suggested by Guilbeault et al. (2005) and Ricker (2008). Three principal steps were followed to calculate the mass flux. The first step was characterizing the plume concentrations with depth across the SZT. Rock core VOC samples collected in 2014 from five shallow wells (MP-22S, MP-23S, MP-24S, MP-25S and MP-26S) were used to determine the two-dimensional (2-D) distribution of contaminant concentration. These five core holes were drilled approximately eighty meters downgradient of the source zone and perpendicular to the general groundwater flow direction (west to east). From each location, over 100 data points were sampled from the rock matrix in the shallow bedrock ranging from 18-61m bgs, with an average sampling rate of 4 samples per meter. The concentration data was interpolated in between the core holes and the result is shown below in Figure 33.
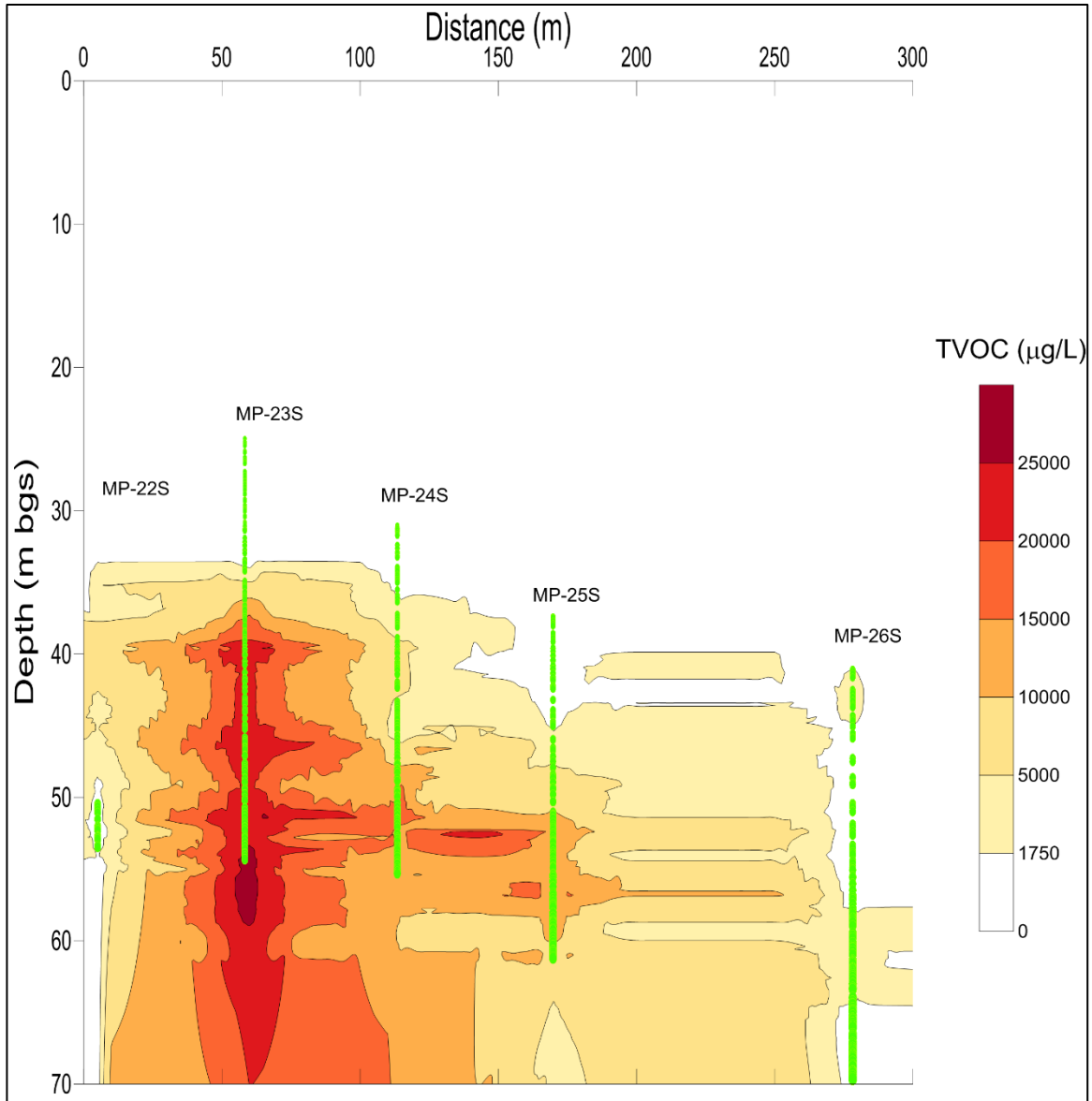
Figure 33: Contour map of concentration data from the shallow cores in the source zone transect.
The green points show the points where samples were collected from. The highest concentration is seen between 40-60 mbgs at a distance of 45-55m from the start of the transect. This zone corresponds to the formation where majority of the contaminants are known to reside from where they serve as a fuel for the plume's persistence. Further away from MP-23S and MP-24S, the groundwater concentration declines and is less than 1750 µg/L at MP-26S and at MP-22S. The zone between 0 and 30m bgs was assumed to have no observable or significant concentrations of TVOC.

The second step involved characterisation of groundwater flow to obtain the horizontal bulk hydraulic conductivity, K_h, and hydraulic gradient, *i*, which would enable calculation of the Darcy flux (q) through each hydrogeological or geologic unit of the source zone. Three of the shallow wells (MP-23S, MP-24S and MP-

25S) were hydraulically characterised in 2017 by researchers at the site (B. Parker et al., 2018). Transmissivity of pre-identified sections was determined using straddle packers which are useful in isolating test intervals, especially in fractured rock sites where transmissivity can vary by large magnitudes over short intervals (Quinn et al., 2012). The three types of transmissivity tests conducted at each test interval were pneumatic slug tests (rising head test and falling head test), constant head step injection test and constant rate pumping and recovery test. The tested zones corresponded to specific geological formations or hydrogeological units (HGUs) that were delineated during previous site investigations. Transmissivity values were divided by the interval over which the test occurred in order to obtain the K_h values at each cored location. Each of these K_h values were grouped into the geology and/or HGUs corresponding to the test interval. Finally, across all three locations, the K_h values from similar geological and/or HGUs were examined. The results are shown below in Table 11. The range of K_h values varied depending on the test interval: K_h values from the upper bedrock units (Tonti, Readstown and Prairie du Chien) varied by one to two orders of magnitude whereas the deeper units (St. Lawrence and Tunnel City) registered larger K_h variations of up to four orders of magnitude. However, given that these are averaged values for each formation from the three test locations, such variations have been noted at previous site investigations. The arithmetic and geometric mean varied by a maximum of one order of magnitude in all formations. For the purposes of calculating the Darcy flux, the geometric mean was selected. Casado (2012) and Meyer (2005) calculated the magnitude of the horizontal hydraulic head gradient for the shallow and deeper bedrock formations at this site respectively. They garnered hydraulic gradients information using two methods: the first involved determining the equation of a water table plane and fitting the plane to measured hydraulic head data (Devlin, 2003) and the other method utilised a three-point estimator using water level data to obtain a series of plots that provided hydraulic gradient values (Silliman and Frost, 1998). Through these methods, the researchers settled on 6×10^{-3} and 4.3×10^{-4} cm/cm for the shallow sediments and deeper bedrock respectively.

Table 11: Variations in the hydraulic conductivity for different formations within the source zone transect

Formation/Unit	Test Interval (mbgs)		Horizontal Bulk Hydraulic Conductivity, K_h (m/s)			
	From	To	Maximum	Minimum	Arithmetic Mean	Geometric Mean
Tonti	30.66	46.33	4.76×10^{-4}	1.56×10^{-6}	1.28×10^{-4}	5.00×10^{-5}
Readstown	38.41	46.76	6.07×10^{-6}	2.63×10^{-7}	2.65×10^{-6}	1.87×10^{-6}
Prairie du Chien	32.90	41.10	7.06×10^{-5}	3.61×10^{-7}	1.08×10^{-5}	1.39×10^{-6}
St. Lawrence	41.34	47.59	2.71×10^{-4}	4.10×10^{-8}	7.45×10^{-5}	1.08×10^{-5}
Tunnel City	47.65	55.64	2.87×10^{-4}	1.56×10^{-7}	5.33×10^{-5}	3.67×10^{-6}
HGU 11	30.66	51.31	4.76×10^{-4}	3.04×10^{-8}	5.85×10^{-5}	6.14×10^{-6}
HGU 8	49.38	52.85	9.84×10^{-6}	3.69×10^{-7}	4.20×10^{-6}	2.05×10^{-6}
HGU 9	48.34	54.37	1.36×10^{-5}	4.02×10^{-7}	4.50×10^{-6}	2.35×10^{-6}

The third and final step involved identifying and calculating the 2-D plane of the SZT whose area contributes to mass flux. The rock core data provided the point variability of contaminant concentration. Each sampled point was assumed to have an area of influence whose vertical length was equal to half the distance between the upper and lower sample. The horizontal length was approximated to be equal to half the distance between the sampling locations along the transect that spanned 273.18m between MP-22S and MP-26S.

The cumulative mass flux across the SZT was calculated according to the method listed in ITRC (2010) modified as shown below:

$$M_f = \sum_{j=1}^{n} C_j K_{h,j} i_j A_j CF$$

where M_f is the cumulative mass flux in g/s, j is the grid number in the SZT, C_j is the concentration in g/L, $K_{h,j}$ is the horizontal bulk hydraulic conductivity of grid j in cm/s, i is the hydraulic gradient, A is the area of the grid in cm^2 and CF the conversion factor of 10^{-3} L/cm^3. The point mass flux from each of the shallow core locations is shown below in Table 12.

Table 12: Total mass flux per area of core at each core location.

MP-23S had the highest point mass flux of the five shallow core locations while MP-22S had the lowest. The difference in mass flux was five orders of magnitude.

Core hole	Depth (m)		$\sum$ Point Mass Flux per core sample $*$ ($\mu g/s/m^2$)	Distance along Transect (m)
	From	To		
MP22S	18.18	54.74	2.00×10^{-4}	5
MP23S	25.07	54.42	4.45×10^{1}	58.34
MP24S	30.46	54.73	2.10×10^{1}	113.43
MP25S	31.48	57.71	5.18×10^{0}	169.77
MP26S	33.47	61.7	2.14×10^{0}	278.18

Given that the rock core data provided point variability of contaminant mass flux, interpolation of the data was required to obtain area A and thus the total mass flux across the entire SZT. Two methods were used to interpolate the data. In the first method, each sampled point was assumed to have an area of influence whose vertical length was equal to half the distance between the upper and lower sample and the horizontal length was approximated to be equal to half the distance between the sampling locations along the transect that spanned 273.18m between MP-22S and MP-26S. The second method used kriging of the point data both vertically and horizontally to obtain the point mass flux per area at each point on the entire transect on SURFER (Figure 34). To translate this into mass flux, an area was required. SURFER offers

an option to calculate the total volume of gridded data following the process described by Ricker (2008). This volume is equal to the total mass flux $\left(\frac{\mu g}{s\,m^2} \times m^2 = \frac{\mu g}{s}\right)$.
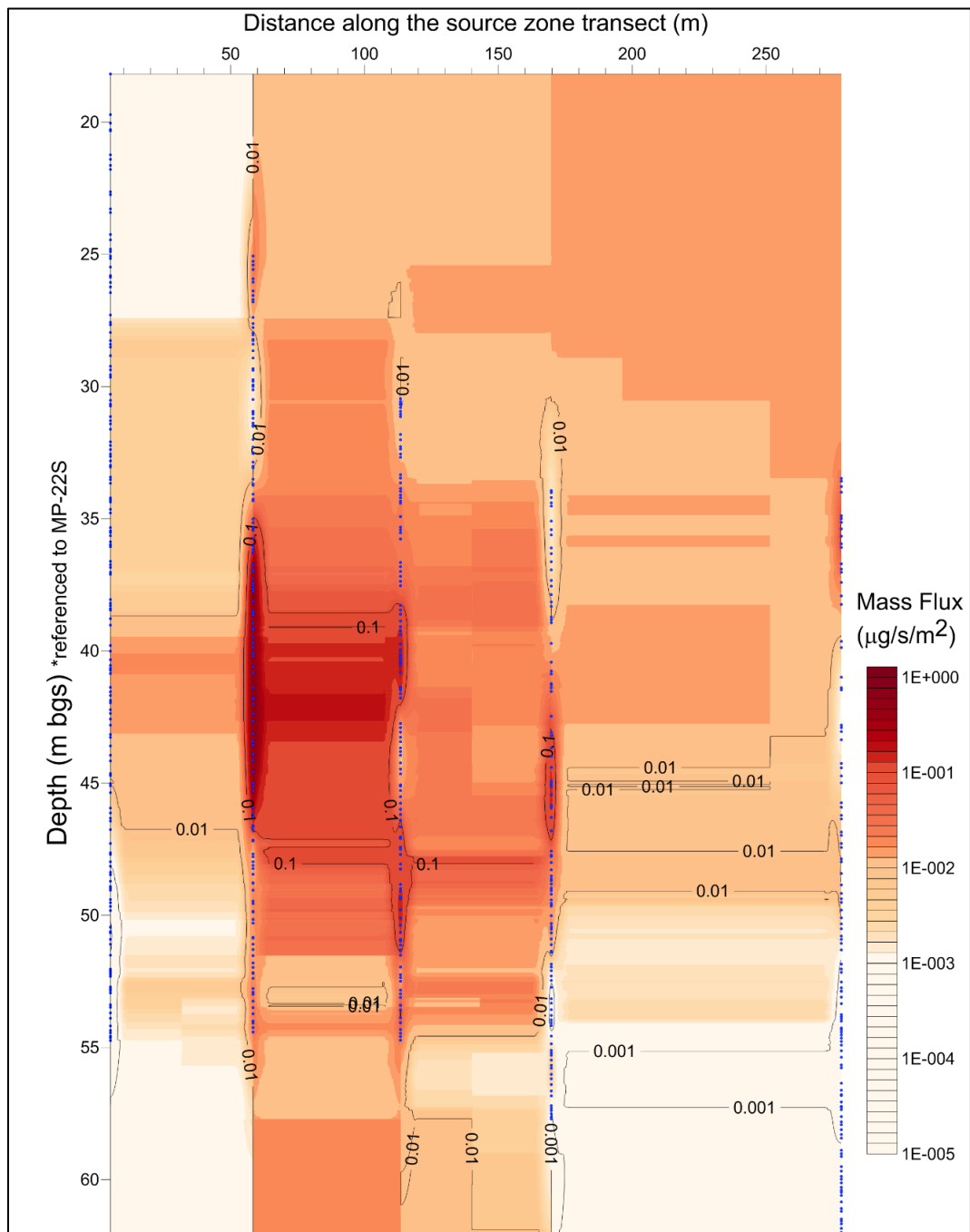

Figure 34: Interpolated mass flux across the SZT.
The blue dots represent the rock core samples from which point mass flux was calculated and then interpolated. The contours generally agree with site observations. Mass flux is lowest close to MP-22S and highest at MP-23S and MP-24S especially between 35 and 45m bgs.

Upon interpolating across the entire SZT using the first method, the total mass flux was found to be 997.42 µg/s. The second method yielded 332.77 µg/s. It is likely that the first method overestimated the mass flux given the half distance interpolation method. The second method is likely to be more accurate but errors in the interpolation could have underestimated this error. However, both values are within an order of magnitude difference which is acceptable given that parameters of hydraulic conductivity and concentration vary by more than two or three orders of magnitude over short intervals. Therefore, the mass flux from the source zone can be said to lie within the range of 332.77 and 997.42 µg/s. This value was assumed to represent the mass flux in 2014 when the "S" wells were cored.

The calculated mass flux from the source zone was used to estimate the maximum concentration of the pumping wells using the approach discussed by Einarson & Mackay (2001) and presented in the equation below:

$$C = \frac{M_d}{Q_{avg}}$$

where M_d is the mass discharge in g/s, C is the concentration of the contaminants sampled from the wells in g/L and Q_{avg} is the monthly average pumping rate in L/s.

In their publication, the authors used a mass balance approach to predict the maximum concentration of the contaminants that could occur in downgradient wells. The assumption underlying this comparison is that the mass flux from the source zone is equal to the maximum mass discharge observed at the downgradient wells. A similar approach was utilised to compare the mass flux and discharge. The observed TVOC concentrations sampled from the wells was combined with the monthly average pumping rates to obtain the mass discharge from the pumping wells. This value was then compared to that from the source zone.

The groundwater samples from the pumping wells were collected every quarter, except in a few instances where sampling did not take place. Given that the pumping schedule was frequently interrupted and the pumping durations irregularly monitored, the monthly average pumping rate was seen as a better representative value than daily pumping rates. The mass discharge from the pumping wells are shown in Figure 35 and Figure 36. A comparison between the mass flux and mass discharge is shown in Figure 37.
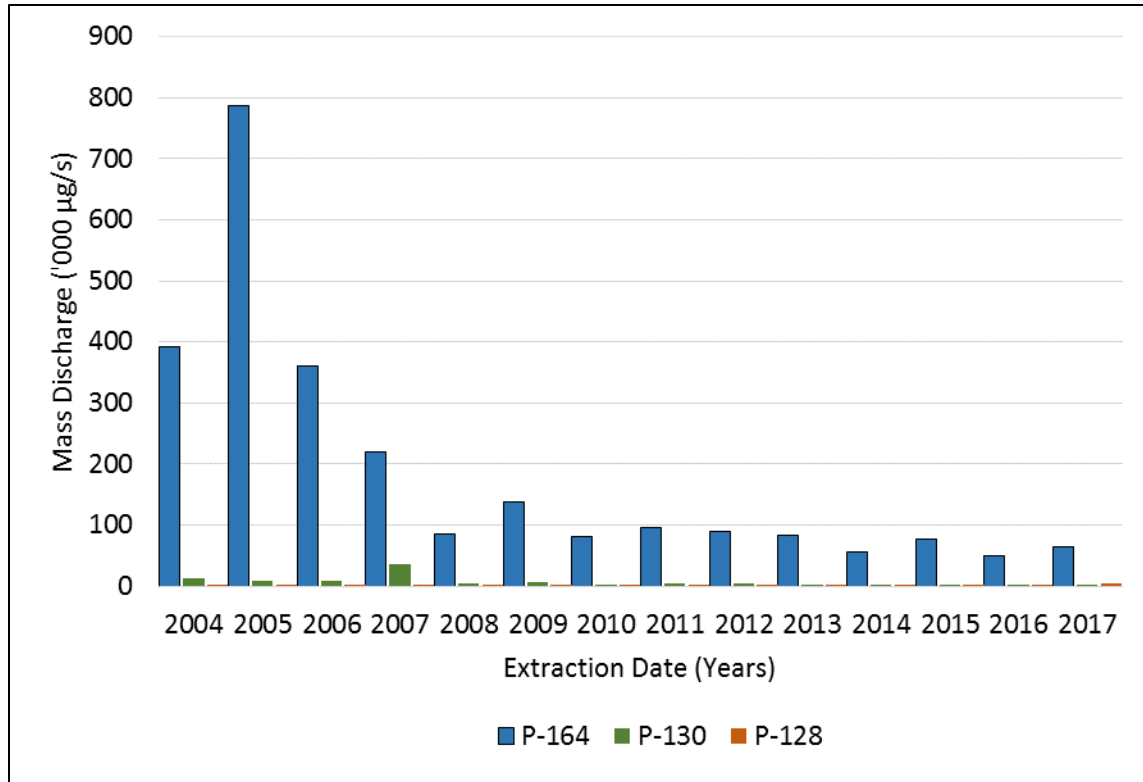
Figure 35: Mass discharge from the HBS.

Since the beginning of operation, mass discharge at P-164 has consistently been higher than the other two pumping wells. Over time, the mass discharge has declined due to a reduction in the concentration of contaminants. P-130 and P-128 that are further downgradient have a mass discharge that is an order of magnitude lower compared to P-164.
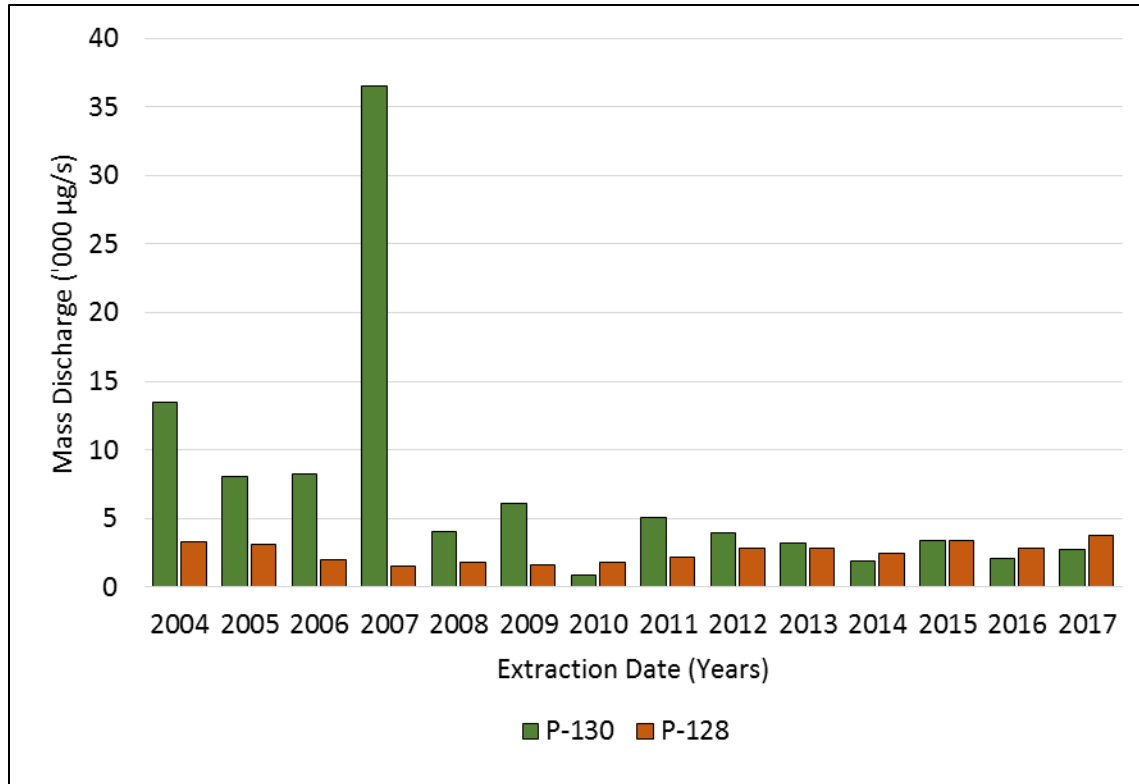
Figure 36: A close-up view of P-130 and P-164 mass discharge.

Between 2004 and 2013, P-130 had a higher mass discharge than P-128 in all years except in 2010. However, between 2013 and 2017, P-128, despite being located further downgradient than P-130, has a higher mass discharge. This may be because of changes in pumping rates, discussed in section 5.3. P-130 displayed a decreasing step trend while P-128 displayed an increasing step trend.

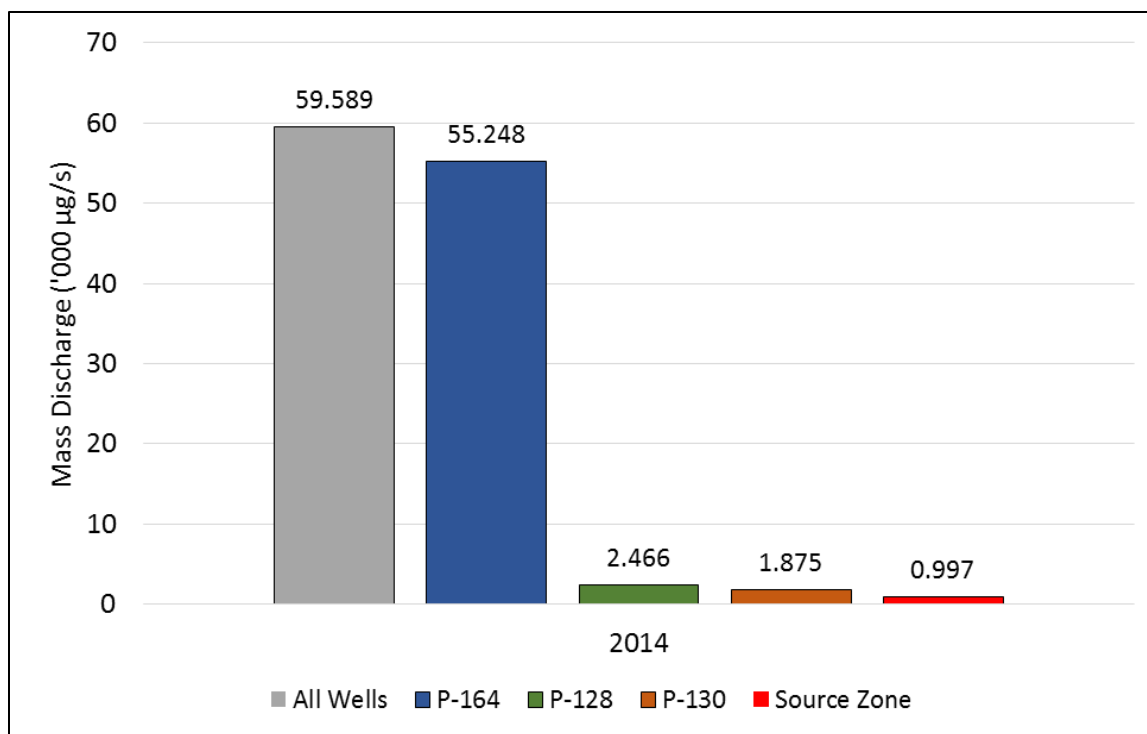Figure 37: A comparison of the source zone mass flux with the barrier system mass discharge. Values are compared in 2014 when the shallow wells were cored. The SZT mass flux is roughly 1.7% of the total mass discharge observed at the pumping wells in 2014. Comparison of the 2014 SZT mass flux with the 2015, 2016 and 2017 HBS results shows that the SZT mass flux is on average, 1.5% of the mass captured by the pumping wells.

Comparing the mass flux from the source zone with the mass discharge from the pumping wells shows that the pumping wells draw contaminants at a rate that is 59.8 times faster than the rate of mass loss from the source zone, according to the 2014 comparison. This comparison is not sensitive to the year of comparison with the barrier system i.e. comparing the source zone mass flux with 2014-2017 results does not yield any significant changes. Therefore, these values are comparable without taking into account the time lag between the source zone and the downgradient barrier system.

The above comparison between the source zone and pumping wells comes with a number of caveats. The first is that the core holes that make up the SZT are only cored in the shallow bedrock that consists of the Prairie du Chien (Tonti and Readstown) and St. Lawrence formations. It is likely that the mass flux calculated is underestimated because it does not include rock core VOC data from some sections of the lower Tunnel City Group, which could potentially increase the total mass flux. However, the calculated flux for 2014 may not significantly change given that most of the mass loss in 2014 occurred in the upper bedrock. The second reason relates to natural source zone depletion. Given the evidence for microbial-mediated attenuation in the source zone (shown by the evolution of chemical composition presented in section 5.1), the mass from the source zone may not all be flowing downgradient to the pumping wells. The

rate of natural attenuation can be estimated and deducted from this mass flux to isolate the fraction that is flushed down-gradient and captured by the barrier system wells. Another limitation is that the mass captured by the barrier system may originate from other sections of the plume created from the contaminant mass between 1970 and 2003. This could explain the relatively high mass captured by the barrier system in comparison to the mass flux originating from the source zone. This last limitation is examined in finer details below.

Understanding the sources of contaminant mass captured by the pumping wells is crucial to qualifying the large difference in mass flux and mass discharge. The composition of the contaminants from the source zone shown in Figure 12 was compared to the composition of the contaminants extracted from the pumping wells (Figure 23 to Figure 29). The results are summarised in Figure 38 below.
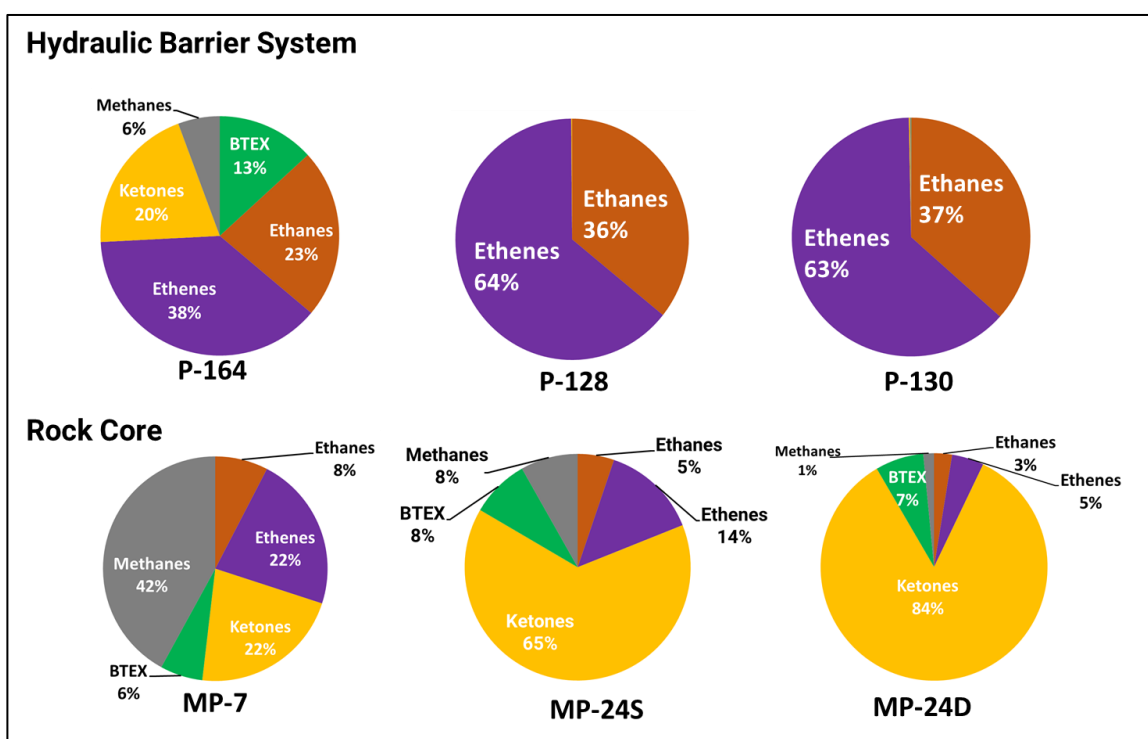
Figure 38: Source zone and barrier system contaminant composition.
Comparison of the overall contaminant composition between the barrier system and the source zone core holes. P-164's contaminant composition is very similar to the three core holes at the SZT whereas P-128 and P-130 are predominantly chlorinated ethanes and ethenes.

The composition of the source zone core holes contained varying percentages of the five key contaminant groups used in this study. Of the three pumping wells, P-164's composition closely resembled that observed from the source zone core holes. P-128 and P-130 were composed primarily of chlorinated ethenes and ethanes. Several hypotheses can be used to suggest mechanisms to explain the composition differences and similarities. The composition of the sampled NAPL (see Figure 30) showed that it was majorly composed of chlorinated ethanes and ethenes (TCA, TCE and PCE). Groundwater flow in the last

four decades dissolved these three contaminants from the source zone and transported them downgradient, creating a plume. Biodegradation of these compounds to lower molecular weight chlorinated ethanes and ethenes occurred both in the rock matrix and along the groundwater flow path. When the pumping wells began operating in 2003, most of the mass captured was most likely from the plume. The composition of P-128 and P-130 support this hypothesis. P-164 is closer to the source zone than the other two wells and therefore likely captures mass from both the plume and the source zone.

Two lines of evidence have been presented to compare the source zone and downgradient wells: mass flux-mass discharge and composition analysis. The first showed that the mass flux emanating from the source zone is over one order of magnitude lower than the total mass flux captured by the barrier wells. The second showed that the composition of two of the three pumping wells is more indicative of the plume characteristics than the source zone composition. However, refining each of these analysis is required to quantify exactly how much of the source zone mass loss is influenced by the downgradient barrier wells.

7   Summary and Conclusion

7.1   Temporal Contaminant Mass Variation

The results presented in section 5.1 showed a significant decline in the rock matrix contaminant mass along the SZT over the fourteen year analysis period. Contaminant concentration trends within the rock matrix varied depending on the position in each core hole as well as with time when the three core holes were examined. In addition to mass, the composition of contaminants varied temporally and also with depth.

Two key groupings were done which enabled key trends to be identified, quantified and discussed. The first grouping was performed by examining cumulative mass curves within each profile and identifying zones based on the mass distribution. Four key zones were identified: two with a high rate of mass loss and two where the mass distribution was lower. A previous analysis showed that majority of the contaminant mass loss occurred in the upper bedrock (Buckley, 2017). This study has refined this mass loss characterisation by showing that between 2014 and 2017, most of the mass loss occurred from the lower bedrock. A key reason for this shift was that after 2014, most of the contaminants in the upper bedrock had already declined to non-detect concentration and thus there was very little mass available to decline in subsequent years. This result implies that the sections of mass loss within the source zones vary with time. Learning more about this variation may be useful when designing depth-targeted remediation systems. Such systems could target zones that are persistent, leaving those where the rate of mass loss is high. On the other hand, delineating sections of the source zone that contribute the highest mass to downgradient plumes can aid in effective plume management strategies.

The second grouping that was done to better understand trends was based on contaminant mass. A closer examination of the contaminant mass at MP-7, MP-24S and MP-24D showed that only 15 of the 35 VOCs that were reported by the laboratory contribute to 99.99% of the total contaminant mass. 13 of these compounds registered mass declines while three displayed an overall mass increase. The declining compounds were primarily higher molecular weight chlorinated compounds as well as compounds whose effective solubilities were relatively high. Each of the three contaminants whose mass increased could have been as a result of different processes within the source zone. Evidence was drawn from previous studies on microbial communities in the rock matrix, geological and hydrogeological characteristics such as erosional unconformities in the upper bedrock, physical parameters such as organic carbon estimations, hydraulic conductivities of the fractures versus matrix and vertical head gradients to understand possible reasons for mass decline, accumulation or persistence. All these contributing mechanisms require closer examination to understand which, if any, are dominant and which ones govern contaminant patterns.

7.2   Evaluating the Efficiency of the Hydraulic Barrier and its Effect on Source Zone Changes

The mass discharge from three down-gradient pumping wells was quantified using quarterly contaminant concentrations and monthly averaged pumping rates. The three wells each experienced a

statistically significant step trend in pumping rates, which had an effect on mass discharge patterns. The mass flux from the source zone was estimated using two interpolation methods which yielded values within the same order of magnitude. On comparing the two, mass discharge from the pumping wells was sixty times higher than the mass flux calculated for the source zone. This discrepancy was attributed to the pumping wells capturing mass from the distal plume that was created from the time the original spill occurred. Given that the size of the plume has decreased since 2003 when it was at its maximum spatial extent, it is likely that the mass captured by the barrier wells has a large contribution from the plume. However, given that one of the wells, P-164, has a similar composition that closely matches that from source zone core analysis, a fraction of the source zone mass decline can be attributed to the pumping wells.

8   Recommendations

Several salient aspects of this research would benefit greatly from further studies. Understanding the reasons behind the variable source zone degradation rates with depth will be a valuable step towards characterising sources of mass loss. Chapelle et al. (2012) estimated a biodegradation rate using contaminant concentrations, effective porosity measurements, estimation of chloride concentrations and groundwater residence time. This simple estimate can be used to provide degradation rates that can be then refined using data such as CSIA results and other chemical data. This quantification is important because it serves as a starting point to assess the contribution of natural source zone depletion to the total declines observed in the source zone. The four zones that have been delineated based on mass distribution patterns would benefit from correlations with visible features such as fracture intensity and aperture, lithological changes and heterogeneity, and inorganic constituents in groundwater. Identifying these zones would enrich the understanding on zones of mass loss and how they contribute to mass flux. The analysis of the mass flux shows that it may vary considerably over time. A key research question would be to investigate whether certain geological formations have a higher propensity for mass loss than others e.g shallow versus deep bedrock. Perhaps other site characteristics are better predictors of mass flux than geology.

Finally, the mass discharge from the pumping wells can be better quantified using an analytical solution such as the integral pumping test approach. However, available analytical solutions should be modified to account for the hydrogeological heterogeneity which influences the capture zone of the wells. Bayer-Raich et al. (2003) develop a particle tracking tool for highly heterogeneous aquifers. A similar approach is required for this site as opposed to more common analytical methods that assume a homogenous aquifer. The capture zone can then be estimated to determine the likelihood of the pumping wells capturing mass from geological units above and below the screened unit. Such a result would be beneficial in informing site managers and environmental regulators on how pump and treat systems alter the contaminant mass and composition in the plume and on the effect of pumping on the source zone.

9   References

Aswasereelert, W., Simo, J. A. T., & Lepain, D. L. (2008). Deposition Of The Cambrian Eau Claire Formation , Wisconsin: Hydrostratigraphic Implications Of Fine-Grained Cratonic Sandstones, *19*.

Austin, D. C. (2005). *Hydrogeologic Controls on Contaminant Distribution Within a Multi- Component DNAPL Zone in a Sedimentary Rock Aquifer in South Central Wisconsin*. University of Waterloo.

Banerjee, S. (1984). Solubility of organic mixtures in water. Environmental Science & Technology, *18*(8), 587–591. https://doi.org/10.1021/es00126a004

Basu, N. B., Rao, P. S. C., Falta, R. W., Annable, M. D., Jawitz, J. W., & Hatfield, K. (2008). Temporal evolution of DNAPL source and contaminant flux distribution: Impacts of source mass depletion. Journal of Contaminant Hydrology, *95*(3–4), 93–109.

Bayer-Raich, M., Jarsjo, J., Holder, T., & Ptak, T. (2003). Numerical estimations of contaminant mass flow rate based on concentration measurements in pumping wells. IAHS Publication, 10–16.

Bradbury, K. R., Swanson, S. K., Krohelski, J. T., & Fritz, A. K. (1999). Hydrogeology of Dane County, Wisconsin, 65. Retrieved from https://wgnhs.uwex.edu/pubs/wofr199904/

Bradley, P. M. (2010). History and Ecology of Chloroethene Biodegradation : A Review History and Ecology of Chloroethene Biodegradation : A Review, *9868*. https://doi.org/10.1080/713607980

Brown, B. A., Massie-Ferch, K. M., Peters, R. M., & Roushar, K. C. (2013). *Preliminary Bedrock Geology of Dane County, Wisconsin*. Madison.

Brusseau, M. L., Nelson, N. T., Zhang, Z., Blue, J. E., Rohrer, J., & Allen, T. (2007). Source-zone characterization of a chlorinated-solvent contaminated Superfund site in Tucson, AZ. Journal of Contaminant Hydrology, *90*(1–2), 21–40. https://doi.org/10.1016/j.jconhyd.2006.09.004

Buckley, A. (2017). *Contaminant Mass Distribution of a Mixed Organic Contaminant Plume Down-Gradient of an Aged DNAPL Source Zone in Sedimentary Rock*. University of Guelph. Retrieved from http://hdl.handle.net/10214/10464

Buckley, A., Meyer, J., Austine-Blaine, D., & Parker, B. (2017). Comparing Rock Matrix Contaminant Profiles Downgradient of a DNAPL Source after 11 Years of Groundwater Dissolution. In *NGWA Conference on Fractured Rock and Groundwater*. Burlington.

Casado, P. (2012). *Fate of a Chlorinated Solvents Plume along the Groundwater Flow System until a Local Discharge Area within a Glacial Sediments and Sedimentary Rock Aquifer*. University of Waterloo.

Chapelle, F. H., Lacombe, P. J., & Bradley, P. M. (2012). Estimated trichloroethene transformation rates due to naturally occurring biodegradation in a fractured rock aquifer. Remediation Journal, *22*(2), 7–20.

Chapman, S. W., Cherry, J. A., & Parker, B. L. (2018). Multiple-scale hydraulic characterization of a surficial

clayey aquitard overlying a regional aquifer in Louisiana. Journal of Hydrology, *558*, 546–563. https://doi.org/10.1016/j.jhydrol.2018.01.059

Cherry, J. A., Barker, J. F., Feenstra, S., Gillham, R. W., Mackay, D. M., & Smyth, D. J. A. (1996). The Borden Site for Groundwater Contamination Experiments: 1978–1995. In *Groundwater and Subsurface Remediation* (pp. 101–127). Springer.

Cherry, J. A., Parker, B., Einarson, M., Chapman, S., & Meyer, J. (2015). Overview of Depth-Discrete Mutilevel Groundwater Monitoring Technologies: Focus on Groundwater Monitoring in Areas of Oil and Gas Well Stimulation in California, 11 Appendix. Recommendations on Model Criteria for Groundwater Sampling, Testing, and Monitoring of Oil and Gas Development in California, Final Report.

Cherry, J. A., Parker, B. L., & Keller, C. (2007). A new depth-discrete multilevel monitoring approach for fractured rock. Ground Water Monitoring and Remediation, *27*(2), 57–70. https://doi.org/10.1111/j.1745-6592.2007.00137.x

Clayton, L., & Attig, J. W. (1997). *Pleistocene geology of Dane County, Wisconsin* (Vol. 95). University of Wisconsin-Extension, Wisconsin Geological and Natural History Survey.

Cline, D. R. (1965). *Geology and ground-water resources of Dane County, Wisconsin*. US Government Printing Office Washington, DC.

Costanza, J., Davis, E. L., Mulholland, J. A., & Pennell, K. D. (2005). Abiotic degradation of trichloroethylene under thermal remediation conditions. Environmental Science & Technology, *39*(17), 6825–6830.

Council, N. R. (1994). *Alternatives for ground water cleanup*. National Academies Press.

Council, N. R. (2013). *Alternatives for managing the nation's complex contaminated groundwater sites*. National Academies Press.

Darlington, R., Lehmicke, L. G., Andrachek, R. G., & Freedman, D. L. (2013). Anaerobic abiotic transformations of cis-1,2-dichloroethene in fractured sandstone. Chemosphere, *90*(8), 2226–2232. https://doi.org/10.1016/j.chemosphere.2012.09.084

Devlin, J. F. (2003). A spreadsheet method of estimating best-fit hydraulic gradients using head data from multiple wells. Groundwater, *41*(3), 316–320.

Einarson, M. D. (2006). Multi-Level Ground Water Monitoring. In D. M. Nielsen (Ed.), *Practical Handbook of Environmental Site Characterization and Ground-Water Monitoring* (2nd ed., pp. 807–848). CRC Press.

Einarson, M. D., & Mackay, D. M. (2001). Peer Reviewed: Predicting Impacts of Groundwater Contamination. Environmental Science & Technology, *35*(3), 66A–73A. https://doi.org/10.1021/es0122647

EPA. (2000). Engineered approaches to in situ bioremediation of chlorinated solvents: Fundamentals and field applications. U. S. Environmental Protection Agency, (EPA 542-R-00-008), 1–144. https://doi.org/EPA 542-R-00-008

Fowler, T., Thompson, B., & Mueller, J. (2011). Acetone and 2-Butanone Creation Associated with Biological and Chemical Remediation of Environmental Contamination, 9–28. https://doi.org/10.1002/rem

Fure, A. D., Jawitz, J. W., & Annable, M. D. (2006). DNAPL source depletion: Linking architecture and flux response. Journal of Contaminant Hydrology, *85*(3–4), 118–140. https://doi.org/10.1016/j.jconhyd.2006.01.002

GeoTrans. (1999). *DNAPL Removal Report*. Cottage Grove.

GeoTrans. (2003). *Additional Characterization Deep DNAPL Bedrock Zone*.

Goldstein, K. J., Vitolins, A. R., Navon, D., Parker, B. L., Chapman, S., & Anderson, G. A. (2004). Characterization and pilot-scale studies for chemical oxidation remediation of fractured shale. Remediation Journal: The Journal of Environmental Cleanup Costs, Technologies & Techniques, *14*(4), 19–37.

Goode, D. J., Imbrigiotta, T. E., & Lacombe, P. J. (2014). High-resolution delineation of chlorinated volatile organic compounds in a dipping, fractured mudstone: Depth- and strata-dependent spatial variability from rock-core sampling. Journal of Contaminant Hydrology, *171*, 1–11. https://doi.org/10.1016/j.jconhyd.2014.10.005

Guilbeault, M. A., Parker, B. L., & Cherry, J. A. (2005). Mass and flux distributions from DNAPL zones in sandy aquifers. Groundwater, *43*(1), 70–86.

Kammerer, P. A. (1995). *Ground-water flow and quality in Wisconsin's shallow aquifer system*. US Department of the Interior, US Geological Survey.

Kokkinaki, A., Werth, C. J., & Sleep, B. E. (2014). Comparison of upscaled models for multistage mass discharge from DNAPL source zones. Water Resources Research, *50*(4), 3187–3205.

Kueper, B. H., Stroo, H. F., Vogel, C. M., & Ward, C. H. (2014). *Chlorinated solvent source zone remediation*. Springer.

Lenczewski, M., Jardine, P., McKay, L., & Layton, A. (2003). Natural attenuation of trichloroethylene in fractured shale bedrock. Journal of Contaminant Hydrology, *64*(3–4), 151–168.

Lima, G., Parker, B., & Meyer, J. (2012). Dechlorinating microorganisms in a sedimentary rock matrix contaminated with a mixture of VOCs. Environmental Science and Technology, *46*(11), 5756–5763. https://doi.org/10.1021/es300214f

Liu, C. X., & Ball, W. P. (2002). Back diffusion of chlorinated solvent contaminants from a natural aquitard

to a remediated aquifer under well-controlled field conditions: Predictions and measurements (vol 40, pg 175, 2002). Ground Water, *40*(3), 220.

Lynn M., M., J.G., F., A.G., F., G.E., G., E.J., S., & S.W., W. (1957). Underground Waste Disposal and Control. Journal (American Water Works Association), *49*(10), 1334–1342. Retrieved from http://www.jstor.org/stable/41255654

Mackay, D. M., & Cherry, J. A. (1989). Groundwater contamination: Pump-and-treat remediation. Environmental Science and Technology, *23*(6), 630–636. https://doi.org/10.1021/es00064a001

Magli, A., Rainey, F. A., & Leisinger, T. (1995). Acetogenesis from dichloromethane by a two-component mixed culture comprising a novel bacterium. Applied and Environmental Microbiology, *61*(8), 2943–2949.

Mai, H., & Dott, R. H. (1985). *A subsurface study of the St. Peter Sandstone in southern and eastern Wisconsin*. Wisconsin Geological & Natural History Survey.

McCarty, P. L., Goltz, M. N., Hopkins, G. D., Dolan, M. E., Allan, J. P., Kawakami, B. T., & Carrothers, T. J. (1998). Full-scale evaluation of in situ cometabolic degradation of trichloroethylene in groundwater through toluene injection. Environmental Science & Technology, *32*(1), 88–100.

Meyer, J. R. (2005). *Migration of a Mixed Organic Contaminant Plume in a Multilayer Sedimentary Rock Aquifer System*. University of Waterloo (M.Sc. Thesis).

Meyer, J. R., Parker, B. L., Arnaud, E., & Runkel, A. C. (2016). Combining high resolution vertical gradients and sequence stratigraphy to delineate hydrogeologic units for a contaminated sedimentary rock aquifer system. Journal of Hydrology, *534*, 505–523. https://doi.org/10.1016/j.jhydrol.2016.01.015

Meyer, J. R., Parker, B. L., & Cherry, J. A. (2008). Detailed hydraulic head profiles as essential data for defining hydrogeologic units in layered fractured sedimentary rock. Environmental Geology, *56*(1), 27–44. https://doi.org/10.1007/s00254-007-1137-4

Meyer, J. R., Parker, B. L., & Cherry, J. A. (2014). Characteristics of high resolution hydraulic head profiles and vertical gradients in fractured sedimentary rocks. Journal of Hydrology, *517*, 493–507. https://doi.org/10.1016/j.jhydrol.2014.05.050

Mickelson, D. M. (1983). *A guide to the glacial landscapes of Dane County, Wisconsin* (Vol. 6). University of Wisconsin--Extension, Geological and Natural History Survey.

Miller, E., Wohlfarth, G., & Diekert, G. (1997). Comparative studies on tetrachloroethene reductive dechlorination mediated by Desulfitobacterium sp. strain PCE-S. Archives of Microbiology, *168*(6), 513–519.

Mintz, J. A. (2011). EPA enforcement of CERCLA: Historical overview and recent trends. Sw. L. REv., *41*, 645.

National Research Council. (2005). *Contaminants in the subsurface: Source zone assessment and remediation*. National Academies Press.

Newell, C. J., Conner, J. A., & Rowen, D. A. (2003). Groundwater Remediation Strategies Tool. Publication No. 4730. API American Petroleum Institute, Houston, TX.

Newell, C. J., Cowie, I., McGuire, T. M., & McNab, W. W. (2006). Multiyear Temporal Changes in Chlorinated Solvent Concentrations at 23 Monitored Natural Attenuation Sites. Journal of Environmental Engineering, *132*(6), 653–663. https://doi.org/10.1061/(ASCE)0733-9372(2006)132:6(653)

Nielsen, D. M. (2005). *Practical Handbook of Environmental Site Characterization and Ground-Water Monitoring* (2nd ed.). CRC Press.

O'Connor, D., Hou, D., Ok, Y. S., Song, Y., Sarmah, A., Li, X., & Tack, F. M. G. (2018). Sustainable in situ remediation of recalcitrant organic pollutants in groundwater with controlled release materials: A review. Journal of Controlled Release, *283*(May), 200–213. https://doi.org/10.1016/j.jconrel.2018.06.007

Odom, E. I. (1978). Lithostratigraphy and sedimentology of the Lone Rock and Mazomanie Formations, upper Mississippi valley. Lithostratigraphy, Petrology, and Sedimentology of Late Cambrian--Early Ordovican Rocks Near Madison, Wisconsin. WGNHS Field Trip Guide Book, *3*.

Odutola, A. O., & Walsh, K. P. (2002). Sorption mechanism of organic compounds in karst: SOM or HSACM dependent? IAHS PUBLICATION, 181–186.

Ostrom, M. E. (1970). Field trip guidebook for Cambrian-Ordovician geology of western Wisconsin: Wisconsin Geological and Natural History Survey Information Circular 11.

Pankow, J. F., & Cherry, J. A. (1996). *Dense Chlorinated Solvents and other DNAPLs in Groundwater: History, Behavior, and Remediation*. *Dense Chlorinated Solvents and other DNAPLs in Groundwater: History, Behavior, and Remediation*.

Parker, B., Cherry, J., & Chapman, S. (2012). Discrete Fracture Network Approach for Studying Contamination in Fractured Rock. AQUAMundi: Journal of Water Science, *3*(2), 101–116. https://doi.org/10.4409/Am-052-12-0046

Parker, B., Cherry, J., Meyer, J., & Casado, P. (2015). *University Consortium for Field Focused Groundwater Contamination Research, Year 2014 Progress Report*.

Parker, B. L., Chapman, S. W., & Cherry, J. A. (2010). Plume persistence in fractured sedimentary rock after source zone removal. Ground Water, *48*(6), 799.

Parker, B. L., Chapman, S. W., Goldstein, K. J., & Cherry, J. A. (2018). Multiple lines of field evidence to inform fracture network connectivity at a shale site contaminated with dense non-aqueous phase

liquids. Geological Society, London, Special Publications, *479*, SP479-8.

Parker, B. L., Cherry, J. A., & Chapman, S. W. (2004). Field study of TCE diffusion profiles below DNAPL to assess aquitard integrity. Journal of Contaminant Hydrology, *74*(1–4), 197–230.

Parker, B. L., Cherry, J. a, & Chapman, S. W. (2012). Discrete fracture network approach for studying contamination in fractured rock. AQUAMundi: Journal of Water Science, *60*(december), 101–116. https://doi.org/10.4409/Am-052-12-0046

Parker, B. L., Gillham, R. W., & Cherry, J. A. (1994). Diffusive disappearance of immiscible-phase organic liquids in fractured geologic media. Groundwater, *32*(5), 805–820.

Parker, B., Meyer, J., & Cherry, J. (2018). *University Consortium for Field Focused Groundwater Contamination Research, Year 2017 Progress Report*.

Parsen, M. J., Bradbury, K. R., Hunt, R. J., & Feinstein, D. T. (2016). *The 2016 Groundwater Flow Model for Dane County , Wisconsin: Wisconsin Geological and Natural History Survey Bulletin 110, 56 p*.

Pierce, A. A., Chapman, S. W., Zimmerman, L. K., Hurley, J. C., Aravena, R., Cherry, J. A., & Parker, B. L. (2018). DFN-M field characterization of sandstone for a process-based site conceptual model and numerical simulations of TCE transport with degradation. Journal of Contaminant Hydrology, *212*(April 2017), 96–114. https://doi.org/10.1016/j.jconhyd.2018.03.001

Quinn, P., Cherry, J. A., & Parker, B. L. (2012). Hydraulic testing using a versatile straddle packer system for improved transmissivity estimation in fractured-rock boreholes. Hydrogeology Journal, *20*(8), 1529–1547.

Ricker, J. A. (2008). A practical method to evaluate ground water contaminant plume stability. Ground Water Monitoring and Remediation, *28*(4), 85–94. https://doi.org/10.1111/j.1745-6592.2008.00215.x

Rivett, M. O., Feenstra, S., & Cherry, J. A. (1994). Transport of a dissolved-phase plume from a residual solvent source in a sand aquifer. Journal of Hydrology, *159*(1–4), 27–41. https://doi.org/10.1016/0022-1694(94)90247-X

Runkel, A. C., Tipping, R. G., Alexander Jr, E. C., & Alexander, S. C. (2006). Hydrostratigraphic characterization of intergranular and secondary porosity in part of the Cambrian sandstone aquifer system of the cratonic interior of North America: Improving predictability of hydrogeologic properties. Sedimentary Geology, *184*(3–4), 281–304.

Schaefer, C. E., White, E. B., Lavorgna, G. M., & Annable, M. D. (2016). Dense Nonaqueous-Phase Liquid Architecture in Fractured Bedrock: Implications for Treatment and Plume Longevity. Environmental Science and Technology, *50*(1), 207–213. https://doi.org/10.1021/acs.est.5b04150

Schwille, F., & Pankow, J. F. (1988). Dense chlorinated solvents in porous and fractured media-model experiments.

Silliman, S. E., & Frost, C. (1998). Monitoring hydraulic gradient using three-point estimator. Journal of Environmental Engineering, *124*(6), 517–523.

Şimşir, B., Yan, J., Im, J., Graves, D., & Löffler, F. E. (2017). Natural Attenuation in Streambed Sediment Receiving Chlorinated Solvents from Underlying Fracture Networks. Environmental Science & Technology, *51*(9), 4821–4830. https://doi.org/10.1021/acs.est.6b05554

Sterling, S. N., Parker, B. L., Cherry, J. A., Williams, J. H., Lane, J. W., & Haeni, F. P. (2005). Vertical cross contamination of trichloroethylene in a borehole in fractured sandstone. Ground Water, *43*(4), 557–573. https://doi.org/10.1111/j.1745-6584.2005.0087.x

Stroo, H. F., Leeson, A., Marqusee, J. A., Johnson, P. C., Ward, C. H., Kavanaugh, M. C., … Unger, M. (2012). Chlorinated Ethene Source Remediation: Lessons Learned. Environmental Science & Technology, *46*(12), 6438–6447. https://doi.org/10.1021/es204714w

Stuetzle, R. J. (2014). *Vertical Profiling Data Sets for Improved Characterization of Hydrologic Units Influencing Contaminant Migration in Strongly Heterogeneous Triassic Sediments*. University of Guelph (MASc. Thesis).

Team, I. I. D. S. S. (2010). Use and Measurement of Mass Flux and Mass Discharge. Integrated DNAPL Site Strategy Team, The Interstate Technology & Regulatory Council, 154.

Tetra Tech. (2017). *Third Quarter 2017 Progress Report July 1 Through September 30, 2017*. Wisconsin.

Toth, J. (1963). A theoretical analysis of groundwater flow in small drainage basins. Journal of Geophysical Research, *68*(16), 4795–4812.

U.S. Environmental Protection Agency. (2004). Cleaning Up the Nation's Waste Sites: Markets and Technology Trends.

UNESCO. (2014). *The United Nations World Water Development Report 2014: Water and Energy* (Vol. 1). https://doi.org/978-92-3-104259-1

Wanner, P., Parker, B. L., Chapman, S. W., Lima, G., Gilmore, A., Mack, E. E., & Aravena, R. (2018). Identi fi cation of Degradation Pathways of Chlorohydrocarbons in Saturated Low-Permeability Sediments Using Compound-Speci fi c Isotope Analysis. https://doi.org/10.1021/acs.est.8b01173

Wiedemeier, T. H., Rifai, H. S., Newell, C. J., & Wilson, J. T. (1999). *Natural attenuation of fuels and chlorinated solvents in the subsurface*. John Wiley & Sons.

Wright, J., Kirchner, V., Bernard, W., Ulrich, N., McLimans, C., Campa, M. F., … McDermott, J. (2017). Bacterial Community Dynamics in Dichloromethane-Contaminated Groundwater Undergoing Natural Attenuation. Frontiers in Microbiology, *8*, 2300.

Yalkowsky, S. H., He, Y., & Jain, P. (2010). *Handbook of Aqueous Solubility Data* (2nd ed.). CRC Press. https://doi.org/10.1017/CBO9781107415324.004